Fluorescent imaging probes for *in vivo* ovarian cancer targeted detection and surgery

Roberta Solidoro, Antonella Centonze, Morena Miciaccia, Olga Maria Baldelli, Domenico Armenise, Savina Ferorelli, Maria Grazia Perrone, Antonio Scilimati*

Department of Pharmacy - Pharmaceutical Sciences, University of Bari, Via E. Orabona 4, 70125 Bari (Italy).

Abstract

Ovarian cancer is the most lethal gynecological cancer, with a survival rate of approximately 40%. The first-line treatment consists of cytoreductive surgery combined with chemotherapy (platinum and taxane-based drugs). To date, the main prognostic factor is related to the complete surgical resection of tumor lesions, including occult micro-metastases. The presence of minimal residual diseases not detected by visual inspection and palpation during surgery significantly increases the risk of disease relapse. Intraoperative fluorescence imaging systems have the potential to improve surgical outcomes. Fluorescent tracers administered to the patient may support surgeons for better real-time visualization of tumor lesions during cytoreductive procedures. In the last decade, consistent with the discovery of an increasing number of ovarian cancer-specific targets, a wide range of fluorescent agents were identified to be employed for intraoperatively detecting ovarian cancer. Here, we present a collection of fluorescent probes designed and developed for fluorescence-guided ovarian cancer surgery. Original articles published between 2011 and November 2022 focusing on fluorescent probes, currently under preclinical and clinical investigation, were searched in PubMed. The keywords used were *targeted detection*, *ovarian cancer*, *fluorescent probe*, *near-infrared fluorescence*, *fluorescence-guided surgery*, and *intraoperative imaging*. All identified papers were English-language full-text papers, and probes were classified based on the location of the biological target: intracellular, membrane, and extracellular.

Key Words:

targeted-detection, ovarian cancer, fluorescent probe, near-infrared fluorescence, fluorescence-guided surgery, intraoperative imaging

1. Introduction

The third most recurrent gynecological cancer globally in 2020, ovarian cancer is the most aggressive of all, with a relative 5-year survival rate of approximately 40%. Referred to as "the silent killer", ovarian cancer is not diagnosed before the advanced stages (III or IV) in 70% of cases. Indeed, vague, and non-specific in the early stage of disease (I-II), the symptoms mainly appear when the disease has already progressed, spreading beyond ovaries inside the abdominal cavity.[1-2] Moreover, the lack of specific biomarkers for ovarian cancer hinders early diagnosis.[3-4] To date, the cornerstone of first-line treatment of ovarian cancer is the combination of cytoreductive surgery and platinum and taxane-based chemotherapy.[4-5] Unfortunately, clinical relapse occurs in 70% of patients, usually within 28 months after primary combined treatment.[6] The presence of minimal residual diseases (<1 cm), not identified during surgery by visual inspection and palpation of surgeons, likely explains the high rate of progression-free survival and recurrences. Indeed, unidentified micro-lesions are often resistant to the following adjuvant chemotherapy treatment and continue to grow after the apparent complete tumor resection.[7] Therefore, the degree of cytoreduction strongly impacts patients' outcomes and represents an important prognostic factor. Until now, an "optimal" cytoreduction possesses minimal residual tumor masses of dimension below 2 cm. Currently, the objective is to achieve complete tumor resection.[8-9] Fluorescence imaging technology constitutes a useful clinical tool to improve real-time intraoperative visualization of primary tumors and occult metastases. Fluorescence-guided surgery (FGS) consists of the combined use of a light source with fitting filters for the excitation of the fluorescence probe, which works as a contrast agent administered to the patient before the surgery procedure, and of a detector of the fluorescent light emitted by the tumor in which the probe is uptaken.[10] Designed to target specific ovarian cancer antigens, fluorescent probes allow the distinction of areas of interest from surrounding healthy tissues through fluorescent signals, with a contrast degree expressed by the tumor-to-background ratio (TBR) value.[11] The increasing number of ovarian cancer-specific biological targets (e.g., folate receptor α,[12] $\alpha v\beta 3$-integrin,[13] prolactin receptor,[14] human follicle-stimulating hormone receptor,[15] β-galactosidase,[16] cyclooxygenase-1[17]) discovered in the last decade has led to the design and development of a wide range of fluorescent probes. The contrast agents generally consist of a moiety that permits the identification of tumor tissues, usually through recognizing and interacting with specific surface antigens, exploiting the high affinity of natural ligands or small molecules, otherwise the high specificity of monoclonal antibodies. [18] Some nano-delivery systems have been investigated to direct the fluorescent probes to the malignancy.[12] Suitably tagged, fluorescent nano-tracers can specifically detect tumor lesions not only through interaction with a specific molecular target but also by exploiting the phenomenon of enhanced permeability and retention effect (EPR). Indeed, the leaky vasculature and compromised lymphatic drainage of tumor microenvironments induce a passive and selective accumulation of nanoparticles (NPs). Depending on the typology of the probe, fluorophores can be differently conjugated targets recognizing moiety. Typically, the antibody- and small-molecule-based probes are connected to the fluorophores either directly or otherwise *via* a linker. Nano-tracers usually include fluorescent dyes or being fluorescently tagged.[19] Moreover, fluorescence-emitting inorganic nanoparticles are being developed, which consist of nano-platforms that emit fluorescent signals at wavelengths lower (down-converting nanoparticles, DCNPs) or higher (up-converting nanoparticles, UCNPs) of the excitation wavelength. DCNPs and UCNPs exhibit interesting spectral characteristics compared to organic fluorophores, such as a higher Stoke shift and enhanced contrast capability.[20] FGS probes may be "always-on" or "activatable" tracers. More diffuse, "always-on" fluorescent probes offer more manageable design and synthesis.18 On the contrary, "activatable" probes emit fluorescence only after being activated *in situ*, usually by a molecular target, such as a tumor-associated enzyme. Activatable tracers possess much lower background signals, thus exhibiting greatly improved TBRs.[21] To date, FGS probes under preclinical and clinical investigation emit in the visible (400 – 700 nm), the near-infrared (NIR, 700 – 900 nm)[22], and the second window of near-infrared (NIR-II, 900 – 1700 nm) spectrum.[23] Nevertheless, the optimal spectral features have been observed in NIR-fluorescent probes, possessing the highest tissue penetration ability among all fluorescent probes. In other spectral windows, the penetrating capability of fluorescent agents was quite limited. When fluorescent probes emit at wavelengths below 700 nm, an overlap occurs between probe-emitted fluorescent signals and cell autofluorescence, strongly limiting the contrast action of visible-emitting probes. Moreover, numerous endogenous molecules, such as hemoglobin and myoglobin, show a high absorbance in the visible spectrum. Similarly, water and lipids absorb at wavelengths above 900 nm.[22-23]

Hereafter, we report a collection of ovarian cancer-associated biological targets and the corresponding fluorescent probes specifically designed and developed for *in vivo* intraoperative fluorescence-guided detection of ovarian cancer. Based on cellular localization, we classified biological targets as intracellular-, membrane-associated- and extracellular.

2. Intracellular targets

2.1 Cyclooxygenase 1 (COX-1)

Cyclooxygenase (COX), also known as prostaglandin-endoperoxide H synthase (PGHS), is a bifunctional, heme-containing, and membrane-bound enzyme located on the endoplasmic reticulum luminal surfaces and catalyzes the intermediated steps of the biosynthesis of prostanoids. Encoded by two different genes, two COX isoforms are known (COX-1 and COX-2). COX-1 is a constitutive enzyme, expressed at low levels in most cell types, whereas at high levels in the gastric mucosa and platelets. In contrast, COX-2 expression is typically inducible by inflammation mediators, such as cytokines and growth factors.[24-25] Different from COX-2 overexpressed in most cancer types, COX-1 is moderate to highly expressed in 99% of high-grade serous ovarian cancer.[26-27] Over the years, several experimental data have proposed COX-1 as an ideal biomarker for ovarian cancer. In a preliminary *in vivo* investigation, [18F]-fluorinated COX-1 highly selective inhibitor ([18F]-P6) demonstrated a reliable potential as a COX-1-targeted PET imaging agent.[17] Encouraging outcomes suggest that COX-1 might represent an effective biological target for *in vivo* detection of ovarian cancer, despite further investigations being necessary.

RR11 probe

The fluorescent compound RR11 (λ_{abs}=610 nm; λ_{em}=672 nm) has been designed and developed for *in vivo* targeted detection of ovarian cancer. Structurally, the fluorescent probe (Figure 1) presents a targeting moiety consisting of one of the most potent and selective COX-1 inhibitors (Mofezolac, (COX-1 IC_{50} =0.0079 µM, COX-2 IC_{50} > 50 µM), connected through an alkyl linker to the fluorescent moiety, consisting of a NIR fluorophore (Nile blue, λ_{ex}=631 nm; λ_{em}=660 nm).

Figure 1.

RR11 inhibits *o*COX-1 with IC_{50}=0.032 µM and *h*COX-2 with IC_{50}=2.4 µM, and a selectivity index SI (COX-2 IC_{50}/ COX-1 IC_{50})=72. According to cytofluorimetry and confocal fluorescence imaging studies, RR11 enters inside the cells (OVCAR-3 cells) and accumulates in the endoplasmic reticulum (ER), which expresses COX-1. RR11 showed a significant change in the fluorescence emission at a concentration of 50 nM. The lipophilicity of the NIR component (Nile blue) likely promotes the entering of RR11 into the cells. Quantified using the Harmony database, fluorescence intensity emitted by RR11 was dose-dependent, increasing in the whole cell from 100 nM (82 f.u) to 100 mM (1,444 f.u). At all concentrations, the membrane fluorescence emission was about 80% of the total fluorescence measured in the whole cell, indicating that RR11 almost exclusively binds to COX-1 on the ER. *In vivo* evaluation of RR11 has been performed in two subcutaneous murine models of ovarian cancer, respectively implanted with COX-1-over-expressing cell lines (OVCAR-3 cells) and COX-1-low-expressing cell lines (SKOV-3 cells). High non-specific fluorescence has been detected in kidneys and gastrointestinal tract after 2 hours from IV injection with 100 µL of 500 µM of RR11. According to *ex vivo* analysis performed on tumor tissues and healthy organs, the non-specific fluorescence was due to an auto-fluorescent alfalfa-containing diet. Tumor-specific fluorescence has been detected only after 4, 6, and 24 hours from RR11 injection, with a mean TBR value of 1.74 at 24 hours post-injection. In addition to significant tumor-specific fluorescence, analyses *ex vivo* revealed a high fluorescence in animal kidneys, gallbladder, stomach, and lungs, suggesting that RR11 exhibits a kidney metabolization. The probe showed a similar biodistribution profile in xenografted mice models of ovarian cancer COX-1-absent (SKOV-3). However, the mean TBR value measured 24 hours post-injection was 1.28, which does not distinguish between healthy organs and malignant tissue. The diffuse fluorescent signals detected among the whole body may be related to mouse and human COX-1 cross-reactivity. Constitutively expressed in many organs, COX-1 may not be specific enough to allow specific *in vivo* detection of ovarian cancer. [28-29]

MSA14 probe

MSA14 (Figure 2) is a NIR fluorescent compound (λ_{abs1}=260 nm, λ_{abs2}=770 nm; λ_{em1}=318 nm, λ_{em2}=822 nm) designed and synthesized for targeting *in vitro* and *in vivo* COX-1.

Figure 2.

Analogously to RR11, MSA14 developed by Scilimati et al.[17] exhibits a COX-1-targeting moiety consisting of the most selective and potent COX-1 inhibitor approved for human use (Mofezolac) conjugated with the fluorescent dye Indocyanine green (ICG, λ_{abs}=7 80 nm; λ_{em}=830 nm) through a flexible alkyl linker. The fluorescent compound possesses a high COX-1-selectivity (SI=874), with a COX-1 IC_{50}=0.087 µM and a COX-2 IC_{50}>50 µM. In the COX-1-overexpressing OVCAR-3 murine model, MSA14 reaches the highest TBR value (1.44) only after 24 hours from IV administration (100 µL of 500 µM). Unfortunately, a residual background fluorescence has been observed, especially in the spine, limbs, and excretion organs. Subsequently, *ex vivo* fluorescence imaging of both tumor tissues and organs excised confirmed the biodistribution data acquired *in vivo*. MSA14 has been *in vivo* evaluated in a clinically compatible intraoperative setting using the FLARE® system (Curadel LLC, Nattick, MA, USA) in subcutaneous OVCAR-3 mice models. Despite high tumor-specific fluorescence in tumors, the gallbladder and lungs exhibited stronger fluorescent signals. To assess the specificity, subcutaneous xenografted mice models of SKOV-3, an ovarian cancer cell line in which COX-1 is absent, have been injected with MSA14. At different dosages of MSA14 (500 µM and 100 µM), fluorescence signals in the tumor have been acquired at 6 and 21 hours post-IV-injection, registering average TBR values of respectively 1.49 and 1.5 for the higher dosage, and 1.23 and 1.96 for the lower. The liver, limbs, and spine exhibited high non-specific fluorescence. Like OVCAR-3 models, in *ex vivo* analysis, the lungs (at the high dose) and spleen showed high signals. Despite intraoperative imaging showing a strong tumor signal at the dose of 500 µM, the tumor fluorescence intensity did not allow the discrimination between healthy organs and malignant tissue. These findings suggest that fluorescence detected in low-COX-1-expressing tumor lesions might be non-specific. The high non-specific signal rate observed in healthy organs and the relatively low TBR values support this consideration. The constitutive expression of COX-1 in many organs, e.g., liver, spleen, intestines, and bone marrow, or the insufficient specificity COX-1 expression of ovarian cancer cells may represent a strong limitation in COX-1 using as a specific ovarian cancer target. However, further investigation is necessary to identify the real target of the newly prepared compounds, which still maintain great potential as contrast agents for ovarian cancer fluorescence-guided surgery.[29]

CMP probe

Developed for COX-1 *in vivo* detection, the fluorescent compound CMP (λ_{ex}=580 nm; λ_{em}=606 nm) consists of the potent COX-1 inhibitor SC-560 as enzyme recognizing moiety, connected with an alkyl linker to the carboxy-X-rhodamine fluorophore (Figure 3).[30]

Figure 3.

The design of the CMP fluorescent probe originated from the discovery of a COX-2-targeted imaging agent (fluorocoxib A), composed of a fluorescent moiety to the carboxyl group of the nonselective COX inhibitor indomethacin. Exhibiting a COX-2-selective inhibitory activity, Fluorocoxib A showed high specificity *in vivo* detection of COX-2-overexpressing tumors in animal models of colon cancer (HCT116 cells).[31-32] CMP showed a selective and potent inhibitory activity towards COX-1 (COX-1 IC_{50}=94 nM; COX-2 IC_{50}>1000 nM). Moreover, the fluorescent compound *in vitro* exhibited high COX-1 inhibitory activity in OVCAR-3 cells, inhibiting the *human* COX-1 with a significative IC_{50} (44 nM). Given that pre-treatment of cells with indomethacin significantly reduces the intensity of the fluorescent signal, CMP possesses a strong specificity for COX-1 detection. Evaluated *in vivo* as a COX-1-targeted optical imaging agent, CMP 3-4 hours post intraperitoneal (IP) injection (at a dosage of 1 mg for 1 kg of body weight) during *in vivo* imaging showed high tumor-specific accumulation in subcutaneous athymic nude mouse models of ovarian cancer (OVCAR-3 cells). The *ex vivo* analyses have confirmed the higher and more specific CMP localization in the OVCAR-3 tumors than in healthy tissues. Furthermore, CMP specifically highlights *in vivo* COX-1 overexpressing tumor lesions within 3-4 hours post IP administration in *a* murine model intraperitoneally implanted with ID8-NGL cells. Moreover, the co-injection of indomethacin compromises the tumor-specific fluorescence.[30]

2.2 Targeting Hunan Nicotinamide adenine dinucleotide phosphate (*h*NQO1)

Human nicotinamide adenine dinucleotide (phosphate): quinone oxidoreductase isozyme 1 (hNQO1) is primarily (~90%) a cytosolic reductase that utilizes NADH or NADPH as a reducing cofactor. The enzyme consists of a homodimer, and each monomer is associated with one molecule of flavin adenine dinucleotide (FAD). *h*NQO1 specifically reduces quinones to hydroquinones through a two-electron reduction, bypassing the formation of the potentially toxic semiquinone, which is highly reactive and can generate reactive oxygen species (ROS).[33] Moreover, the enzyme action contributes to maintaining endogenous lipid-soluble antioxidants such as α-tocopherol-hydroquinone and ubiquinol in their reduced and active forms. In addition, it is known that INQO1 enhances the accumulation of the p53 protein, negatively affecting one of its degradation pathways under oxidative stress conditions. Thus, INQO1 is historically known as an endogenous detoxifying cellular agent, having antioxidant and cytoprotective functions.[34] Despite the *h*NQO1 expression being typically suppressed during chronic inflammation with a consequent increasing cellular susceptibility to injuries, several studies have reported that an elevated *h*NQO1 expression at early phases of carcinogenesis may be associated with cancer cell growth promotion.[35-37] Indeed, it has been observed that *h*NQO1 is overexpressed in many solid tumors, including ovarian cancer.[38] Furthermore, Cui *et al.* have shown that the high rate of enzyme expression is also associated with higher histological grade, advanced clinical stage, and lower survival rates. Although its role remains partially unclear thus far, the high positive rate of *h*NQO1 protein may represent an effective biomarker for serous ovarian carcinomas.[39]

Q$_3$STCy probe

Q$_3$STCy is a NIR fluorescent probe activated in situ by the human nicotinamide adenine dinucleotide (phosphate): quinone oxidoreductase isozyme 1 (*h*NQO1). In the presence of cofactor NADH, *h*NQO1 reducing the quinone propionic acid group allows its cleavage and the consequent self-cleavage of the 2-mercaptoethanol, turning on the NIR fluorescence of the probe (Figure 4).[40]

Figure 4.

During intraoperative imaging performed in an intraperitoneal murine model of human ovarian cancer (SHIN3-DsRed cells), at excitation wavelengths of 672.5–747.5 nm and emission wavelengths of 765–855 nm, the probe (λ_{em}=755 nm) showed high sensitivity (96.9%) *in vivo* detecting 124 of 128 tumor lesions. The whole-body fluorescence imaging was carried out 10 minutes post IP injection with Q$_3$STCy (300 μL of 25 μM) after euthanasia of all animals. Since intra-abdominal organs, especially the small bowel, emitted fluorescent signals, the Q$_3$STCy specificity did not reach 61%, even though the fluorescence intensity of healthy cells was significantly weaker than that of malignant tissues.[40] Being activable in situ, Q$_3$STCy is topically sprayable onto the surface of tumors during the surgical procedure, resulting in an advantageous tool providing a cancer-specific fluorescence using small doses that reduce potential toxic complications.[41] The *ex vivo* fluorescence imaging has shown significantly different levels of fluorescence intensity in the small intestine tissues and SHIN3 tumors when topically sprayed by the NIR activable probe, which creates a high contrast between the disease and the background healthy tissue, even though both show the same emitting profile. Indeed, in both healthy and malignant tissues, the fluorescent signal immediately increases post-injection and further intensifies during monitoring (60 minutes). Collecting the *ex vivo* fluorescent images at different time points has allowed the construction of a time-fluorescence intensity curve and the acquisition of three different parameters: the maximum fluorescence signal (MF), the wash-in rate (WIR), and the area under the curve (AUC). [40] While MF is the maximum in fluorescence observed, WIR is the maximum slope approaching the MF. AUC is instead the area measured under the time-fluorescence curve.[42] These kinetics parameters allow the differentiation between signals associated with tumors from the background, showing a significantly improved specificity of Q$_3$STCy to 80%, 100%, and 100% for MF, WIR, and AUC, respectively, beyond the moderate improvement in sensitivity (100% for all approaches). Since it is a NIR-light emitting probe, Q$_3$STCy possesses a high tissue penetration ability. Moreover, being topically administrable during the surgical procedure, Q$_3$STCy may be particularly useful for detecting tiny, and consequently undetectable by the naked eye, metastatic tumor lesions, usually disseminated throughout the abdomen in advanced ovarian cancer stages. These findings demonstrate that Q_3STCy represents a potential imaging agent in aiding the targeted detection of ovarian cancer during intraoperative real-time fluorescence imaging.[40]

2.3 Lysosomal hydrolase *β*-Galactosidase (*β*-Gal)

β-Gal specifically catalyzes the hydrolysis of *β*-glycosidic bond.[16] In cancer, high levels of *β*-Gal expression and activity may lead to the degradation of proteoglycan, the main component of the extracellular matrix, and consequently to the destruction of the basement membrane as well as the extracellular interstitial barrier, promoting the infiltration and metastasis of cancer cells.[43] Extensive research has reported that primary ovarian cancer overexpresses *β*-Gal. Therefore, the enzyme has been considered an ovarian cancer biomarker, both *in vitro* and *in vivo*. Indeed, over the last decades, several activatable molecular probes for the specific detection of *β*-Gal have been developed.[16]

HMRef-βGal probe

Asanuma *et al.* have developed a highly sensitive fluorescent probe for *in vivo* imaging of metastatic ovarian cancer by detecting intracellular *β*-Gal activity. The fluorescent probe structure consists of a hydroxymethyl rhodol (HMR) derivative conjugated to a molecule of *β*-galactose (βGal). HMRef-βGal (Figure 5) at physiological pH 7.4 exists in the non-fluorescent spirocyclic form (pK_{cycl}=4.5), possessing high membrane permeability (LogP=2.61 (ALOGPS 2.1 program).[44]

Figure 5.

Moreover, at physiological pH, existing in a non-fluorescent spirocyclic form, HMRef-βGal exhibits a strongly reduced background noise. Indeed, only inside the cell can the probe be converted in its highly fluorescent form (HMR-Ref, Figure 6) by *β*-Gal action (Figure 25), which determines a fluorescence enhancement in the intensity of >1,400 fold. [44]

Figure 6.

Tested *in vitro*, HMRef-βGal determined fluorescence in several cultured ovarian cancer cell lines (SHIN3, SKOV3, OVK18, OVCAR3, OVCAR4, OVCAR5, and OVCAR8). Moreover, the fluorescence intensity strongly decreased in the presence of a *β*-Gal inhibitor (*β*-galactosylamidine; β-GA).[45] Since HMRef-βGal showed almost no toxicity up to 100 mM (MTT assay) and any significant body weight change or even death in mice during a preliminary *in vivo* toxicity evaluation at ten times higher dose, the activatable probe demonstrated to be suitable for further *in vivo* preclinical evaluation. Based on these findings, HMRef-βGal was evaluated in an intraperitoneal murine model of metastatic ovarian cancer (SHIN3 cells). 5 minutes after IP injection with HMRef-βGal (300 ml of 100 mM solution), metastases down to 1 mm in size were visible inside the peritoneal cavity of the sacrificed mice. 1 hour post-administration, the fluorescence intensity in the tumor increased as much to be discriminated from healthy tissues by the naked eye. All the tumor lesions detected were confirmed to be malignant by the colocalization with a lectin-targeted stain.[46] Moreover, co-administration of HMRef-βGal with the *β*-Gal inhibitor (β-GA) determined the almost complete suppression of fluorescence, confirming the probe *β*-Gal-specific targeting. HMRef-βGal achieved similar outcomes in metastatic ovarian cancer mice models IP administered with the probe. The fluorescent probe has been tested for *in vivo* fluorescence laparoscopy to detect metastases. The activatable agent successfully identified tumor lesions, allowing the resection of tumor nodules down to 1 mm in size in the real-time fluorescence-guided laparotomy. HMRef-βGal allowed the localization of metastases in a direct three-dimensional view by visible fluorescence. Despite further investigations being necessary before clinical evaluation, HMRef-βGal has surgical cytoreduction of ovarian cancer under fluorescence imaging guidance.[44]

BOD-M-βGal

Chen *et al.* developed an activatable NIR-II fluorescent probe for *in vivo* targeted detection of ovarian cancer. The fluorescent probe exhibits a β-galactose residue for *in vivo* tracking of the β-Gal activity, increased in primary ovarian cancer. Consisting of a boron dipyrromethene (BODIPY) derivative, the fluorescent dye is connected to the monosaccharide through a benzyl thioether linker. The electron-withdrawing group (3-ethyl-1,1,2-trimethyl-1H-benz[e]indolium) has been inserted in position 3 of the BODIPY core *via* a vinylene linker (Figure 7) to elongate the π-conjugation, obtaining the BOD-M-βGal probe.[47]

Figure 7.

After treatment with β-Gal, the absorption/emission bands of BODIPY (λ_{abs}=533 nm, and λ_{em}=565 nm) decreased until a complete quenching within 20 minutes. β-Gal triggers the 1,6-elimination reaction and the subsequent releasing of the BODIPY-based fluorophore (BOD-M-SH), which exhibits a Stokes shift of 130 nm, being excitable at λ=723 nm and emitting in the NIR region at λ=853 nm. The action of β-Gal generates a 35-fold increase in NIR fluorescence emission. Furthermore, the probe exhibited a fluorescence tail in the NIR-II region (λ=1000 - 1200 nm), which is advantageous for *in vivo* cancer imaging and offers a higher resolution and deeper tissue penetration. BOD-M-βGal showed only weak changes in fluorescence intensity when treated with various analytes such as enzymes, amino acids, and biomolecules. A strong NIR fluorescence emission is turned on by the exclusive addition of βGal, showing BOD-M-βGal exhibits high selectivity for *β*-Gal. The kinetics of enzyme-catalyzed hydrolysis of BOD-M-βGal has been examined, determining Vmax and Km (0.36 µM ·s-1 and 40.16 µM respectively). Whereas increased β-Gal concentration enhances the rate of the enzymatic reaction, in contrast, the addition of D-galactose reduces the rate of the reaction, likely establishing a competition mechanism, confirming the specific interaction between the probe and the hydrolase. According to docking calculations, performed considering the protein *E. coli β*-Gal (PDB ID 1JYN), BOD-M-βGal is a good substrate of *β*-Gal. Docking analysis has shown that the galactosyl moiety occupies almost the same location as lactose, maintaining the interactions of the natural substrate with *β*-Gal. Indeed, while the galactosyl moiety is located in the active pocket, in a typical *β*-Gal substrate mode, the fluorescent group is out of the binding site, not interfering with the hydrolysis of BOD-M-*β*Gal. Over 24 hours, no cytotoxic effect has been observed in normal human umbilical vein endothelial cell lines (HUVEC cells) treated with BOD-M-βGal, using cell counting kit-8 (CCK-8) assay. In subcutaneous murine models of ovarian cancer (SKOV-3 cells) administered with an intra-tumoral injection with BOD-M-βGal (30 nmol), the probe reached the maximum specific NIR-II fluorescence intensity 10 minutes post-injection. When injected with BOD-M-βGal, muscles showed no fluorescence, confirming the advantage of activatable probes over the "always-on" probes due to not generating non-specific fluorescence in healthy tissues. NIR-II fluorescent signals marked the tumor lesions with a TBR value of 17.38 at a depth of 0 mm and a TBR value of 6.43 at a depth of 2 mm. Tumor implants pre-treated with an inhibitor of β-Gal (D-galactose) showed an effectively suppressed fluorescent signal, indicating that BOD-M-βGal allows the visualization of ovarian cancer by specifically detecting β-Gal activity.[47]

3. Membrane-associated targets

3.1 Folate Receptor α (FRα)

The folate receptor-α (FRα) is a folate-binding protein anchored to the cellular membrane by glycosylphosphatidylinositol (GPI) with a molecular weight ranging from 38 up to 45 kDa. Encoded by the FOLR1 gene, FRα is part of the folate-receptors family, consisting of four isoforms (α, β, γ, δ) involved in the uptake and transport of various forms of folic acid (FA). Dietary acquired FA is metabolized in the liver and released as 5-methyltetrahydrofolate (5-MTHF) in the systemic circulation. Primarily taken up by ubiquitous reduced folate carrier (RFC) and proton-coupled folate transporter (PCFT), folate (folic acid, vitamin B_9) is a water-soluble vitamin crucial for the synthesis of nucleic acids as well as involved in numerous human metabolic pathways. Three molecular moieties can be identified in the FA chemical structure: a pteridine ring covalently bonded to a *p*-aminobenzoic acid that, in turn, is connected to the glutamic acid by an amidic bond (Figure 8).[48]

Figure 8.

FRα binds folic acid with a very high affinity ($Kd \approx 1–10$ nM), differently from the other folate transporters, which present an affinity for folate in the micromolar range. FRα mediates the FA cellular internalization *via* potocytosis, a non-classical endocytosis. Similarly to other receptor-mediated endocytosis, in potocytosis, the clustering on the cell surface of the receptor-ligand complexes induces plasma membrane invagination and a subsequent formation of endocytic vesicles. However, in potocytosis, molecules are transported *via* caveolae (rather than clathrin-coated vesicles). Caveolae are a small membrane invagination rich in proteins and lipids like cholesterol and sphingolipids. After internalization, besides joining with lysosomes ($pH \approx 4$-5) as in the pinocytosis, caveolae-vesicles (caveosomes, pH~ 6) may release the content directly in the cytosol ($pH \approx 7$), bypassing the low lysosomal pH. The caveosomes can also deliver small molecules to the endoplasmic reticulum (RE).[19,49] FRα is scarcely present in healthy tissues and has a limited physiological function, except for the crucial role in embryogenesis. Indeed, FRα is highly expressed in the yolk sac and provides the essential folate supply during embryo neurulation. Dietary folate supplementation is often recommended in the periconceptional period for preventing congenital malformations, especially for neural tube defects prevention. As involved in cancer progression, FRα is overexpressed in numerous solid tumors, especially of epithelial origin. FRα not only acts as a folate transporter but it also plays a crucial role in intracellular signalling and genic transcription. A recent study reported that, after folate uptake, separated from caveosomes by a phospholipase and translocating in the nucleus, FRα could regulate the expression of genes detrimental to cancer development. FRα overexpression has been associated with enhanced cellular proliferation, migration, and loss of adhesion, leading to uncontrolled cellular motility and metastasis progression. Among FRα-expressing epithelial malignancies, the α-subtype of folate receptor is in 80% of epithelial ovarian cancers (EOCs), and its expression is associated with histological grade and stage. Data from 12 separate studies showed that FRα expression is present in 32% of clear-cell ovarian malignancies, 50% of low-grade serous tumors, and 76% of high-grade serous tumors. Chemotherapy resistance development has also been correlated to FRα overexpression. Nevertheless, according to several studies, chemotherapy treatments do not have an impact on FRα-expression. FRα-positivity can be used as an ovarian cancer biomarker, supporting the potential utility of FRα-targeting in therapy/diagnosis of ovarian cancer in both the earliest stage and relapsed disease.[12,50] It follows the description of fluorescent probes developed to detect ovarian cancer targeting FRα.

FA-HDL(DiR-BOA) NPs

The NIR fluorescent nano-probe (λ_{ex}=748 nm; λ_{em}=780 nm) consisting of high-density lipoprotein nanoparticles (HDL NPs) conjugated with FA and loaded with the NIR fluorescent dye DiR-BOA (Figure 9) has been developed and *in vitro* and *in vivo* evaluated for fluorescent imaging of metastatic FRα-overexpressing ovarian cancer.[12]

Figure 9.

Unlike other plasma lipoproteins, HDL particles are commonly known as "good cholesterol" because they remove lipids (such as cholesterol, phospholipids, and triglycerides) from cells, carrying them back to the liver. Their highest density is due to the predominance of the protein components, mainly apolipoprotein types A-I and A-II. The primary HDL receptor is the class B scavenger receptor type I (SR-BI) that is principally expressed in liver cells and binds with high affinity to the lipoprotein, allowing selective cholesterol uptake by hepatocytes. Unfortunately, for cancer targeting, SR-BI does not offer the specificity required. Therefore, to improve the selective uptake of HDL, Corbin *et al.* have shown both *in vitro* and *in vivo* that labeling the apoprotein component with FA enables the active and targeted delivery of the HDL-based nanocarriers to FRα-positive cancer cells by selective uptake of the nanocarriers via FRα interaction.[51] HDL NPs represent a versatile and efficient drug-delivery nanosystem. The HDL apoA-I establishing a network of hydrophobic interactions between its helixes and the NPs lipids allows NPs size control, and by coating and fastening nanoparticles' phospholipidic layer on the outside, offers a discrete number of sites for tumor ligands conjugation. HDL NPs exhibit nanoscale size and a phospholipid shell, which allows them to elude the reticular endothelial system (RES), HDL NPs have nano-sized dimensions and a phospholipid shell, which allows them to evade the reticular endothelial system (RES), thereby conferring the non-immunogenic characteristics of these nanocarriers and long blood circulation. The fully biocompatible HDL NPs can easily pass through the endothelium, accessing most tissue compartments.[52] According to compositional data analyses, in FA-HDL(DiR-BOA) NPs 44 molecules of FA are covalently bonded to the apoA-I external amino acid residues. Instead, the NIR dye DiR-BOA shows sufficient hydrophobicity to be trapped in the nonpolar HDL NPs core, and, four fluorophore molecules are successfully included in each particle. FA-conjugated HDL NPs, selected for *in vitro* and *in vivo* experiments, have an average hydrodynamic diameter of 14.17 ± 3.29 nm according to DLS measurements and were prepared using a co-sonication method. The FRα-targeting efficiency of FA-HDL (DiR-BOA) NPs has been *in vitro* assessed in FRα-overexpressing malignant murine ovarian cell lines (IC5-MOSEC), incubated with FA-conjugated NPs and non-conjugated NPs. A high amount of FA-HDL(DiR-BOA) NPs accumulated in the IC5-MOSEC cells after 3 hours of incubation. In contrast, the absence of FA in HDL(DiR-BOA) NPs has almost completely compromised the nano-probe uptake, and the negligible amount of un-functionalized NPs detected was likely due to uptake via SR-BI. Indeed, the subsequent western blot analyses confirmed that IC5-MOSEC exhibits a weak SR-BI expression. The FRα-mediated enhancement of the NPs' cellular uptake has been verified by further inhibition studies using an excess of free FA, which inhibited the cellular accumulation of fluorescent NPs. On the contrary, FA HDL(DiR-BOA) NPs internalization has not been markedly conditioned by the excess HDL, confirming that SR-BI is not involved in the notable increased cellular uptake observed in IC5-MOSECs. Following intravenous

(IV) or intraperitoneal (IP) administration, fluorescent FA-HDL NPs were *in vivo* evaluated for their ability to target FRα-positive cancer in an intraperitoneal mouse model of metastatic ovarian cancer (IC5-MOSEC). Whole-body fluorescence imaging was performed on sacrificed mice 24 hours post-injection to monitor the bio-distribution of fluorescent nano-probe. Little to no tumor fluorescence was observed following IV FA-HDL(DiR-BOA) NPs administration at a dose of 4 nmol of DiR-BOA/mouse. In contrast, the liver was the primary site of the fluorescence detection. In contrast, fluorescent signals following IP injection of the same dosage of NPs revealed a significant NPs accumulation in the tumor lesions dispersed throughout the abdomen and in free-floating metastatic cells in the ascites. Instead, in mice IP administered, the liver showed almost no fluorescence. The local delivery of FA-HDL(DiR-BOA) into the IP cavity most likely allows the IC5-MOSEC cancer cells to extract the fluorescent nanoparticles from surrounding compartments, bypassing the first-pass metabolism. *Ex vivo* images of the tissues and organs excised were later collected from mice IV and IP administered with the FA-HDL(DiR-BOA) NPs, showing consistency with the whole-body images. To demonstrate the improvement of specific tumor-targeting by the FA-functionalization of NPs, the un-functionalized ones were IP injected into metastatic ovarian cancer-bearing mice. The following whole-body fluorescence imaging showed that the non-functionalized nano-probe failed to highlight the IC5-MOSEC tumors. Moreover, fluorescent images of ascitic fluids and cells showed a moderate uptake of NPs by free-floating metastatic ovarian cancer cells inside the ascites of mice. Previous flow cytometry analyses had shown that the IC5-MOSEC cell lines exhibit a low level of expression of SR-BI. The majority uptake of HDL NPs by these cells has been likely due to the nonspecific interactions. In summary, the local–regional administration of FA-HDL(DiR-BOA) NPs offers a promising approach for specific FRα-positive ovarian cancer-targeted fluorescence imaging for diagnosis and guided surgery, with a lower systemic toxicity.[12]

Folate-specific activatable probe

The folate-specific activatable probe (FSA) has been designed for *in vivo* NIR fluorescence imaging of ovarian cancer. In FSA (λ_{abs}=655 nm; λ_{em}=688 nm), FA is connected to the NIR dye ATT655 throughout a peptide linker (Figure 10). In contrast to most NIR "always-on" type agents currently developed; the FSA fluorescent signal is "turned on" only inside the FRα-positive tumor cells. Indeed, after internalization *via* FRα-mediated endocytosis, the tumor-associated lysosomal enzyme cathepsin B catalyzes the peptide linker cleavage, releasing the fluorescent-free dye.

Figure 10.

The design of the *in situ* activatable fluorescent type of probes is justified by the need to minimize background signals to improve the tumor-background ratio (TBR). Cathepsin B activates the FSA fluorescence emission. FSA treated with a catalytic amount of the enzyme increases its basal fluorescence intensity by 3-fold. The enzyme-inducted fluorescence is suppressed by pre-treating cathepsin B with its inhibitor E64. Treating FSA with other cathepsins did not lead to fluorescence emission. Neither human serum albumin (HSA) nor bovine serum albumin (BSA) implicates the non-specific fluorescence activation of FSA. Indeed, after 4 hours of incubation of FSA with serum proteins, no fluorescence has been turned on. FRα-overexpressing SKOV-3 cell lines were treated with 1 μM of FSA probe and with 1 μM of free dye ATTO655. Except for a weak signal in the extracellular space, the strongest fluorescent signal derives from the inside of the cell lines treated with FSA. Instead, cell lines treated with the free dye showed the opposite scenario: the fluorescence was detected only outside the cells. An excess of FA or its competitor, otherwise the pre-treatment of SKOV-3 cells with the cell-permeable cathepsin B inhibitor (E64), resulted in a significant reduction of fluorescence within the cells. The NIR probe has been *in vivo* evaluated in subcutaneous xenografted mouse models of SKOV-3, giving promising results. In mice IV administered with FSA (15 nmol/20 g body weight), strong fluorescence signals were detected in tumor lesions with a high TBS value (7.76 ± 0.88), data confirmed also by the *ex vivo* NIR fluorescence imaging performed on excised organs and tissues. Instead, 3 hours post-injection, healthy tissues are not distinguishable from tumors due to the high background signals in mice treated only with ATTO655. These findings suggest that the FSA could represent a promising tool for FGS, as it can accumulate specifically in FRα-positive tumors where its fluorescence is turned on, with a consequent lowest background signal.[53]

FA-fluoresceine (EC17) probe

EC17 (Figure 11) is an FRα-targeted fluorescence imaging agent currently in clinical investigations and consists of folate conjugated with fluorescein (FITC) (EC17 λ_{abs}=470 nm and λ_{em}=520 nm; Stoke shift=50 nm). As a contrast agent in fluorescence image-guided surgery, EC17 is currently under clinical investigation for ovarian cancer as well as other conditions that overexpress the FRα, including hyperparathyroidism, breast cancer, renal cell carcinoma, and pleural and pulmonary malignancies.[54]

Figure11.

Regarding feasibility as a fluorescent imaging agent for intraoperative ovarian cancer detection, EC17 is currently in clinical investigation phase 2 for FDA authorization. Ten patients aged between 50 and 72 years had been included in the first human clinical trial. Patients were diagnosed with epithelial ovarian cancer (four patients), borderline serous tumor (one patient), and benign ovarian cancer (five patients). During laparoscopic exploration in three of the four patients with a diagnosis of malignant ovarian cancer, it was possible to detect FRα -positive malignancies by an intense fluorescent signal 10 minutes after IV administration of 0.1 mg/kg of EC17 (reduced from initial 0.3 mg/kg with the intent to contain mild abdominal side effects). The mean TBR (considering the healthy peritoneal surface as background) has been measured for 10 fluorescent tumor deposits in two patients with ovarian cancer and was 3.1±0.8. In patients with the widespread disease (stage III, FRα -positive) tumor-specific fluorescent signals allowed the excision of cancer deposits up to 1.0 mm. Malignant tumor tissue not highlighted by EC17 fluorescence (1 patient with malignant ovarian cancer), as well as benign ovarian cancer tissues, did not express FRα, according to post-operative immunohistochemistry analyses, which in contrast showed a strong expression of the FRα in the probe-illuminated samples. The fluorescent signals generated by EC17 remained detectable up to 8 hours after systemic administration, providing a surgical window also suitable for prolonged surgical procedures.[54] On a further twelve patients with malignant ovarian cancer at various stages of the disease, receiving intravenously 0.1 mg/kg over 10 minutes of EC17, nearly 50% developed mild and no clinically relevant adverse reactions, just like in the previous human trial. After 2 hours from the injection of fluorescein-probe, EC17 detected 57 lesions with a mean TBR=7.0 ± 1.2. Histopathologic post-operative analyses demonstrated that almost 77% (44 lesions) were malignant, while the remaining excised fluorescence-highlighted tissues (28%) were benign. EC17 allowed the detection of an additional 16% of malignant lesions during surgery that were benign-looking or too small to be detected by manual palpation or the naked eye. Post-operative investigations have detected 3 false-positive lesions that were not identifiable during surgery but revealed a strong fluorescence when dissected. The intraoperative identification of these lesions has probably not been achievable because of poor tissue penetration of light at λ=500 nm. 5 out of 13 benign excised lesions were false positives that expressed FRα and were detected by EC17 and removed. Instead, the 6 remaining false positive lesions were rich in collagen, which causes autofluorescence at λ=500 nm. Unfortunately, the mean TBR of the false positives (5.4±1.0) was not significantly different from the TBR of true-positives one (7.0 vs. 5.4). Even while EC17 has a short half-life (about 86.6 minutes) and excreted quickly, tumor fluorescence remains strong with high TBR from almost 2 hours post-injection until 5 h later. These pharmacokinetic properties of EC17 favor intra-operative imaging of ovarian cancer starting two hours after dosage and over for a long period, confirming the results of the first human study. Although EC17 has excellent pharmacokinetic properties and high specificity, being FRα a specific tumor target, it does not have all the requisites necessary for fluorescence-guided surgery in ovarian cancer. The visible emission of the probe with the consequently overlapping with the natural autofluorescence of biological tissues and the reduced penetrative properties of light at λ=500 nm constitutes a significant limit for EC17 feasibility.[55] Clinical investigations on the sensitivity and specificity of EC17 in the intra-operative imaging of ovarian cancer have not been completed.[56-57]

In-farletuzumab-IRDye800CW dual probe

^{111}In-farletuzumab-IRDye800CW is a hybrid probe because it simultaneously bears a radionuclide (^{111}In) and a fluorescent moiety (IRDye800CW, Figure 12).

Figure 12.

^{111}In-farletuzumab-IRDye800CW is an FRα-targeted antibody-based probe designed for pre-operative and intra-operative detection of ovarian cancer lesions. Farletuzumab is an anti-FRα humanized antibody, developed under the name MORAb-003 by Morphoteck Inc., currently also studied as a therapeutic agent for ovarian cancer. The monoclonal antibody is labeled with the NIR fluorescent dye IRDye800CW (λ_{abs}=774 nm, λ_{em}=789 nm in water) and with the radionuclide 111Indium allows both fluorescence imaging and microSPECT/CT analysis. In a dose-escalation study on subcutaneous IGROV-1 xenograft models, optimal tumor-to-blood ratios (3.4 - 3.7) have been observed at dual-probe doses up to 30 µg. After 3 days post-injection, tumor uptake rate remains stable (39.3 ± 5.8 % - 43.6 ± 4.8 % injected dose/gram, ID/g %) in mice IV administrated with 3, 10 and 30 µg of dual-labeled farletuzumab. A decreasing tumor-to-blood ratio and consequently lower tumor uptake has been observed at higher protein doses, probably due to the antigen saturation. The dual-modality imaging was then investigated in an intraperitoneal IGROV-1 mice model IV injected with 10 µg of ^{111}In-farletuzumab-IRDye800CW. The pre-operative microSPECT/CT imaging and intraoperative fluorescence imaging detected multiple abdominal lesions. The fluorescent moiety allowed the resection of superficial and macroscopic tumor lesions and micro-metastases located deeper within the abdominal cavity, which have been fluorescently highlighted and successfully removed. Several tumor deposits under 1 mm were detected in the abdomen through fluorescence imaging, even those barely visible to the naked eye. The histopathological analyses of the excised lesions revealed that the radioactive and fluorescent signals observed during the pre-operative and intraoperative imaging corresponded to malignant lesions expressing FRα. A consisting decrease of dual-labelled probe uptake was observed in the mice co-injected with 10 µg of ^{111}In-farletuzumab-IRDye800CW and 1 mg of unlabelled farletuzumab (69.4 ± 27.6 versus 18.3 ± 2.2 % ID/g). Over-injection of unlabeled mAb has likely induced a competitive antagonism, confirming the FRα-mediated tumor uptake. Farletuzumab's lack of cross-reactivity to murine FRα led to high tumor-to-normal tissue contrast. Therefore, this dual probe has shown high sensitivity in preclinical investigations.[58]

HSA&ICG-FA NPs and HSA&FITC-FA NPs

HSA&ICG-FA NPs and HSA&FITC-FA NPs are fluorescent dye-loaded human serum albumin nanoparticles conjugated with folic acid (FA) to obtain a selective fluorescent probe for FRα-overexpressing ovarian cancer. NPs characterized by suitable biocompatibility and biodegradability are promising targeted drug-delivery systems, especially in cancer theragnostics. Indeed, the enhanced permeability and retention effect (EPR) in solid tumors induces a passive targeted delivery of NPs. Leaky vasculature and the reduced lymphatic drainage system that characterizes tumor microenvironments establish a selective accumulation of NPs in tumor cells. Therefore, labeling and biofunctionalization of NPs with specific ligands is a strategy to strengthen NPs selective tumor uptake. Being a scaffold susceptible to various functional modifications, the HSA was used as a building block to produce protein-based nanoparticles (NPs). Then, HSA NPs were loaded with the FDA-approved ICG and FITC dyes, emitting respectively in the near-infrared and visible. Fluorescent HSA NPs, obtained with a yield > 75% and a loading efficiency almost equal to 50% for ICG and higher than 30% for FITC, exhibit an optimal diameter for passive targeting by the EPR effect, which almost remains unvaried even after conjugation with FA (26.63 ± 0.22 nm a polydispersity index (PDI) of 0.24 ± 0.01 for the HSA&ICG-FA NPs and 33.70 ± 0.29 nm with a PDI of 0.23 ± 0.01 for the HSA&FITC-FA NPs). The two-fluorescent protein-based nanoparticles (HSA&ICG-FA NPs λ_{abs}=802 nm, λ_{em}=814 nm; HSA&FITC-FA NPs λ_{abs}=491 nm, λ_{em}=525 nm) showed high photostability; the fluorescence intensity remained almost stable after 15 days. Folic acid was covalently conjugated with the aminic groups on the NPs surface by an amide bond. MTT assays performed using FA-conjugated NPson NIH: OVCAR-3, an ovarian cancer cell line known for the FRα-overexpression, confirmed the non-toxicity of the nanoprobe. According to competitive assay outcomes, NPs conjugation with the natural ligand of FRα improves target-specific cellular internalization of nanoprobe. In addition, FA, HSA, and other small molecules trigger a specific cellular uptake, consisting of the caveolin-mediated potocytosis, during which NPs are included in caveosomes, bypassing the lysosomal digestive low pH, thus maintaining their structural integrity. Collected fluorescence microscopic images show that fluorescent vesicles do a noteworthy number of round-oval NP-containing vesicles of 200-400 nm in cells treated with FA-labeled nanoparticles. TEM images show NPs localized in an enlarged ER lumen, which appears normal even in cells treated with unlabeled NPs. In addition, if treated with unlabeled NPs, fewer and smaller NP-containing vesicles can enter cells, supporting the existence of a specific and increased cellular uptake established by the NPs conjugated with FA, which results in high specificity of fluorescent HAS-FA NPs, as fluorescence imaging tools for ovarian cancer detection.[19]

HSA&phthaloNO_2-AB NPs

Protein-based nanoparticle technology has been employed to achieve a nanosized theragnostic agent for targeted fluorescence imaging and multimodal therapy for ovarian cancer. HSA-based nanoparticles obtained with a high particle yield (> 70%) have been loaded (loading efficiency ~ 88%) with the phthalocyanine fluorescent dye Zn(II)-2,9,16,23-tetranitrophthalocyanine (phthaloNO_2) endowed with a triple action. PhthaloNO_2 absorbs and emits light in the deep-red and near-infrared (NIR) regions, but it also acts as a photothermal agent, as entering an excited state, when irradiated by NIR light, generates heat to return to equilibrium. Indeed, temperatures higher than 40

°C in the cancer cell microenvironment determine thermal ablation of solid tumor lesions. Moreover, phthaloNO_2 has photodynamic properties, and its photochemical interaction with light in the presence of molecular oxygen (O_2) leads to the formation of toxic radicals, such as reactive oxygen species (ROS) in which the oxygen is in a singlet state ($^1O_2$), that induce cell death (apoptosis, necrosis, and autophagy). To target FRα-overexpressing ovarian cancer, HSA&phthaloNO_2 NPs were labeled with anti-FRα antibodies. HSA&phthaloNO_2-AB NPs exhibit the size for the passive tumor-targeting driven by enhanced permeability and retention (EPR) effect (28.3 ± 1.2 nm with PDI=0.32 ± 0.05). Furthermore, HSA&phthaloNO_2-AB NPs, concerning the free phthaloNO_2, have a slightly hypsochromic shift (2 nm) in the absorbance spectrum (λ_{abs}=668 nm from λ_{abs}=670 nm of free naphtholNO_2), 27 nm blue shift in the fluorescence emission spectrum (λ_{em}=663 nm from λ_{em}=690 nm), and a fluorescence intensity reduction. An i*n vitro* study (MTT assay) performed on A2780 ovarian cancer cell lines overexpressing FRα showed that no significant change in cell viability occurs when treated with HSA&phthaloNO_2-AB NPs. I*n vitro,* fluorescence imaging confirmed that labelling fluorescent NPs with anti-FRα antibody enhances NPs internalization by the cancer cells if compared to non-specific uptake of HSA&phthaloNO_2 NPs. Moreover, the presence of the antibody and the phthaloNO_2-encapsulation inside the protein-based nanoparticles increases fluorescence lifetime decay times (2.31 ns for HSA&phthaloNO_2-AB NPs, 2.08 ns for HSA&phthaloNO_2 NPs and 1.90 ns for free-phthaloNO2). Deep-red/NIR fluorescent dye bounding HSA within the nanoparticle probably does not dimerize to the non-fluorescent form. On the other hand, the 0.23 ns increase in the lifetime decay time of antibody-decorated nanoparticles compared to undecorated nanoparticles suggests the existence of different intracellular localization and/or internalization pathways of the fluorescent agent when FRα is involved. Although further *in vivo* investigations are needed, HSA&phthaloNO_2-AB NPs have great optical potential as FRα-targeted fluorescence imaging nano-sized agents.[59]

FolateSiR 1 probe

The NIR fluorescent probe FolateSiR consists of xanthene-based dye conjugated with folic acid (FA).[60] The folate-linked NIR probes currently under preclinical investigation have very low tumor-to-background ratios and consequently longer washout procedures, up to 24 h, due to an extended non-specific absorption on normal tissues. FolateSiR 1 was designed and developed to reduce non-specific absorption and achieve quick and high-contrast detection of FRα-expressing tumors, including ovarian cancer. The fluorophore selected was the xanthene-based dye Si-Rhodamine with a carboxylic group inserted in phenyl-C2 (2-COOH SiR650, λ_{abs}=652 nm and λ_{em}=674 nm). Indeed, a hydrophobic environment, such as plasma/inner membranes, promotes intramolecular cyclization of 2-COOH SiR650 in its uncharged and nonfluorescent spironolactone form (Figure 13).[61] The cyclization combined with an intrinsic low level of non-specific binding probably contributes to decreased background interferences.

Figure13.

In the crystal structure of FA complexed with human FRα,[62]the pteridine nucleus is placed inside the receptor binding pocket, thus leaving the glutamate moiety exposed to the solvent. Therefore, to maintain the high ligand-receptor affinity, in FolateSiR 1, the fluorescent dye has been connected to glutamate moiety through a negatively charged peptide linker, consisting of Asp-Lys-Gly, which should also reduce the cell-membrane permeability of the fluorescent probe (Figure 14).[63]

Figure 14.

At first, FolateSir 1 (λ_{abs} = 652 nm and λ_{em} = 674 nm) was *in vitro* evaluated on FRα-expressing (KB) and FRα-non-expressing (OVCAR-3) cell lines. Strong fluorescent signals on cell surface were observed on KB cells treated with 5 μM of FolateSiR 1. This peripheral fluorescence disappears in the presence of 1 mM FA, confirming the specific interaction with the membrane-associated target. Considering that the fluorescence was limited to the cell membrane and no bright dots were detected inside the cells, the folate-linked fluorescent dye should not be internalized *via* non-FRα-mediated mechanisms. Besides, no fluorescence was detected on FRα-non-expressing cells. Then, FolateSiR 1 was evaluated in subcutaneous animal models of FRα-(+)-tumor (KB cells). Mice have been IV injected with 100 μM of folate-linked fluorescent probe for *in vivo* fluorescence imaging. From the images obtained at different time points, using the Maestro In vivo Imaging System (CRi Inc., Woburn, MA), changes in the value of the tumor-to-background ratio (TBR) have been monitored. Using a grey intensity scale (from 0 to 255), the ratio of fluorescentscent intensity of tumor masses to healthy tissue used as a reference (muscle in this case) was determined. As shown in Image 1, 30 minutes after FolateSiR-1 injection, the TBR value was 83 and the tumors were distinctly visible with high contrast; up to 6 hours after injection, TBR remained high.

Image 1.

In subcutaneous mice models of FRα-(-)-tumors (HT1080 cells) no fluorescence has been detected. Furthermore, when 6 mM FA saline was IV administrated to KB-tumor-bearing mice, followed by 100 μM FolateSiR 1, fluorescence showed no signals (except those in the stomach probably due to feeding). Therefore, FA acts as a competitor for FRα, indicating that the NIR probe specifically interacts with the target. FolateSiR 1 was able to selectively *ex vivo* highlight patient-derived ovarian cancer tissue. Despite little binding to normal tissues (collected from normal tissues adjacent to tumor lesions), matching the immunostaining images with fluorescence images suggests the potential applicability of FolateSiR 1 for intraoperative tumor detection.[60]

FA-BSA-AuNCs

Hada *et al.* propose FA-BSA-AuNCs as a contrast agent for fluorescent-guided imaging of ovarian cancer. The nanoprobe consists of BSA-stabilized photoluminescent gold nanoclusters (BSA-AuNCs) functionalized with folic acid to obtain FRα-targeted detection. AuNCs are made up of a few up to 200 gold atoms usually protected by macromolecules, and exhibit peculiar physical and chemical features, that make them suitable for several applications such as ions detection, catalysis, molecular identification, sensing, biolabeling, cell and tissue imaging. BSA-AuNCs are potential fluorescent contrast agents since they have a strong red-emission (λ=670 nm) under an excitation wavelength of λ=530 nm. Furthermore, under excitation at λ=280 nm, BSA-AuNCs exhibit two additional emission bands at λ=350 and λ=415 nm assigned to the BSA and oxidized-BSA (oBSA), which show visible-emitting fluorescence as biomolecules. According to dynamic light scattering (DLS) and Transmission Electron Microscopy (TEM) measurements, BSA-AuNCs have an average size of 25±12 nm. Moreover, at high-resolution TEM images (HRTEM images), the AuNCs appear as defined structures of approximately 2–3 nm located within a corona made up of BSA chains. Afterward, the functionalization with FA increases the BSA-AuNCs' average size of 3 nm and alters slightly their photoluminescence. Under excitation at λ=350 nm and λ=530 nm, a 15 nm bathochromic shift of the BSA-specific emission band has been observed, while the BSA-AuNCs photoluminescence has a moderate hypsochromic shift (12 nm). These spectral alterations do not compromise their functionality but show that biofunctionalization successfully occurred. The contrast agent biocompatibility has been evaluated up to a concentration of 40 mg/ml *via* MTT assays that were performed on FRα-overexpressing NIH:OVCAR-3 cell lines, treated with both unfunctionalized and FA-functionalized BSA-AuNCs. The latter showed slightly superior biocompatibility, probably due to the FA's important role in cell division. Using wide-field conventional epi-fluorescence microscopy and confocal fluorescence lifetime imaging microscopy the agent cellular uptake was *in vitro* evaluated. The accumulation of the targeted and untargeted tracers in the cytoplasm, particularly in the perinuclear area, was observed using microscopic imaging. Instead, no fluorescence was detected in the nuclei. This evidence demonstrates that the agent can cross the cell membrane in a specific and non-specific manner. Compared to BSA-AuNCs, the functionalized-BSA-AuNCs have demonstrated a higher cellular uptake by NIH:OVCAR-3 cell lines, confirming the occurrence of a specific and more advantageous FRα-mediated internalization. Instead, the untreated control samples have shown no fluorescence, except for a weak auto-fluorescence that is typical of biological structures. These results suggest that the FA-BSA-AuNCs represent promising contrast agents for early diagnosis and image-guided surgery of FRα-positive ovarian cancer.[63]

FA-ZW800-1-Forte probe

To obtain a fluorescent imaging agent that specifically targets FRα-positive-ovarian cancer, García de Jalón *et al.* have conjugated the NIR fluorescent dye ZW800-1-Forte (λ_{ex}=774 nm, and λ_{em}=802 nm) to folic acid (FA) throughout an ethylenediamine (EDA) linker (Figure 15). ZW800-1 Forte is the more stable analogue of the ZW800-1 dye. Indeed, ZW800-1 Forte has a stronger C-C bond than the ether linkage on the *meso* carbon present in ZW800-1. Being a zwitterion with a net charge of zero ZW800-1 Forte shows a reduced non-specific binding to, e.g., serum proteins, and as a result has a lower background signal as a contrast agent.[64]

Figure 15.

To assess the specificity of the conjugated FA-ZW800-1 Forte-binding to FRα, low intermediate and high FRα-expressing cell lines were treated with three different concentrations (10 µM, 1 µM, and 0.1 µM) of the agent. After 4 hours of incubation, fluorescence imaging of the cell lines showed that the most intense fluorescent signal derived from the endometrial cancer cell line HeLa, which had the highest extent of FRα-expression. In addition, a specific binding assay was performed on HeLa cells at the three previous concentrations in the absence and presence of 100-fold excess FA. The presence of the natural ligand of FRα strongly reduced the fluorescent signal, especially at the lowest concentration of the agent, indicating the specific interaction between the NIR probe and the target. Using a water-soluble tetrazolium salt assay kit (WST-1, Roche Applied Science, Germany) the *in vitro* toxicity of FA-ZW800-1 Forte was assessed in SKOV-3 cell lines. At concentrations between 0.1 and 100 µM, neither cytotoxicity nor cellular proliferation inhibition was observed. The FA-ZW800-1 Forte biodistribution was *in vivo* performed on subcutaneous SKOV-3 ovarian cancer models. Mice were intravenously injected with the tracer when mean tumor volumes reached a size of approximately 150 mm3. Each mouse received a selected dose of 500 nmol of FA-ZW800-1 Forte, based on the results of the prior preclinical study using another folate-NIR conjugate agent for *in vivo* fluorescence imaging (OTL38[64]). At first time point, the agent exhibited a strong background signal; however, with time, a rapid renal clearance reduces the background noise, perhaps because of the high hydrophilicity of the tracer. Indeed, a strong fluorescent signal was detected in kidneys in the following *ex vivo* fluorescence analysis of excised tumor lesions and organs. FA-ZW800-1 Forte has an acceptable value of TBR (2.0 ± 0.2) 4 hours post-injection, the best timing for fluorescence imaging purposes. Fluorescence imaging detection was performed in the subcutaneous xenograft of two FRα-positive tumor cell lines (SKOV-3 and A549) that exhibited a different rate of the target expression. As evidence of the FA-ZW800-1 Forte's capability to specifically detect FRα-tumors, tumor models with higher FRα-expression (SKOV-3) displayed the most fluorescent signal intensities. Therefore, ZW800-1 Forte has shown some potential as a fluorescent contrast agent for ovarian cancer fluorescence-guided surgery, but further investigations are still needed.[65]

Plu-IR780-chit-FA nanoprobe

The Plu-IR780-chit-FA is a NIR-fluorescent and responsive nano-platform designed for targeted theragnostic applications against FRα-overexpressing ovarian cancer. The nanosystem consists of water-soluble micelles made up of amphiphilic copolymer Pluronic F127 and then loaded with the hydrophobic NIR dye IR780 (Figure 16).

Figure 16.

The Plu-IR780 micelles are coated with a shell of FA-functionalized chitosan for FRα-targeted ovarian cancer recognition. Pluronic F127 is a synthetic and thermo-sensitive copolymer approved by the FDA and selected for its ability to self-assemble into nano-micelles in an aqueous solution Structurally, it consists of a modification of a block of poly-(ethylene oxide) (PEO) and poly-(propylene oxide) (PPO). The Pluronic micelles have been loaded with the NIR dye *via* a rapid and reproducible synthesis. The encapsulation efficiency was 69%. Externally covering Plu-IR780 micelles by the chitosan, a biopolymer that presents in its structure many aminic residues, offering binding sites for various targeting ligands such as FA. In contrast to the majority of nanocarriers under development, designed to only satisfy one purpose at a time, Plu-IR780-chit-FA is a cancer-targeted theragnostic agent that has been realized with the intent to combine the NIR fluorescence optical proprieties of a contrast agent with the photothermal and photodynamic effect of a therapeutic agent. Indeed, in addition to strong fluorescence emission and high photostability, IR780 displays NIR-light-induced photo-cytotoxic properties, releasing heat and generating high reactive-oxygen species (ROS) under laser line irradiation (λ=785 nm). Nevertheless, the nanoprobe has shown superior heating efficiency compared to the free IR780 in water. In contrast, its singlet oxygen generation efficiency was comparable to that of the free dye in an organic solvent. Made up of a thermo-sensitive copolymer, the Plu-IR780-chi-FA nano-probe shows both a temperature-dependent size distribution and spectral characteristics. Pluronic micelles' dimensions decrease with the increase in temperature from a few hundred to around ten nanometers. At physiological conditions (37 °C) the diameter of the nano-probe corresponds to 32 nm, according to DLS measurements. Regarding fluorescence spectral profiles, the temperature affects both fluorescent signal intensity and absorption/emission band position reversibly. At physiological temperature (37°C) Plu-IR780-chi-FA exhibits a maximum absorption intensity (λ_{abs}=790 nm) and an emission profile comparable in intensity to standard conditions' one (25 °C) with a position red-shift of 18 nm (λ_{em}=808 nm). The fluorescent nanoprobe also presents an additional absorption peak at 290 nm corresponding to the folic acid absorption band, proving that FA-conjugation successfully occurs. Being Plu-IR780-chi-FA designed for biomedical use, its cytotoxicity has been *in vitro* evaluated on NIH:OVCAR-3 cell line using WST-1 assay. After 24 hours, the fluorescent nano-probe showed no significant effects on cell viability, except at the highest concentration (23 µg/mL). The dye encapsulation markedly limits the known cytotoxicity of free IR780, which has been observed even at the lowest concentrations (2.4 µg/mL). A series of targeting assays performed on ovarian cancer cell lines have *in vitro* demonstrated the high FRα-targeting capability of Plu-IR780-chi-FA. Differently from the FA-unlabelled micellar nanoparticles (Plu-IR780-chi), Plu-IR780-chi-FA have shown an FRα-targeting ability considerably improved. Indeed, the strongest fluorescence intensity was observed in FRα-overexpressing NIH:OVCAR-3 cells treated with the nano-probe FA-conjugated. Comparing images obtained by NIR fluorescence confocal microscopy of FRα-positive (NIH:OVCAR-3) and FRα-negative (A2780-Cis) ovarian cancer cell lines treated with the Plu-IR780-chi-FA, the strongest fluorescent signals were detected in the FRα-expressing cells. The fluorescence detected in NIH:OVCAR-3 appeared immediately intense maintaining stability up to 30 minutes of incubation. In contrast, in A2780-Cis cells a weaker fluorescence was observed, which presented a slight increase in intensity during incubation, indicating a continuous cellular non-specific uptake. Recorded NIR fluorescent images revealed that after specifically internalized *via* FA-FRα, the FA-functionalized nanoparticles mainly localize in the perinuclear region of cytoplasm without penetrating the nuclear membrane, differently from a free dye which after cellular uptake shown to be uniformly distributed in the whole cytoplasm. Based on these results, the Plu-IR780-chi-FA revealed a real potential as a contrast FRα-targeted-agent for *in vivo* imaging-assisted ovarian cancer surgery.[66]

FA-IR780&PFOB-SNPs

FA-IR780&PFOB-SNPs is an acid-responsive IR780-loaded nanoprobe, designed for FRα-targeted fluorescent detection of ovarian cancer. According to TEM analyses, FA-IR780&PFOB-SNPs exhibit a spherical structure consisting of a perfluorooctyl bromide (PFOB) internal nanocore, and an external polymeric shell made up of poly (lactic-co-glycolic-acid) functionalized with folic acid, poly (2-ethyl-2-oxazoline), and poly (ethylene glycol) (FA-PEOz-PEG-PLGA). Song *et al.* has engineered an activatable fluorescent nanoplatform that exploits the self-quenching property of the NIR fluorescent dye IR780 (λ_{abs}=795 nm), whose fluorescence is quenched when the dye aggregated at high concentrations, turning on when a greater distance between molecules of dye is re-established. [67-69] Being characterized by a pH-responsive framework, the nano-probe can disassemble in a specific way in the acidic tumor microenvironment, releasing the IR780 dye molecules, which become fluorescent again as they move away from each other. Indeed, measured by a NanoSight NS300 (Malvern Instruments, Malvern, United Kingdom), the activatable nanoparticles size decreased from 291.20 ± 82.70 nm at pH 7.4 to 115.50 ± 28.00 nm at pH 4.0, confirming previous study results on IR780-loaded nanoparticles.[70] FA-IR780&PFOB-SNPs possess a mitochondrial targeting capability in ovarian cancer cells and respect to the dye-unloaded SNPs, enter inside the cell more rapidly, showing a better distribution in the mitochondria. At the concentrations of 20-80 μg/mL, FA-IR780&PFOB-SNPs showed no *in vitro* toxicity on ovarian cancer cell lines (SKOV-3 cells, CCK-8 assay), even if cell viability decreases significantly when the nano-probes reach the 120 μg/mL, likely due to the increased amount of IR780.[71] According to *in vivo* safety evaluations, no significant toxicity was observed at dosages below 50 mg/kg of FA-IR780&PFOB-SNPs. For *in vivo* fluorescence imaging of ovarian cancer, the fluorescent nanoparticles are IP administered (10 mg/kg) in xenografted ovarian cancer mice models, to exploit the passive accumulation in peritoneal tumors of the nanoparticles,[72] in addition to the folate-mediated active targeted-internalization. After IP injection, FA-IR780&PFOB-SNPs reach the peak in serum concentration in 24 h, showing a half-life of 40.16 ±10.88 h. The complete elimination of the nano-probe occurs approximately in 9 days, consequently, the fluorescence imaging is performed 72 hours after IP administration. The activatable FA-IR780&PFOB-SNPs have shown a modestly improved NIR fluorescence imaging ability in subcutaneous ovarian cancer mice models, in comparison to IR780-loaded folate-targeted ordinary nanoparticles (fluorescence always on nanoparticles) and used as control.[68] Indeed, FA-IR780&PFOB-SNPs can detect the subcutaneous tumor implants with higher contrast, due to a lower intensity of the background fluorescent signals, from the surrounding normal tissues. Despite, according to histopathology analyses, the two types of fluorescent nanoparticles, both the ordinary and activatable, specifically accumulate in cancerous tissues, TBR for FA-IR780&PFOB-SNPs (3.05 ± 0.15) is significantly higher than that of the control group (2.24 ± 0.15). Nonetheless, the best outcomes have been achieved evaluating the NIR fluorescence imaging of FA-IR780&PFOB-SNPs in intraperitoneal mice models of ovarian cancer. Indeed, FA-IR780&PFOB-SNPs can delineate tumor boundaries, since the fluorescence signals detected in cancerous lesions have significantly higher intensity, in comparison to those observed in the surrounding normal tissues. In the intraperitoneal models, the average of TBRs obtained for FA-IR780&PFOB-SNPs is 30-fold higher than that of the controls, which were treated with ordinary IR780-loaded nanoparticles (62.71 ± 4.84 for FA-IR780&PFOB-SNPs, and 2.45±0.07 for control). Moreover, the activatable nano-probe can be detected with high contrast (TBR average=7.62 ± 2.07) micro-metastases characterized by maximum diameters less than 2 mm. In conclusion, the FA-IR780&PFOB-SNPs have demonstrated concrete potential as a contrast agent for intraoperative NIR fluorescence imaging of ovarian cancer.[67]

Pafolacianine (OTL38)

Pafolacianine (named OTL38 in clinical trials phase I and phase II), commercialized as Cytalux™, is the first fluorescent imaging agent for ovarian cancer fluorescence-guided surgery that received FDA approval. The probe consists of folic acid conjugated to an indocyanine green-like near-infrared dye (λ_{ex}=776 nm, λ_{em}=796 nm) (Figure 17), that allows targeted detection of FRα, expressed in more than 90% of epithelial ovarian cancers. Furthermore, pafolacianine is currently under clinical investigation as a contrast agent for fluorescence-guided surgery for FRα-positive lung, pituitary, bladder, stomach, and kidney neoplasms.

Figure 17.

In phase I, the tolerability and pharmacokinetics of increasing doses of OTL38 have been investigated in 30 healthy volunteers. Then, its feasibility as a contrast agent for the intraoperative detection of FRα-positive ovarian cancer was assessed in 12 patients undergoing cytoreductive surgery. At first, in the safety investigation, hypersensitivity-like reactions were observed after injection with the selected lowest dose of OTL38. According to DLS and TEM analyses, formulation of the contrast agent (diluted in 0.9% NaCl solution) inducing OTL38 aggregation, was considered the cause of pseudo-allergic reactions. Therefore, to avoid OTL38 aggregation, the NIR agent was diluted in 5% dextrose and infused for 60 minutes in another trial, which showed dose-dependent adverse events. Nevertheless, being such events not clinically meaningful, OTL38 was considered endowed with a toxicity profile suitable for IV administration. Scheduled for cytoreductive surgery, ovarian cancer patients were intravenously infused with the contrast agent 2-3 hours before the procedures, the time window necessary to clear it from the blood, as seen in the pharmacokinetic-profile study in healthy volunteers. Accumulated in FRα-positive tumors and metastases, the NIR agent enabled surgeons to resect and collect 83 lesions. Out of the total, 62 were found to be malignant on histological examination, achieving approximately 75% of true positives. More specifically, OTL38 allowed the detection of 29% more tumor lesions not identifiable by visual inspection and/or palpation, highlighting malignant lesions up to 8 mm below the tissue surface. The highest value of the tumor-to-background ratio (TBR, mean=4.4, range: 1.7–9.8), was reached at a dosage of 0.0125 mg/kg, which was lower than the doses selected at the beginning of the trial, and it remained stable until 6 hours after injection. It was observed that the TBR value decreased at an increasing dose of OTL38, probably due to the non-saturable and nonspecific background binding of the fluorescent probe.[64] Data collected in the phase I study has provided the guidelines to proceed to the phase II clinical trial, in which the safety and efficacy of OTL38 have been assessed on a larger cohort consisting of 44 subjects. In this phase, patients were strictly monitored from the IV administration time up to 28 days after the surgical procedure. Although almost all patients (90.9%) reported at least one treatment-emergent adverse event (TEAE), just 18.2% (8/44) were drug-related, consisting of mild gastrointestinal disorders that resolved within 24 hours. Instead, the majority of TEAEs were procedure-associated. To reduce image acquisition time, 2-3 h before the surgery all patients were infused with 0.025 mg/kg of OTL38, rather than 0.0125 mg/kg identified as the optimal dosage in phase I. The efficacy analyses were performed exclusively on those subjects (29/44) who had received the drug and were exposed to fluorescent light, presenting at least one FRα-positive ovarian cancer lesion. From the 29 patients, 225 lesions were collected, 75% of which were proved to be true positive (TP), which were the FRα-positive tumor lesions confirmed by both fluorescence of OTL38 and/or immunohistochemistry. However, according to the data, just 10% of false positives (FP) were confirmed and the majority of these were lymph node-located FRβ-expressing lesions. In the phase II trial, the agent sensitivity was defined as the ratio of the number of the TP over the number of FRα-positive cancer lesions confirmed just by immunohistochemistry. Since the study used two different statistical models to evaluate the data, depending on the model employed, the sensitivity of the NIR agent measured was 85.93–97.97% for FRα-positive ovarian cancer with lower 95% confidence interval boundaries of 81.19–87.75. Assuming a possible correlation of lesions within the patient, the Generalized Linear Mixed Model (GLMM) analysis has estimated a higher sensitivity of 97.97%. Furthermore, as compared to the phase I trial, the phase II expanded cohort of subjects underwent in the clinical trial has revealed an additional 48% of patients who have at least one lesion that was identified by imaging alone and was not detectable by the naked eye or through manual inspection during the surgery.[73] The phase III clinical trial led to FDA approval in November 2021 and involved 178 subjects, who should have to underwent cytoreductive surgery for known or suspected ovarian cancer. The open-label study was conducted from March 2018 through November 2020 in 11 centers in the United States (10 sites) and the Netherlands (one site). After an initial screening, among all the deemed suitable patients and administered pafolacianine (150 of 178), only 134 were randomly assigned to undergo intraoperative fluorescence imaging. Instead, 6 subjects were examined just by white normal light and palpation. The remaining 10 were excluded from the study for disease extension, adverse events, or benign biopsy. The pafolacianine safety was evaluated in all patients who received it (150). Only 45 subjects have signaled drug-related TEAEs, reporting mostly mild symptoms (69% of the cases). Instead, in 28 cases the infusion was interrupted for a mean interruption duration of 13.7 minutes. The infusion was then resumed, and the agent-planned dose was entirely administered in 22 patients, while the dosage was reduced in 3 subjects. However, adverse events or infusion reactions had both onset and resolution on the same day as the infusion. Notwithstanding, the safety profile has been shown consistent with pafolacianine phase I and phase II clinical studies. The secondary but not less important objective of the phase III trial was to assess the efficacy of the NIR agent in providing detection and resection of FRα-positive lesions not detectable by palpation and normal white light. Therefore, like phase II, efficacy has been assessed on data collected from those subjects who received pafolacianine and, were assigned to undergo NIR imaging, and had pathology histologic confirmation of at least one FR-positive ovarian cancer lesion (109 of 178 patients). Subjects have been infused with 0.025 mg/kg of Pafolacianine more than 1 h before the surgery and they first have been examined for lesion detection under normal white light and palpation. After that, patients underwent NIR imaging, and the lesions identified by the pafolacianine were compared to those detected by normal white light and palpation (Image 2).[74]

Image 2.

The contrast agent allowed to resection of at least one more FRα-positive ovarian cancer lesion, confirmed by the central pathology analyses in 33% of the 109 subjects. NIR agent alone detected the smallest lesions excised, which were mostly peritoneal and retroperitoneal micro-metastases; while the largest one measured approximately 1 cm, the smallest one measured 3 mm in its longest dimension. Based on the identification of 221 FP lesions out of 616 NIR-positive lesions, the FP rate at the lesion level was estimated to be approximately 33%. It is right to keep in mind that the resection of false-positive lesions, especially those situated in lymph nodes, might represent a concern. The presence of fluorescence in lymph nodes has been also observed in the preceding phase I and phase II study of pafolacianine and it was mostly due to FRβ expression. The lymphadenectomy in the Ovarian Neoplasms (LION) trial reported that the removal of clinically negative lymph nodes could implicate an increase in morbidity and mortality. Nevertheless, although further studies are needed to exclude the potential increased surgical risk of the use of pafolacianine, up to now it represents the first and the only fluorescent imaging agent clinically approved for ovarian cancer intraoperative detection.[74]

3.2 Integrin $\alpha_v\beta_3$

Integrins are cellular membrane-anchored heterodimeric glycoproteins, which structurally consist of two subunits α and *β*.[13] Integrins mediate cellular adhesion to extracellular matrix (ECM) proteins as well as to other cells. In addition, integrins can establish transmembrane connections with the cytoskeleton and activate several intracellular signaling pathways. To date, 24 different heterodimers are known and characterized by different combinations of the 18 variants of α-subunit and 8 of β-subunit. Each heterodimer has its specificity toward extracellular components such as collagen, laminin, fibronectin, and vitronectin. The adhesion and signaling events mediated by integrins are involved in physiological functions such as immune response, hemostasis, cell survival, and cell differentiation. Thus, dysregulation of integrin functions is associated with the pathogenesis of thrombotic vascular disorders, auto-immune disease, and cancer metastasis.[75-76] Being particularly expressed in endothelial cells of developing vessels, $\alpha_v\beta_3$-integrin is known especially for its crucial role in angiogenesis.[77] Although interacting predominantly with vitronectin, $\alpha_v\beta_3$-integrin also interacts with fibrinogen, fibronectin, and thrombospondin, and the signals generated within the cell have a significant impact on growth, migration, invasion, differentiation, and survival. In several tumors including breast, prostate, glioblastoma, metastatic human melanoma, and ovarian cancer, upregulation of $\alpha v\beta_3$-integrin expression has been associated with the development of the malignant phenotype. In particular, Landen *et al.* have reported that $\alpha_v\beta_3$-integrin contributes to increasing the proliferation and invasion of ovarian cancer cells. Although the expression of the β_3 subunit is not yet examined, the αv subunit has been found in 100% (of 30 samples) of ovarian tumors and cells from effusions in 96% (of 121 samples) of patients. *In vitro*, $\alpha_v\beta_3$-integrin has been demonstrated to play a crucial role in ovarian cancer cell migration and motility, through interaction with the ECM proteins, especially with its primary ligand, vitronectin. Thus, having the further advantage of being little expressed in healthy tissues, $\alpha_v\beta_3$-integrin represents a promising tumor-specific target.[78]

Fluorescent RAFT-(cRGDfK)$_4$ (AngioStamp®)

The AngioStamp® molecule (Fluoptics, Grenoble) is a NIR fluorescent tracer evaluated for the intraoperative $\alpha_v\beta_3$-targeting detection of tumors.[79-80] AngioStamp® (λ_{ex}=690 nm; the wavelength of emission ranging within the 690–700 nm) is a regioselectively addressable functionalized template (RAFT), formed by a cyclic decapeptide platform onto which a targeting domain consisting of four cyclopeptides (cRGDfK = c[Arg-Gly-Asp-D-Phe-Lys) and a NIR fluorescent moiety (chemical structure not available) have been inserted (Figure 18).[81]

Figure 18.

Since ECM proteins such as fibronectin, vitronectin, osteopontin, and thrombospondin specifically interact with integrins through the RGD (Arg-Gly-Asp) peptide motif, over the last thirty years, several researches were performed to develop specific RGD-like ligands for selective distinguish various integrins.[82] The RAFT-(cRGDfK)$_4$ platform was developed by Boturyn *et al.* as a molecular tool RAFT-based which has in a spatially controlled manner a four-ligand domain for $\alpha_v\beta_3$-integrin recognition, a cell targeting (cRGDfK) and a labelling domain for attachment of a radiolabel or a fluorophore. The *in vitro* biological activity evaluation of several multivalent RAFT-(cRGDfK)$_4$-conjugates has shown that they retain the recognition and selectivity for $\alpha_v\beta_3$-integrin of the cyclopeptide module cRGDfK. In addition, it has been observed that RAFT-(cRGDfK)$_4$-conjugates are efficiently internalized inside the cells via receptor-mediated endocytosis, suggesting the potential efficacy of the RAFT-based system as a biological active platform for $\alpha_v\beta_3$-targeted drug delivery for diagnostic or therapeutic purposes.[83] Garanger *et al.* have shown that RAFT(cRGDfK)$_4$ conjugated with a NIR fluorescent dye (Cy5) can detect human $\alpha_v\beta_3$-positive IGROV1 ovarian carcinoma metastasis disseminated in the peritoneal cavity of subcutaneous murine models with a low level of nonspecific binding.[84] Based on these findings, Mery *et al.* have performed a preclinical investigation of AngioStamp® as a NIR fluorescent agent for real-time intraoperative detection of ovarian cancer which overexpresses $\alpha_v\beta_3$-integrin. To validate its specificity and sensitivity, AngioStamp® has been *in vivo* evaluated in xenograft murine models of $\alpha_v\beta_3$-overexpressing human ovarian cancer (SKOV-3 cells, IGROV-1 cells, or OVCAR-3 cells). Tumor lesions were easily detectable 18-24 h following IV injection of AngioStamp® (10 nM). Moreover, in intraperitoneal mice models of metastatic ovarian carcinoma, AngioStamp® allowed the detection and removal even of infra-millimetric nodules (0.25 mm), undetectable without fluorescent imaging. Since 70% of ovarian cancer patients undergoing chemotherapies and surgical treatment experiments intraperitoneal recurrence, the capability of AngioStamp® to detect tumor lesions even after chemotherapy treatment has been assessed *in vivo*. Frequently, relapse is connected to minimal residual lesions that being unidentified during surgery, are left *in situ*, silently spreading in the intraperitoneal cavity. Therefore, to simulate the typical clinical condition, mice intraperitoneally grafted with ovarian cancer cells (OVCAR-3) were injected with AngioStamp® (10 nM) when the disease relapsed, exactly following 60 days of treatment with topotecan. AngioStamp® showed the same high sensitivity, allowing detection and resection of the tiny widespread metastases, unidentifiable by the naked eye. Moreover, AngioStamp® has shown high sensitivity and efficacy in the identification of tumor lesions in patient-derived xenograft murine models, established using samples of serous papillary adenocarcinomas or tubal carcinomas (low or high-grade) collected from patients before or after carboplatin/paclitaxel treatment. $\alpha_v\beta_3$-Integrins expression in samples employed had been previously confirmed using immunohistochemistry analyses, which had detected high levels of the target's expression. Nevertheless, among all the experiments carried out, nonspecific fluorescence has been observed in the bladder, kidneys, and uterus of 20% of animals. Whereas uterine fluorescence may be explained by an up-regulation of $\alpha_v\beta_3$-integrin, during the endometrial phase of the menstrual cycle in mammals,[85] the nonspecific signal found in the urinary organ is probably connected with the processes of agent elimination. Moreover, even if all the lesions resected showed malignancy, the detection of a false positive lesion in lymph nodes was reported in 3 of 60 mice.[80] Despite AngioStamp® demonstrated to be an efficient and specifically $\alpha_v\beta_3$-targeted contrast agent, Mery *et al.* conducted a further study, deepening the capability of AngioStamp® to be used as a fluorescent tracer for different types of tumors, to assess its potential in wider clinical use. Supporting this purpose, an *in vivo* study performed on patient-derived xenograft murine models of $\alpha_v\beta_3$-positive and $\alpha_v\beta_3$-negative ovarian tumors showed that AngioStamp® can detect ovarian tumor lesions in an $\alpha_v\beta_3$-integrin-independent manner. The study had been accomplished since only 50% of human ovarian cancer overexpresses the $\alpha_v\beta_3$-integrin. Therefore, AngioStamp® has been evaluated as a fluorescent tracer in subcutaneous models of several solid cancers including carcinoma (HCT 116), adenoma (SKOV-3), and glioma (U87), which were characterized by different levels of $\alpha_v\beta_3$-integrins expression. Although with different fluorescence intensity which was directly related to integrins expression level, AngioStamp® (2 nmol) can highlight tumor nodules in all investigated mice. Data from previous studies have been confirmed, and a nonspecific fluorescence has been detected in the kidneys and bladder. After a first rapid increase, in both cases, the unspecific fluorescent signal decreases to reach a basal level at 5 hours post-injection. However, the best tumor-to-background ratio has been reached between 17 and 24 hours post-injection, the range which has been indeed the perfect time window for surgery. Even though AngioStamp® was initially developed as a tumor angiogenesis tracer, the high level of neo-vascularization of solid tumors does not explain the agent's efficacy in the targeted detection of several tumors. Indeed, AngioStamp® has demonstrated the ability to label non-$\alpha_v\beta_3$-integrin-expressing tumor cells as well as endothelial cells located inside tumor nodules, according to the macroscopic and microscopic fluorescence analyses of resected lesions collected from murine models. These findings suggest that other phenomena could be involved, such as the well-known "enhanced permeability and retention" (EPR) effect, which has a significant role in the passive targeting of drugs to tumor tissues. Moreover, a proof-of-concept trial has been performed on three dogs and a cat bearing different types of cancers (breast tumors, ovarian cancer, and cutaneous carcinoma). The use of the tracer AngioStamp® enabled intraoperative detection of carcinomatosis sites 18-24 hours post a single injection of 0.15 mg/kg for dogs, and 0.3 mg/kg for cats. All the nodules which exhibited low, moderate, or high fluorescence have been resected from pets and all turned out to be malignant according to post-operative pathological analyses. AngioStamp® did help veterinary surgeons to perform a more accurate tumor removal, highlighting small nodules undetectable by only visual inspection by the surgeon. Since AngioStamp showed good tolerability and no significant toxic effect in mice models as well as in pets, it proved to be a promising fluorescent imaging agent for intraoperative tumor-specific detection.[86] In a work published in 2022, Josserand *et al.* used a NIR fluorescent labeled AngioStamp (AngioStamp800, labeled with IRDye800CW, Figure 12) to compare conventional surgery and fluorescence-guided surgery. Moreover, the action of AngioStamp800 was compared to the clinically approved fluorescent tracer ICG. Finally, the influence of neoadjuvant chemotherapy was investigated.[87-88] Indeed, in orthotopic peritoneal carcinomatosis mice models of ovarian cancer, the surgeon performed a tumor resection in 2 steps. Firstly, they performed a conventional laparotomy procedure under normal light including hysterectomy, bilateral adenectomy, and resection of all tumor nodules detectable by the naked eye. Then, cytoreduction was further completed under fluorescence guidance using the Fluobeam®800. Finally, the mouse body was imaged by bioluminescence to assess the final tumor residues in mice after the surgery. Mice were implanted with 107 SKOV3-Luc cells to monitor tumor growth and peritoneal invasion by *in vivo* bioluminescence imaging (IVIS Kinetic, Perkin Elmer, Waltham, MA, USA). Animals received an IV injection of 1.6 mg/kg Angiostamp800 (10 nmol/mouse) and 4 mg/kg ICG (113 nmol/mouse). The posology used was selected based on literature data.[89-90] Then, 16 hours after administration of Angiostamp800, mice were intraperitoneally injected with 150 mg/kg of D-luciferin for imaging by bioluminescence to assess the final tumor residues in mice after the surgery. The same surgical procedure was applied three days after neoadjuvant chemotherapy in intraperitoneal mice model of carcinomatosis of ovarian origin. Animals received two cures four days apart: paclitaxel (IV injection of 10 mg/kg) and carboplatin (IV injection of 40 mg/kg). Angiostamp800 as well as ICG showed an immediate fluorescence signal in the tumor followed by a gradual decrease up to 24 h. The fluorescent probes' clearances were kidney-mediated and liver-mediated, for Angiostamp800 and ICG respectively. Indeed, high signals were observed in the kidneys and liver, which showed a higher signal than the tumor. However, *in vivo*, fluorescence imaging demonstrated specific and high tumor uptake of poth probes after intravenous injection, and data were confirmed by *ex vivo* fluorescence imaging on collected organs at 24 h. Conventional surgery allowed the removal of 88.0 ± 1.2% of the total tumor mass in mice. Employing AngioStamp for performing fluorescence-guided surgery allowed the resection of additional nodules, enhancing the total tumor resection by 9.8 ± 0.7%, with only 1.4% of false positives. Instead, ICG allowed only the additional 3.9 ± 1.2% of tumor resection. After neoadjuvant chemotherapy treatment, fluorescence-guided surgery with Angiostamp800 allowed the resection of 88.7 ± 4.3% of the total tumor, while with conventional surgery only 69.0 ± 3.9% of total tumor masses had been removed. On the contrary, ICG did not improve surgery at all. Angiostamp800 confirms its-self as a promising fluorescent probe for better detection of ovarian tumors and metastases than the clinically used fluorescent tracer ICG and can help surgeons completely remove tumors, even in surgery procedures after neoadjuvant chemotherapy treatment.[87]

IntegriSense 680

IntegriSense 680 (Perkin & Elmer Medical, Woburn, MA, USA) is a commercial fluorescent $\alpha v\beta 3$-integrin targeted probe, currently approved for research use only. The probe is a non-peptide small molecule (chemical structure not available), having a selective and potent antagonist action against $\alpha v\beta 3$-integrin, linked to a NIR fluorophore. IntegriSense has λ_{ex}=675 nm and λ_{em}=693 nm. Harlaar *et al.* have *in vivo* evaluated IntegriSense's feasibility as a fluorescent imaging agent for intraoperative ovarian cancer detection on intraperitoneal xenograft mice models of ovarian adenocarcinoma (A2780 cells). Mice have been IV injected with IntegriSense (dosage not available) 24 hours before the surgery. Out of a total of 58 fluorescent lesions collected during the procedure, only 17 were false positive (FP) according to post-operative histopathological analyses. Thus, IntegriSense has shown a sensitivity of 100%, measured as the ratio of true positive (TP), fluorescent lesions revealing to be malignant at histological assay, and the sum of TP and false negative (FN), consisting of non-fluorescent tumor lesions. Instead, the specificity (ratio of the number of true negatives (TN) lesions excised, i.e., non-fluorescent healthy lesions, and the sum of TN and FP) obtained by IntegriSense did not reach 88%. In summary, this NIR fluorescent probe has demonstrated a diagnostic accuracy of 96 % (measured as the (TP + TN)/(TP + TN + FP + FN). On the contrary, obtained TBR values were below the average generally required. Indeed, measured using image analysis software ImageJ (National Institutes of Health, Bethesda, USA), TBR has been calculated as the ratio of tumor intensity and the background tissue intensity. With a mean of 2.2, TBR related to skin was 4.2, and TBR related to muscle was 5.5. Nevertheless, IntegriSense could offer a practical advantage in intraoperative ovarian cancer detection, even if further investigations are needed.[91]

RGD-based probe SqRGD2

SqRGD2 is a fluorescent RGD-based probe designed for the targeted detection of $\alpha_v\beta_3$-integrin overexpressing ovarian cancer.[92] The targeting moiety consists of an RGD motif, which is known to be specifically recognized by $\alpha_v\beta_3$-integrins.[82] In SqRGD2 (Figure 19), two RGD-sequence-containing cyclopeptides (cRGDfK) are connected to a central fluorophore (NIR-emitting squaraine dye, Sq). SqRGD2 (λ_{ex}=667 nm, λ_{em}=679 nm) has been *in vitro* evaluated on OVCAR-4 cell lines, in which $\alpha_v\beta_3$-integrin receptors expression is up-regulated. After 30 h from the treatment with SqRGD2, the fluorescence intensity detected in the cells was 2.3 ± 0.7 times greater than the intensity of cells treated with the corresponding monovalent analogous probe (SqRGD). SqRGD2 is taken up by endocytosis specifically $\alpha_v\beta_3$-integrin mediated, through an active transport membrane process. Pre-treatment of cells with hypertonic sucrose and nystatin, known inhibitors of the clathrin- and caveolae-mediated endocytosis, strongly reduces cellular uptake of SqRGD2, which occurs following two specific pathways. Moreover, SqRGD2 and its monovalent analogous have been *in vivo* evaluated on OVCAR-4 tumor-bearing mice, that were IV injected with 3 nmol of either probe. 3 hours post-injection, mice were sacrificed and organs, as well as the tumor masses, were excised and imaged using an *in vivo* imaging system. The *ex vivo* analysis of samples collected has revealed that tumors were lighted in a 3 times greater manner by SqRGD2 in comparison with the monovalent SqRGD. A strong fluorescent signal has been also detected in the kidneys, liver, and lungs, which is consistent with previous studies on RGD-based probes, which showed to require many hours for completion of body clearance. Indeed, the majority of peptide-based fluorescent agent shows an increased non-specific accumulation in healthy organs.[93-94] Thus, despite further *in vivo* investigations being necessary, the deep-red fluorescent RGD-divalent squaraine probe (SqRGD2) has the potential as an αvβ3-integrin targeted agent for fluorescent-guided surgery of ovarian cancer.[92]

Figure 19.

3.3 Epidermal Growth Factor Receptor (EGFR)/human Epidermal Growth Factor Receptors 2 (HER-2)

Human epidermal growth factor receptor-2 (HER-2) belongs to the epidermal growth factor receptor (EGFR) family, which includes four members: HER-1(or EGFR1), HER-2 (or ErbB2), HER-3, and HER-4. EGFRs are tyrosine kinases transmembrane receptors that work as dimers. They form four homodimers and six heterodimers. Binding with transmembrane receptor tyrosine kinase ligands through the ectodomain, EGF receptors undergo an allosteric transition which leads to dimerization, and the subsequent protein kinase activation, trans-auto-phosphorylation, and initiation of signaling cascades.[95-96] HER-2 is a transmembrane glycoprotein of 185 kDa which, differently from other EGFRs, does not directly bind with ligands and its activation is dimerization-mediated. While the HER-2 homodimers do not interact with any of the known growth factors, when HER-2 dimerizes with other EGF receptors can recognize growth factors and be activated.[97-98] Involved in the activation of intracellular signaling pathways related to cell proliferation, differentiation, and survival, HER-2 is overexpressed in a variety of tumor types including breast, ovarian, cervical, colon, cervical, endometrial, esophageal, lung, and pancreatic cancers.[98-100] In particular, the amplification of HER-2 induces phenotypic changes associated with more aggressive disease, including increased cell motility, cell proliferation, and/or invasive ability.[101] HER2 status is a well-known prognostic and predictive marker in invasive breast cancer. Still, several investigations report that HER-2 is overexpressed in 52.5% of epithelial ovarian cancer patients. As for breast cancer, the high level of HER-2 expression has been associated with more aggressive tumor phenotypes and poorer clinical outcomes.[95,102-103]

AF680-labeled phage-J18

Asar *et al.* have employed peptide-displaying bacteriophage technology for obtaining biological nanoparticles that have been adequately modified for allowing a targeted *in vivo* detection of ovarian cancer cells.[104] Using a two-tier through phage display technique, which involves *in vivo* selection rounds in tumor-bearing mice followed by *in vitro* screening against cultured tumor cells, Soendergaard *et al.* have identified the ovarian-cancer-targeting peptide RSLWSDFYASASRGP (J18).[105] After labelling with the NIR dye AlexaFluor 680 (Figure 15, λ_{ex}=679 nm; λ_{em}=702 nm), it has been investigated *in vitro* the phage clone (pJ18) binding ability and its specificity for ovarian cancer cells, using fluorescent microscopy and modified ELISA. According to fluorescent microscopy analysis, the *in vitro* evaluation in cancerous and non-cancerous cell lines has shown the biotinylated-peptide J18 to possess a marked affinity for ovarian cancer cell lines (SKOV-3 and OVCAR-3), whereas only a minimal-level of binding has been observed in both breast cancer cells (MDA-MB-435) and embryonic kidney cells (HEK293). Moreover, in contrast to wild-type (WT) phage, which lacked foreign peptides, pJ18 has shown a significantly increased binding capability to adenocarcinoma cell lines (SKOV-3 cells), confirming the occurrence of a specific interaction J18-mediated. Since the peptide J18 exhibited an enhanced affinity towards SKOV-3 cells compared to OVCAR-3 cells, based on differences between their expression profiles, Asar *et al.* hypothesized that EGFR may be the potential surface antigen intercepted by J18. Indeed, known for their higher invasiveness potential, SKOV-3 cells exhibit a higher EGFR expression than OVCAR-3 cells.[106-108] Moreover, in support of this, it has been observed minimal binding to breast cancer cell lines that lack EGFR expression (MDA-MB-435 cells) by J18.[109] However, further studies are needed for the exact J18-target identification. According to a cell-based dose-response assay, performed at peptide concentrations ranging from 10 nM to 300 μM, J18 displayed saturation binding kinetics to SKOV-3 cells with EC_{50}=22.2 ± 10.6 μM, consistent with previously identified peptides using phage display technology.[110-111] A biodistribution study of AF680-labeled pJ18, performed on subcutaneous xenograft models of ovarian cancer (SKOV-3 cells), has revealed that the bacteriophagic optical agents undergo a rapid clearance in early hours after IV injection, by the reticuloendothelial system (RES), as already been observed for nanoparticles in general.[112-1139] Indeed, at 4 hours post-injection, while tumors do not exhibit a strong NIR fluorescence, high fluorescence intensities have been detected in the liver, spleen, and lungs. Similar results were obtained previously in phage biodistribution studies.[106,114-117] Therefore, 2 hours following IV injection with pJ18 (1012 transducing units, TU), NIR fluorescence imaging performed on SKOV-3-xenografted mice showed strong fluorescence in tumors, combined at sufficient tumor-to-background ratio values (data not reported). In conclusion, enabling easy tumor *in vivo* visualization, AF680-labeled pJ18 deserves further investigation as an ovarian cancer-targeting fluorescent nano-agent for the detection and diagnosis of the disease.[113]

BrCy106-NHS-doped optical viral ghosts (OVGs)

Vankayala *et al.* have developed virus-mimicking nanoparticles, hereafter named optical viral ghosts (OVGs), for targeted NIR fluorescence imaging of ovarian cancer. OVGs have been functionalized with antibodies against HER-2 and doped with the NIR bromo-cyanine dye BrCy106-NHS (Figure 20) to obtain a targeted detection of tumors.[118]

Figure 20.

These virus-mimicking nanoparticles consist of capsid protein (CP) subunits derived from genome-depleted plant infecting brome mosaic virus (BMV). The wild-type BMV genomic contents have been deleted, and only the CP subunits of the virus have been used to encapsulate the bromo-cyanine dye. In a prior *in vitro* investigation, Guerrero *et al.* demonstrated the specificity of ICG-doped anti-HER2 OVGs in targeting SKOV3 cells, which express high levels of HER-2, using fluorescent imaging microscopy and flow cytometry. Moreover, a competitive binding assay, in which SKOV3 cells were incubated with free antibodies and anti-HER2 OVGs for two hours, demonstrated the specific antibody-mediated internalization of virus-mimicking nanoparticles by tumor cells. Indeed, the mean fraction of fluorescent SKOV3 cells decreased by 1.5 and 5.4 times, respectively, when the amount of free antibody increased from 300 ng to 1.2 µg.[119] About spectral characteristics, in addition to the absorption in the 700-900 nm spectral band, consistent with BrCy106-NHS-dye-loading, anti-HER-2 OVGs present an absorption peak at 280 nm, attributable to the tyrosine, tryptophan, and cysteine residues of the CP. Instead, the fluorescent emission reaches the peak at 750 nm, and in the emission spectrum, an additional blue-sided shoulder (ranging from 675 nm to 715 nm) is present, likely originating from the monomeric and H-like aggregate forms of BrCy106-NHS.[120] According to DLS analyses, the average size of OVGs measures 37.8 ± 2.3 nm, with a poly-dispersibility index (PDI) in the range of 0.1–0.4, exactly 0.289.[118] Since do not exceed 200 nm in dimension, virus-mimicking nanoparticles may reach tumors driven by the enhanced permeability retention (EPR) effect.[121-122] The OVG's efficacy has been evaluated in intraperitoneal mice models of human ovarian cancer (SKOV3 cells). Anti-HER2-OVGs were suspended in a particles-stabilizing buffer (RNA assembly buffer lacking DTT) before injection into mice, and then, the OVGs pellet was combined to achieve an effective dye concentration of ~120 µg/ mL for injection. Following an IV administration, mice have undergone fluorescence imaging investigations for a timepoint range of 2–24 hours. At 24 hours post-injection, the fluorescence from tumors reaches its highest level in intensity, with a TBR value of ~ seven (7.6). TBR, measured as signal-to-noise ratio (SNR), considers the respective average fluorescence intensities associated with a given region of interest (ROI) of tumors that have received the optical agent or the RNA assembly buffer (as control). In mice injected with anti-HER-2 OVGs, the fluorescence intensity is significantly higher than that observed in animals injected with non-functionalized OVGs or non-encapsulated BrCy106-NHS. That has confirmed the improvement generated by both functionalization and encapsulation of optical viral ghosts. The use of anti-HER2 OVGs may offer a useful technique for real-time intraoperative detection of ovarian tumors, thus providing a technology for image-guided surgery.[118]

3.4 Claudin-3 and Claudin-4

Claudins belong to a large family of integral membrane proteins. Together with occludin, claudin proteins are essential components of the tight junctions (TJs). The TJs tie polarized epithelial and endothelial cells through a continuous network at their most apical region. TJs carry out a barrier function, preventing the paracellular transport of solutes, and, a fence function, maintaining the membrane polarity. Much evidence suggests that claudin proteins also have signaling functions, this is supported by the presence of *C*-terminal PDZ (postsynaptic density protein (PSD95), Drosophila disc large tumor suppressor (Dlg1), and zonula occludens-1 protein (zo-1)) binding domains in their protein sequence.[123-125] Serial analyses of gene expression (SAGE) allowed the investigation of ovarian cancer genetic fingerprints.[124] The genes encoding claudin proteins have been identified among the most highly up-regulated and overexpression of claudin 3 and claudin 4 was found in all ovarian cancer subtypes (80 - 84% of the cases were positive for claudin-3, whereas 60 - 71% for claudin-4).[123] Significantly higher levels of these TJs proteins were found in chemotherapy-resistant/recurrent ovarian tumors when compared with chemotherapy-naïve ovarian cancers. Localized in the cellular membrane, claudins are mis-localized in cancer cells, often detected in the cytoplasm. Claudin-3 and only a low rate of claudin-4 were detected in healthy ovarian epithelial tissues. Therefore, the overexpression in all ovarian cancer subtypes of these proteins is correlated with malignancy, and up-regulation of claudin-3 and 4 is correlated to ovarian cancer development. Their overexpression could prevent normal TJs formation and function. Indeed, cancer cells typically show a deficiency of TJs, with a consequent loss of physiologic cellular polarity and permeability. This permits an easier diffusion of substances necessary for the growth and survival of cancer cells. Claudin 3 and 4 represent the natural interaction sites for *Clostridium perfringens* enterotoxin (CPE) and are the only claudin protein family members able to bind CPE mediating the toxin cytolytic mechanism. CPE is a single polypeptide consisting of 319 amino acids. CPE generates epithelial cell permeability alteration up to cellular osmotic lysis through the interaction with claudin 3 and 4. Structure-activity relationship studies of the polypeptide revealed that the CPE290-319 COOH-terminus fragment (cCPE) is responsible for the high-affinity binding with targets but unable to form the small molecular complex that brings to cytolysis, hence it is not toxic.[125] These characteristics make cCPE an ideal carrier for targeting theragnostic agents to ovarian cancer cells overexpressing claudin 3 and 4.[127]

FITC-conjugated CPE peptide

cCPE has been conjugated to fluorescein isothiocyanate (FITC, λ_{abs}=490 nm, λ_{em}=525 nm), giving a FITC-conjugated CPE peptide, which was evaluated in vitro and in vivo as ovarian cancer fluorescent-tracer. FITC-cCPE accuracy and specificity have been assessed *in vitro* using patients-derived ovarian cancer cells. The cells OSPC-ARK-1 and CC-ARK-1 were proven to express claudin 3 and 4 by RT-PCR. Flow cytometry analysis confirmed that the carboxy-terminal fragment of CPE conjugated to FITC was able to label all primary ovarian cancer cells expressing claudin 3 and 4. The probe identifies ovarian cancer cells with 100% specificity and high mean fluorescence intensity (MFI) values. In agreement with the flow cytometry results, fluorescent images confirm that the probe lights all primary ovarian tumor cells, which had not shown intrinsic fluorescence before the treatment with FITC-cCPE. The fluorescence intensity of the fluorescently labelled peptide proved to be time and dose-dependent. Fluorescence, detected after 30 minutes, emitted by chemotherapy-resistant ovarian cancer cells, increased in intensity until 6 hours of incubation. Furthermore, a specific staining pattern is appreciable: localized spots on the tumor cell surface. This patterning suggests that the probe could be internalized and compartmentalized inside the tumor cell after binding with claudins. Confocal microscopic images 3D reconstruction supports this evidence. FITC-cCPE internalization, observed after 30 minutes of incubation, likely increases the probe's ability to concentrate and mark tumor burden. To determine the ability of FITC-cCPE to *in vivo* localize ovarian cancer cells, mice harbouring OSPC-ARK-1-derived tumors were IV injected with FITC-cCPE (100 μg). At different time points (30 minutes to 48 hours), tumors, normal organs, and ascites were examined for fluorescence by a whole-body optical imaging system. The images show a strong and selective fluorescent signal derived from the tumor, with the highest MFI value 24 hours after IV injection (2592 ± 1303). Interestingly, the fluorescent peptide was able to target tumor spheroids and even single chemotherapy-resistant ovarian cancer cells floating in the ascites of the OSPC-ARK-1 xenografted model.[127] IP administration has been *in vivo* investigated for FITC-cCPE on animals harbouring chemotherapy-resistant human ovarian cancer. The fluorescence signals of tumors rapidly increase, showing the highest MFI (741.7 ± 124.2) at 6 hours after IP injection (10 μg). Compared to MFI calculated for multiple normal organs excised, MFI values of disease were significantly higher. As observed after IV administration of FITC-cCPE (100 μg), millimetric metastases (i.e., micro-implants disseminated in the abdominal cavity and tumor spheroids floating in the ascites) have been fluorescent-targeted by FITC-cCPE after IP injection (10 μg) into mice harboring OSPC-ARK-1 primary chemotherapy-resistant ovarian cancer. These data suggest the ability of the probe to detect occult micro-metastases not clinically identifiable. Despite the great potential, the use of FITC-cCPE as an intraoperative fluorescent probe for fluorescence image-guided surgery (FIGS) has relevant limitations associated with the fluorescent moiety. FITC absorbs and emits (480/535 nm, respectively) in the visible light range (between 390 and 700 nm), which also includes the high absorption and scattering of biological tissues. The interferences associated with biological tissue autofluorescence may significantly compromise the ability of FITC-cCPE to discriminate between normal and malignant tissues.[128]

CW800-cCPE

A modified version of cCPE, with a residue of cysteine at *the N*-terminus, has been conjugated to IRDye CW800 maleimide (Figure 12, λ_{abs}=774 and λ_{em}=789 in water and PBS), generating the near-infrared (NIR) probe CW800-cCPE. CW800 is widely used in cancer optical imaging due to its safety profile. As NIR dye provides a good tissue penetration and optimal tumor-to-background ratio, because of low absorption and emission of biological tissues at these high wavelengths ($\lambda > 750$ nm) and the resulting low background interference. Furthermore, the chemical structure of CW800 allows for suitable and stable conjugation to target moieties such as peptides or small molecules. CW800-cCPE has been previously *in vitro* evaluated for its binding affinity to claudin 3 and 4: peptide binding properties remain unchanged after the NIR dye conjugation. Kinetics and biodistribution of CW800-cCPE have been *in vivo* investigated, following IP and IV administration on subcutaneous and intraperitoneal models of chemotherapy-resistant primary ovarian serous papillary carcinoma (OSPC-ARK-1). OSPC-ARK-1 cell lines were established from samples collected from patients at the time of disease recurrence (stage IV OSPC). After 30 minutes of IP injection of CW800-cCPE (10 µg) in intraperitoneal models of human ovarian cancer, the NIR probe was able to detect the disease with satisfying specificity. MFI calculated (considering an area of 5396 pixels) for the tumor was significantly higher (156.55 ± 23.73) than the MFI of other excised normal organs (ranging from 13.46 ± 1.35 in the brain to 95.72 ± 18.19 in the kidney). CW800-cCPE detected small metastatic lesions (a few millimeters) disseminated in the abdominal cavity of mice (10 µg of IP. CW800-cCPE) harboring intraperitoneal metastatic OSPC-ARK-1-derived tumors. The small-sized tumors disseminated in healthy organs were likely detectable due to the absence of background interference, with negligible signals coming from surrounding healthy tissues. The tumor-targeting capacity of CW800-cCPE has been *in vivo* evaluated in mice harboring subcutaneous human chemotherapy-resistant ovarian cancer following systemic (IV) injection. After IV administration of 25 µg of NIR probe, total body fluorescence distribution has been visualized at different time points. At first (6 h), CW800-cCPE spreads throughout the animal body, in the tumor as well as in normal organs. After longer incubation times (24 - 96 hours), a specific and progressive accumulation in the tumor occurs. TBR peaked after 48 hours of injection. The same value (48 hours) is obtained on the patient-derived xenograft (PDX) model generated from chemotherapy-naıve ovarian cancer patients injected with 25 µg of CW800-cCPE. After IV injection with equimolar concentration of the free NIR dye into size-matched subcutaneous models of OSPC-ARK-1, negligible fluorescent targeting was detected. These results confirm that the specificity of the probe is related to the binding of cCPE with the targets (claudin 3 and 4). *In vivo*, toxicity studies have been carried out on mice with sized-match OSPC-ARK-1-derived subcutaneous tumors. Mice have been injected IP and/or IV with different doses of CW800-cCPE (ranging from 10 to 100 µg) and monitored over three months. No acute and/or chronic toxicity has been observed. CW800-cCPE (25 µg, IV administration) has proved to be able to detect micro-metastatic lesions (<1 mm) located in the abdominal cavity of mice harbouring intraperitoneal metastatic OSPC-ARK-1-derived ovarian tumors (Image 3).[128]

Image 3.

Using real-time fluorescence imaging technology, the NIR probe (25 µg, IV administration) allows a highly sensitive and specific detection of disease in a PDX model of chemo-naıve ovarian cancer and, in a xenograft model of chemotherapy-resistant uterine serous carcinoma (USC, highly aggressive subtype of endometrial cancer overexpressing claudin-3 and 4). These data suggest that CW800-peptide may represent a safe and highly sensitive optical probe for the real-time intraoperative visualization of averagely large (i.e., 10 – 12 mm) tumor masses but also micrometastatic lesions (<1mm), not clinically visible.[128]

3.5 Cluster of Differentiation 44 (CD44)

CD44 (cluster of differentiation 44) antigens form a ubiquitously expressed family. CD44 is a glycoprotein located on the cellular surface and involved in cell-cell interactions, cell adhesion, and migration. Indeed, the integral component of the extracellular matrix, hyaluronic acid, represents its principal ligand. Other CD44 ligands include osteopontin, serglycin, collagens, fibronectin, and laminin. CD44 is involved in a wide range of physiologic and pathological processes such as lymphocyte activation, recirculation and homing, hematopoiesis, and tumor metastasis.[129] Among markers of ovarian cancer stem cell (CSC), CD44 is the most common, and according to several studies, CD44 may be a reliable indicator for the identification of ovarian CSCs.[130] Bhattacharya *et al.* associated CD44 expression and stem-like characteristics and chemoresistance in ovarian cancer cells.[131] Moreover, Suarez *et al.* demonstrated that CD44 could play a role in spheroids formation in ovarian cancer, promoting invasion and metastasis dissemination.[132]

LbL DCNPs

Using the layer-by-layer (LbL) assembly technology, Dang *et al.* have fabricated a NIR-II fluorescent nanoprobe for *in vivo* targeted detection of ovarian cancer. The nanoprobe consists of a multilayer structure that contains the inorganic fluorescent dye DCNP ($NaY_{0.78}Yb_{0.2}Er_{0.02}2F_4$) encapsulated in the amphiphilic partially alkyl amide functionalized poly(acrylic acid) (PAA). PAA provides a fully negatively charged core suitable to be subsequently coated with two barrier layers, the biocompatible poly(L-arginine) (PLA) and dextran sulfate (DXS), respectively. Finally, the outmost layer consists of a natural polysaccharide, hyaluronic acid (HA), which provides not only a surface suitable for further functionalization but also a targeting capability; indeed, HA represents the primary ligand of CD44, over-expressed in ovarian cancer cells. Negatively charged, with a $\zeta_{potential}=-30$ mV, the completed LbL DCNPs possess an optimal hydro-dynamic diameter for systemic delivery (within 200 nm) and establish a monodisperse system, with a PDI between 0.1 and 0.2, according to DLS measurements. The LbL DCNPs reach the excitation peak at $\lambda=980$ nm and the maximum in emission at $\lambda=1{,}575$ nm, showing a very high Stoke's shift. *In vivo,* biodistribution and pharmacokinetics studies revealed that LbL NIR-II nanoprobe after an IV administration rapidly (1-second post-injection) firstly accumulates in the heart and within 30 seconds in the other major organs (lungs, liver, spleen, and circulatory system). The whole-body diffused fluorescent signals remain stable for 1 hour. Up to 72 hours post-injection, the liver and spleen constitute the main fluorescence sources, which, being part of the reticuloendothelial system, as expected, are responsible for NPs clearance. Likely due to the highly hydrophilic external HA layer, which prevents above all binding with hematic proteins, LbL DCNPs exhibit an extended blood half-life of 24 hours. Histopathological *ex vivo* analyses performed on excised organs show that LbL DCNPs are functionally nontoxic and suitable for biomedical applications. In xenografted murine models of ovarian metastatic cancer (COV362 cells), it has been *in vivo* assessed the LbL DCNPs' ability to detect tumor lesions. After IV injection with a single dose of the nano-agent (1 mg/mL, 200 μL), the whole-body NIR-II fluorescence imaging performed on mice indicated a preferential targeting of LbL DCNPs to tumorous tissue. 72 hours post-injection, the contrast action of LbL DCNPs facilitated the excision of organs and tumor lesions. The nano-agent down-converted NIR-II fluorescence emission permits the individuation of in-depth small lesions in the abdominal cavity, while the up-converted green fluorescence emission, which is visible by the human eye, allows cellular-level detection with a low level of autofluorescence interference. Substantially, several tumor lesions, distributed within the abdominal cavity or invading vital organs such as the liver, pancreas, and intestine have been successfully detected in a tumor-specific and non-invasive manner. Thus, despite further investigation being essential, this fluorescent nanoplatform may represent a useful contrast agent for real-time imaging-guided surgery, as well as for monitoring the progression and treatment response of tumors.[133]

3.6 Lysophosphatidic acid (LPA)

Lysophosphatidic acid (LPA: mono-acyl-sn-glycerol-3-phosphate, Figure 21) is a small and structurally simple phospholipid, that carries only one fatty group.

Figure 21.

LPA is a cell membrane lipid derivative and a metabolic intermediate that is involved in several biochemical, physiological, and pathological processes, ranging from vascular development and neurite remodeling to inflammation and tumor progression.[134-135] Seeing as it has been observed a significantly higher LPA concentration in patients with gynecologic malignancies in comparison with healthy controls, Xu *et al.* first demonstrated that LPA may represent a potential biomarker for gynecological cancers, and for ovarian cancer in particular. Indeed, 98% of patients with ovarian cancer, and 95% of patients affected by gynecological cancers, present high levels of LPA.[136] Subsequently, several studies demonstrated the presence of LPA at high concentrations in both ascitic fluid and plasma of patients with ovarian cancer, suggesting that LPA represents a promising biomarker of ovarian cancer with high specificity and sensitivity.[137]

G4RGDSq2

G4RGDSq2 is a NIR fluorescent imaging agent designed for sensing and detection of LPA, an ovarian cancer-specific biomarker widely distributed in cells and tissues. The probe selectivity relies on two structural elements. First, consisting of a peptide skeleton on which are inserted four guanines and two squaraine dyes (Figure 22), the fluorescent probe responds to the polarity change of the surrounding environment. Indeed, in aqueous solutions, G4RGDSq2 assumes a folded state stabilized by hydrogen bonds between the guanines, and this conformational restriction turns off the probe fluorescence. In contrast, the fluorescence turns on when the probe binds the target, which establishes polarity changes in the tumor microenvironment, inducing the break of intramolecular hydrogen bonds and a subsequent conformational change to an extended and fluorescent form. The second element consists of the presence of two sequences of arginine-glycine-aspartic (RGD) repeated in the chemical structure. RGD moiety is a targeting ligand to integrin receptor $\alpha_v\beta_3$, which is over-expressed in ovarian cancer, and it improves the probe cellular uptake.

Figure 22.

The NIR fluorescent probe exhibits two absorption bands at 650 nm and 710 nm that correspond to the absorption of RGDSq2 and G4RGDSq2, respectively, and emits at 720 nm. According to spectrofluorometer analyses, LPA strongly enhanced intensities of absorption and emission. Indeed, the quantum yield increases from 0.37% in the absence of LPA up to 6.0% in the presence of 10 equivalents of LPA. G4RGDSq2 can detect down to a minimum of 0.5 μM of LPA. G4RGDSq2 (385 nm) and LPA (126 nm) compose a complex of 585 nm, according to DLS and TEM analyses. The measurement of the $\zeta_{potential}$ of G4RGDSq2−LPA, free LPA, and G4RGDSq2 has permitted the identification of the nature of the binding between the fluorescent probe and the target, kept together by electrostatic interactions established among RGD motif and LPA. Firstly, the G4RGDSq2 capability to detect LPA has been *in vitro* assessed. After incubation with G4RGDSq2 at a concentration ranging between 0.5 and 2.0 μM, mean fluorescence intensity (MFI) measured on LPA-overexpressing SKOV-3 cells is approximately 3−6 fold higher than human normal ovarian surface epithelial cell lines (IOSE80) used as control due to their low level of LPA-expression. Observed at confocal laser scanning microscopy (CLSM), both cell lines SKOV-3 and IOSE80 have shown red fluorescence in the cytoplasm. Nevertheless, the higher cellular concentration of LPA of SKOV-3 likely has determined a stronger red fluorescent light emission than the control. Showing no cytotoxicity *in vitro* (MTT assay), the turn-on fluorescent probe has been *in vivo* evaluated in subcutaneous murine xenograft models of SKOV-3. After 24 h of IV injection (120 nm), G4RGDSq2 has successfully detected the tumor lesion only in the mouse not previously IV administered with the LPA-inhibitor (S32826, 486 nmol) or αvβ3 integrin inhibitor (cilengitide, 170 nmol). Since no fluorescence has been observed in the tumor lesions of the mice treated with the inhibitors, G4RGDSq2 presumably enters SKOV-3 cells *via* $\alpha_v\beta_3$ integrin receptor, and it emits a red fluorescent signal only in the presence of high levels of LPA in the tumor. Exhibiting no significant *in vivo* toxicity, measured as histological alterations observed in excised normal organs, G4RGDSq2 has created promising expectations about its potential use as a detection tool for LPA-targeted NIR fluorescence imaging of ovarian cancer suitable for both diagnosis and surgery procedures.[138]

3.7 OC183B2 antigen

OC183B2 belongs to the Ig family and is an ovarian cancer-associated antigen.[139] The OC183B2 expression has been *in vivo* evaluated in patients-derived tissue samples of ovarian cancer and FT (fallopian tube) using IHC staining, employing COC183B2 as primary mAb. Indirect enzyme-linked immunosorbent assay (ELISA) has been performed to determine COC183B2 binding specificity for ovarian cancer-associated antigen. The level of OC183B2 expression has been found significantly higher in ovarian cancer specimens than in FTs. With a higher OC183B2 rate in serous ovarian cancer than in non-serous ovarian cancer, a relationship between OC183B2 expression and ovarian cancer clinicopathological characteristics has been observed. In particular, the presence of the antigen is associated with a positive prognosis. IF staining of samples with AlexaFluor488-COC183B2 reveals the antigen cellular collocation. Strong fluorescent signals in the cytoplasm and dots of fluorescence in the nucleus have been observed.[140] IHC experiments have detected the expression of OC183B2 in different histological subtypes of epithelial ovarian cancer (i.e., serous, mucinous, clear cell and, endometrioid), different clinical stages and, different pathological grades. In addition, OC183B2 has been detected in patients with derived epithelial ovarian cancer metastatic lymph nodes. The simultaneous absence of OC183B2 expression in normal tissues and normal lymph nodes makes the ovarian cancer antigen an epithelial ovarian cancer-specific target.[140-141]

COC183B2-Cy7

COC183B2, a mouse MAb OC183B2-specific generated using hybridoma technology, is conjugated to the NIR dye Cy7 *N*-hydroxy succinimide (NHS) ester (Figure 23, λ_{ex}=750 nm, λ_{em}=773 nm). Dye-to-protein ratio measured using the UV-Vis spectrophotometry is 2.4:1.

Figure 23.

COC183B2-Cy7 target efficacy has been *in vivo* investigated on subcutaneous xenograft mouse models of serous epithelial ovarian cancer (SKOV3-Luc). Mice were subcutaneously implanted with cell lines injected in BALB/c (Bagg albino laboratory-bred strain), which were previously evaluated for OC183B2 antigen expression by IF staining (strongly positive signals were detected both in the plasma membrane and cytoplasm of SKOV3-Luc). Performed using an IVIS spectrum imaging system, NIRF imaging revealed that COC183B2-Cy7 is mainly taken up by xenografts and the liver. The highest fluorescent signal in xenografts is detected 96 hours after IV injection with 30 µg of COC183B2-Cy7. TBR, which increases with fluorescent MAb dose, peaks 24 hours after IV injection (30 µg), keeping high up to 96 hours after injection. IVIS images show intense fluorescence until 264 hours post-injection in tumors and the liver, which represents the main metabolic organ. No toxic or chronic effects have been observed in mice during the experiments.[140] Considering that expression of OC183B2 has been detected also in metastatic lymph nodes of epithelial ovarian cancer, COC183B2-Cy7's ability to identify tiny metastatic lymph nodal lesions has been investigated in a subcutaneous mouse model of metastatic ovarian cancer. Mice-bearing tumors (SKOV3-Luc) with 0.4 - 0.7 cm in diameter were IV injected with fluorescent mAb. NIR fluorescence imaging showed that the highest TBR value was detected 168 hours after COC183B2-Cy7 (20 µg) IV injection. The probe (half-life=86.24 hours) induces a strong, specific, and long-lasting (168-240 hours post-injection) fluorescent signal in xenograft ovarian cancer models. A strong fluorescent signal in the liver has been detected, performing *in vivo* NIR fluorescence imaging, which confirms the previous results that identified the liver as the main metabolic organ. Nevertheless, liver fluorescence decreases from 168 hours post-injection, further reducing the background fluorescent interference. To further investigate COC183B2-Cy7 sensitivity, metastatic ovarian cancer intraperitoneal models have been IV injected with Cy7-labeled mAb (20 µg). Tumor-harbouring mice (SKOV3-Luc) with micro-metastases disseminated throughout the animal abdominal cavity, were IV injected with COC183b2-Cy7 (20 µg). 7 days after injection, NIR fluorescence *in vivo* imaging showed that the fluorescent agent had been able to detect tiny cancerous metastases, approximately 1 mm in diameter. These results have been confirmed by *ex vivo* imaging performed on the excised multiple micro-lesions, which showed not only strong fluorescent signals in the liver but also a discrete accumulation of fluorescent mAb in the lungs. Unfortunately, fluorescent signals from the ovaries and uterus of nontumor-bearing mice have been observed, probably correlated to COC183B2-Cy7 non-specific binding to mouse ovarian and uterine tissues. With high sensitivity and low background fluorescence, COC183B2-Cy7 proves to be a promising fluorescent imaging agent for real-time detection of average-size lesions as well as micro lesions, such as lymph nodal occult metastases, often not identifiable through palpation or with the naked eye.[141]

COC183B2-800

In COC183B2-800, the NIR fluorescent dye IRDye800CW (Figure 12, λ_{abs}=774 nm; λ_{em}=789 nm) is conjugated to COC183B2 (dye-to-protein ratio=2.2:1), the mouse mAb against ovarian cancer-associated antigen OC183B2, generated using hybridoma technology. IRDye800CW has been extensively used on humans in clinical studies, and it has shown a safe administration profile. The targeting ability of COC183B2-800 has been *in vivo* evaluated on a subcutaneous mouse model of epithelial ovarian cancer (SKOV3-Luc). Subcutaneously implanted mice have been IV injected with the fluorescent mAb. NIRF imaging, performed with IVIS technology, shows a strong tumor-specific fluorescence, except for the significant fluorescent signals in the liver. High TBR values were observed with the injection of 25 µg and 50 µg of COC183B2-800 from 24 up to 72 hours after administration. TBR value increases according to the enhancement of fluorescent protein dose. Mainly metabolized in the liver, no fluorescence was detected in the other excised organs by the *ex vivo* NIRF imaging, except for a weak fluorescence in the kidneys. COC183B2-800 stands out as a safe and ovarian cancer-specific imaging agent for FIGS.[141]

3.8 Cancer Antigen 125 (CA125)

The transmembrane cell-surface protein CA125 (cancer antigen 125) is a member of the mucin family of glycoproteins and is encoded by the MUC16 gene.[142-144] It is a part of the epithelia of the female reproductive tract, the respiratory tract, and the ocular surface. Due to its high glycosylation, it produces a hydrophilic environment on the apical membrane of epithelial cells that functions as a lubricating barrier against external particles and pathogens.[145] Moreover, CA125 has in its structure a cytoplasmic tail that interacts with the cytoskeleton binding members of the ERM (ezrin/radixin/moesin) protein family.[146] Over the years, several studies have reported that CA125 plays multiple roles in tumorigenesis and tumor proliferation. It has been shown that CA125 participates in cell-to-cell interactions that enable metastasis formation.[147] Furthermore, due to its cytoplasmic tail, it is involved in enabling tumor cells to grow, promoting cell motility, and facilitating invasion. Promoting expression of *N*-cadherin and vimentin, CA125 participates in cancer epithelial-mesenchymal transition.[148] Finally, it may also contribute to reducing the sensitivity of cancer cells to drugs.[149] Based on these findings, in the last two decades, CA125 has found application as a tumor marker or biomarker in many cancer types, most notably in ovarian cancer.[150] Numerous studies have demonstrated elevated levels of CA125 in ovarian cancer tissues when compared to healthy,[151-152] and to date, the transmembrane cell-surface protein CA125 remains the most-used molecular ovarian cancer marker.[153] Moreover, despite CA125 mainly representing a serum biomarker, since high concentrations of *MUC16*/CA125 remain on the surface of ovarian cancer cells, it could represent a reliable biomarker for targeted detection of ovarian cancer through imaging techniques.[154]

^{ss}B43.13-IR800

Fung *et al.* produced a fluorescent imaging agent for the *in vivo* detection of CA125-expressing ovarian cancer. The probe mAb-based targeting moiety (B43.13) conjugated to a NIR-fluorophore (IRDye® 800CW, Figure 12), with a degree of labeling of approximately 0.75 fluorophores/mAb.[155] The heavy chain glycans have been site-specifically modified (^{ss}B43.13) using a chemoenzymatic reaction. The mAb was previously used to develop the PET imaging agent [^{89}Zr]Zr-DFO-B43.13, which showed *in vivo* high capability to delineate primary tumor tissue, but also the metastatic spread of ovarian cancer through the ipsilateral chain of lymph nodes.[154] B43.13 is a CA125-targeting murine antibody (K_d for CA125=1.2 nM), currently investigated in clinical trials, as oregovomab (OvaRex®), in combination with several therapeutic agents, for targeted chemotherapy and immunotherapy of epithelial ovarian cancer.[156-163] Since flow cytometry and fluorescence microscopes exhibit superior compatibility with visible-emitting fluorophores, the *in vitro* experiments were performed using ^{ss}B43.13-AF488 (λ_{abs1}=280 nm, λ_{abs2}=494 nm; λ_{em} 516 nm), where the mAb is labelled with the green fluorescent dye Alexa Fluor™ 488 (AF488). ^{ss}B43.13-AF488 has shown high specificity binding to Ca125-positive OVCAR3 cells but not CA125-negative SKOV3 cells at an incubation concentration of 1-16 µg/mL. Near-infrared fluorescence imaging evaluation was performed with ^{ss}B43.13-IR800 (λ_{abs1}=280 nm, λ_{abs2}=774 nm; λ_{em}=820 nm) as a contrast agent on subcutaneous xenografts (OVCAR3 cells) mice models of ovarian cancer. After 120 hours from IV injection of ^{ss}B43.13-IR800 (100 µg; 0.66 nmol), a high accumulation of the fluorescent probe in the tumor was detected. In some mice, fluorescent signals were also observed in the lymph nodes adjacent to the tumor. Based on data from the preclinical evaluation of the hybrid immune-PET agent [^{89}Zr]Zr-DFO-B43.13, fluorescence detected in lymph nodes may be due to the uptake of the immunoconjugate by metastatic lesions, diffused through the ipsilateral lymph node chain.[154] Mostly weak fluorescence was observed in healthy organs, except for the liver, where likely accumulate immune complexes of shed serum CA125 with the contrast agent, and takes place the clearance of the exogen murine labelled-mAb by hepatocytes or resident macrophages (Kupffer cells). To simulate the application of ^{ss}B43-IR800 as a fluorescent agent for intraoperative imaging, athymic nude mice bearing orthotopic OVCAR3 xenografts implanted in the left ovary underwent NIR fluorescence imaging and post-mortem excision. ^{ss}B43-IR800 (100 μg; 0.66 nmol) has detected the primary tumor in the left ovary, and in addition, it highlighted the presence of a peritoneal implant and lesions in renal lymph nodes, that at the later histopathological *ex vivo* analyses revealed to be malignant. The feasibility of ^{ss}B43.13-IR800 was also evaluated in subcutaneous, orthotopic, and patient-derived xenograft (PDX) Nod-Scid-Gamma (NSG) mice models of high-grade serous ovarian cancer. Since in athymic nude mice, OVCAR3 xenografts exhibit a low take rate, slow growth, and inconsistent size, NSG mice have been used for subsequent *in vivo* evaluation. Moreover, beyond showing an approximately 100% take rate of OVCAR3 xenografts in the absence of functional NK cells, the highly immunocompromised NSG mice are the preferred strain for the propagation of frozen parent PDX tumors. In NSG mice bearing orthotopic OVCAR3 tumors and subcutaneous, CA125-positive PDXs, after IV injection with ^{ss}B43.13-IR800 (50 μg; 0.33 nmol), high NIR fluorescent signals have been detected in the tumors. In contrast, weaker fluorescence was emitted by most healthy organs, in comparison with the previous athymic mice model. A moderate liver fluorescence was observed, which was however lower than that observed in athymic mice, likely due to the higher dosage administered in these latter. These data suggest that it is necessary to determine an optimal dosage to facilitate the target-mediated clearance of the NIRF probe maintaining high contrast signals essential to achieve efficient surgical cytoreduction. Finally, similarly to the free antibody (B43.13) and another commercially available anti-CA125 antibody, ^{ss}B43.13-IR800 has demonstrated *in vitro* a strong capability to specifically stain CA125-positive tissue sections, obtained from tumors and metastatic lymph nodes harvested during the surgical debulking of patients with high-grade serous ovarian cancer. These findings confirmed the conjugation with the NIR dye does not compromise the binding affinity of mAb with the target. In conclusion, despite more investigation needed, the fluorescent probe ^{ss}B43.13-IR800 possesses a concrete potential as a contrast agent for fluorescence-guided surgery of ovarian cancer.[155]

3.9 Prolactin receptor (PRLR)

The prolactin receptor (PRLR) is a membrane receptor that belongs to the hematopoietic cytokine receptor superfamily. It is structurally constituted by three domains: an extracellular domain (ED), that contains two binding domains (D_1 and D_2), a well-conserved transmembrane domain (TD), and an intracellular domain (ID). Up to now, several isoforms of PRLR have been identified, and they are encoded by the same gene (PRLR) which undergoes alternative splicing. Isoforms mainly differ in size and sequence of the ID which can be long, intermediate, or short. The main human isoform is the "long" PRLP consisting of 598 amino acids. It can interact with prolactin (PRL), and two additional ligands: placental lactogen, and growth hormone. PRL is a polypeptide hormone structurally constituted by a sequence of 199 amino acids, and it is primarily synthesized and secreted by anterior hypophysis lactotroph cells. Nevertheless, its production is not restricted to the pituitary gland, indeed recently several studies reported a peripheral and extra-pituitary production of prolactin which has disclosed a wide range of other functions of the hormone. In addition to promoting the proliferation and differentiation of the mammary cells for lactation, PRL also exhibits a wide range of other functions, including the regulation of the hair cycle, the maintenance of bone homeostasis, and the adrenal response to stress. The PRLR dimerizes through TDs and, upon binding with ligand, transmits the signal through several associated cytoplasmic proteins, triggering downstream signaling pathways that result in different cell responses that explain the pleiotropic effects of PRL.[164] Nowadays numerous investigations have revealed that PRL plays a significant role in oncogenic processes, including survival, cellular proliferation, migration, invasion, metastasis, and treatment resistance. Consequently, due to the high level of female production, PRL and its receptor are particularly overexpressed in gynecological cancers such as ovarian cancer.[165] In addition to the pituitary PRL having endocrine action, tumoral tissues can also synthesize and secrete PRL with paracrine/autocrine functions.[166] Furthermore, several studies have reported that tumoral PRL is an important survival factor, inhibiting apoptosis and having a significant impact on the growth of ovarian cancer cells.[14,167] Regardless of stage, grade, and histology, PRLR is expressed in more than 80% of ovarian cancers, and the serum level of PRL is considerably elevated in women affected by ovarian cancers.[168] According to microarrays analysis of tissues collected from 152 patients affected with ovarian cancer from early to the advanced stage, and from 10 healthy subjects, the PRLR expression is moderate to high in more than 98% of malignant samples. On the contrary, a lower level of PRLR expression has been detected in normal tissues. In comparison to primary tumors, samples belonging to peritoneal metastases have shown no significant differences in PRLR level of expression. These findings suggest that PRLR has a noteworthy potential as an ovarian cancer biomarker for the targeted detection of disease through imaging systems.[169]

NIR fluorescent hPL*-conjugates

Sundaram *et al.* have designed and evaluated *in vitro* and *in vivo* ovarian cancer-targeted fluorescent probes that take advantage of the high affinity for PRLR of human placental lactogen (hPL), a specific ligand of prolactin receptor, which is overexpressed in most ovarian tumors. By rDNA technology, a point mutation has been inserted in the native hPL gene, and a recombinant human placental lactogen* (hPL*) has been expressed in an *E. coli* cell line. Differently from native hPL, hPL* contains a residue of cysteine rather than isoleucine in position 138 in its sequence. Differently from isoleucine, cysteine through its thiol group conjugates with fluorescent dyes Cyanine 5 maleimide (λ_{abs}=498 nm; λ_{em}=517 nm), and Cyanine 5.5 maleimide (λ_{abs}=683 nm; λ_{em}=703 nm), allowing the obtain respectively hPL*-Cy5 and hPL*-Cy5.5 (Figure 24), which maintains a certain affinity for PRLR. Indeed, the mutation has been inserted in a strategic position that does not compromise interaction with the target.[169] Indeed, according to the crystal structure of the rat PRLR extracellular domain complexed with ovine placental lactogen, residue 138 of hPL is in a flexible loop region of the polypeptide that remains outside the binding interface during the interaction with the target.[170]

Figure 24.

As evidence of this, the hPL*-conjugates have demonstrated the ability to activate *in vitro* the downstream signaling pathways of both long-PRLR and short-PRLR isoform, confirming that the site-specific modification of flexible loop of hPL did not compromise the probe affinity for the target. Since triggering signaling pathways by the hPL*-conjugates may result in dangerous side effects, the *in vivo* use of the fluorescent probes must be restricted to an average of 6 hours, a time term suitable for diagnostic purposes. Indeed, following 15 days of exposure to hPL*-conjugated, an increase in probe tumorigenic activity has been observed.[169] Similar to the native ligand,[171] hPL*-Cy5 binding the receptor can induce a zinc-dependent internalization of the complex of hPL*-conjugate and PRLR via clathrin-mediated endocytosis, thus enabling a targeted accumulation of the imaging agent in the PRLR-overexpressing cancer cells. At first, the hPL*-Cy5 capability to discriminate malignant against normal ovarian tissues has been *in vitro* evaluated. After overnight incubation of the ovarian-derived tissues with 500 nM hPL*-Cy5 in the presence of 20 µM $ZnCl_2$, the fundamental cofactor for interaction between hPL* and PRLR, only malignant tissues showed fluorescence. Subsequently, the NIR fluorescent probe hPL*-Cy5.5 has been evaluated *in vivo* in animal xenograft models of PRLR-expressing and PRLR-non-expressing ovarian cancer. Since ovarian cancer is highly heterogeneous, subcutaneous animal models of two different histological subtypes of ovarian cancer (Heya8 and CaOV3) have been employed to *in vivo* assess the targeted detection capability of the hPL*-conjugate. 24 hours after injection with hPL*-Cy5.5 (0.21 μM/kg), the NIR probe showed a specific accumulation in the tumor lesions of both subcutaneous murine models of ovarian cancer which overexpresses the prolactin receptor. The NIR probe undergoes a time-dependent internalization by tumor tissues, and the tumor fluorescence reaches the peak in intensity after 72 hours from the injection, vanishing only 192 hours following injection. In the *ex vivo* imaging of excised tissues and organs, fluorescence has been observed in tumor tissues as well as organs such as the liver and kidneys, where likely the probe is metabolized. In contrast, no fluorescence signals have been detected in surrounding muscles, suggesting efficient discrimination between healthy and malignant tissues. Indeed, the probe demonstrated high efficacy in discrimination *in vivo* of PRLR-positive lesions from PRLR-negative ones in subcutaneous models, distinguishing within the same PRLR-positive lesion different levels of PRLR expression. Moreover, the NIR probe showed high sensitivity, proving to be able to detect *in vivo* small metastatic lesions (10 mg) spread in the peritoneal region of an intraperitoneal murine model of ovarian cancer (Heya8). Despite these advantages, since hPL*-conjugates can activate PRLR signaling, its actual clinical use generates concerns regarding the tumorigenic potential risk which arises mainly from prolonged exposure to hPL*-conjugates. Therefore, further preclinical validations must be performed before proceeding to clinical experimentation of hPL*-conjugates as a fluorescent imaging agent for real-time intraoperative ovarian cancer detection.[169]

3.10 Human follicle-stimulating hormone receptor (FSHR)

FSHR is a G protein-coupled receptor (GPCR) of 75 kDa mainly expressed in gonads (testis and ovary), it is scarcely present in normal tissues. Currently, there are 4 known human isoforms of FSHR: FSHR-1 (G protein-coupled form), FSHR-2 (dominant negative form), FSHR-3 (growth factor type-1), and FSHR-4 (soluble FSHR). Structurally, the FSHR consists of 7 transmembrane domains connected with 6 loops, an intracellular C-terminal tail, and a large *N*-terminal extracellular for interaction with a specific hormone, the follicle-stimulating hormone (FSH). Secreted by the anterior pituitary gland, FSH, also known as Follitropin, is a dimeric glycoprotein consisting of alpha and beta subunits. Made up of 96 amino acids, the alpha unit (FSHα) is identical to other glycoprotein hormones such as luteinizing hormone (LH), thyroid-stimulating hormone (TSH), and human chorionic gonadotropin (hCG), while the beta subunit (FSHβ) is hormone-specific, and in FSH consists in 111 amino acids. FSH is involved in growth and pubertal maturation during development. Instead in adults, usually stimulates Sertoli cells' function in males, and induces the growth and maturation of ovarian follicles, and estrogenic production through the activation of FSHR in granulosa cells in females. FSH also plays an important role in the carcinogenesis of ovarian cancer, being highly present in the malignancy. Therefore, the overexpression of FSHR may contribute to uncontrolled cell proliferation, invasion, and migration, and consequently in tumor progression.[172-173] Indeed, FSH stimulates ovarian epithelial stem cells that are involved in the creation of new oocytes and the assembly of primordial follicles, thus FSHR-overexpression inducing abnormal activation of this process leads to ovarian cancer cell proliferation.[15] Zhang *et al.* have reported that FSH also increases ovarian cancer proliferation by stimulating the signaling pathway of octamer-binding transcription factor 4 (OCT4) cancer stem cells.[174] Several studies shed light on the connection between the phosphatidylinositol-3-kinase/protein kinase B (PI3K/Akt) pathway and ovarian cancer cell proliferation and invasion. Through inducing the transient receptor potential channel C3 (TRPC3), FSH triggers the PI3K/Akt cascade that modulates different molecules involved in epithelial-to-mesenchymal transition (EMT), proliferation, differentiation, and migration.[175-178] Moreover, inducing ROS production, FSH leads to the upregulation of Nrf2 and hypoxia-inducible factor 1α (HIF1α) and promotes the binding of HIF1α to the vascular endothelial growth factor (VEGF) notoriously associated with cancer angiogenesis.[179] In conclusion, due to its specific correlation with the malignancy microenvironment and the relative lack of its expression in normal tissues, FSHR has significant potential as a biomarker in the detection of ovarian cancer.[180]

DCNPs-$L_{1/2}$-FSH_{β}

The NIR-II lanthanide-based FHSR-targeted *in vivo* self-assembly nanoparticles (NPs) have been designed to improve intraoperative ovarian cancer-specific fluorescence imaging. NIR-II-emitting inorganic NPs have been functionalized through a ligand exchange strategy with a fragment of DNA (L_1/L_2) and the targeting moiety FSH_{β}, *via* EDC/NHS reaction. Wang *et al.* developed lanthanide-based downconversion nanoparticles (DCNPs) which exhibit attractive optical properties, and a penetration depth (8 mm) almost three times higher than indocyanine green (ICG) and superior signal-to-background ratio.[180] Indeed, DCNPs made up of rare-hearth (RE) NIR-II emitting elements, are species excited by photons with a short wavelength emitting a longer wavelength photon. Compared to organic fluorophores, DCNPs have a larger stroke shift and a narrower emission band.[20,181] The nanoplatforms of DCNPs-$L_{1/2}$-FSH_{β} have been produced by the successive layer-by-layer (SILAR) method presenting a core@shell structure. The hexagonal host matrix consisting of alkaline lanthanide tetrafluoride ($NaGdF_4$) has been doped at 5% with trivalent Nd^{3+} ions. The 5 nm size luminescent DCNPs core ($NaGdF_4$:5% Nd^{3+}) has been coated with a 2.5 nm of inert $NaGdF_4$ shell ($NaGdF_4$: 5% Nd@$NaGdF_4$ DCNPs). Thus, once functionalized with the DNA fragment (L_1 or L_2) and the FSH_{β}, nanoprobes reach a size ranging within ~8–17 nm and exhibit as well as the not labeled DCNPs a large Stoke shift of 252 nm (λ_{abs}=808 nm; λ_{em}~1060 nm). Due to labeling with specific and complementary DNA sequences (L_1 and L_2), the two modified DCNPs act as building blocks and can assemble *in vivo* in organized superstructures sized between ~100–500 nm that have shown *in vitro* high photostability and low cytotoxicity. The self-assembly nanoprobes have been evaluated *in vivo* in a subcutaneous murine model of human ovarian adenocarcinoma (CaOV3). Using a two-staged in-sequence injection strategy, enhanced nanoprobe tumor retention attended by rapid and efficient body clearance has been obtained, which led to the highest tumor-to-background ratio (TBR) values. At first, mice are IV administered with 7.5 mg/kg of the DCNPs-L_1-FSH_{β}, and following 8 hours the same dosage of the second complementary nanoprobe (DCNPs-L_2-FSH_{β}) is injected. With an 8 hours interval time between the first and second administration, the in-blood assembly of the two complementary nanoprobes is prevented, resulting in a hematic half-life of 2 hours after the second injection. Significantly increased 20 hours after the first injection, the TBR value (~12.5) stays stably high up to 28 hours later, providing an optimal surgical time window of 6 hours. The fluorescent imaging agent has afforded accurate tumor margin identification in mice subcutaneous models of metastatic ovarian adenocarcinoma ($CaVO_3$), as confirmed by magnetic resonance imaging (MRI). The accurate discrimination between malignant and normal tissue types allows for avoiding incomplete resections which may lead to relapse or unnecessary healthy tissue removal. Under the guidance of fluorescent signals of DCNPs-$L_{1/2}$-FSH_{β}, tumor lesions sized up to ≤1 mm have been detected with high sensitivity, and successfully removed. According to post-operative immunohistochemical analyses, all resected fluorescent lesions proved to be malignant. Finally, the

NIR-II emitting imaging nano-agent that employs an *in vivo* self-assembly strategy has demonstrated great potential as a tracer for intraoperative ovarian cancer-specific NIR-II fluorescence imaging, providing solid bases for the design of nanomaterials for medical applications.[180]

DSNPs@FSHP

Wang *et al*. have fabricated NIR-II fluorescent lanthanide-based down-shifting nanoparticles (DSNPs) for FHSR-targeted fluorescence imaging-guided surgery of ovarian cancer.[182] Employing the successive layer-by-lay method (SILAR), an oleic acid-capped host matrix consisting of alkaline lanthanide tetrafluoride ($NaGdF_4$) has been doped at 5% with trivalent Nd^{3+} ion, obtaining ultrasmall core of ~5.0 ($NaGdF_4$:5% Nd^{3+}), which in turn has been coated with an inert NaGdF4 shell ($NaGdF_4$: 5% Nd@$NaGdF_4$ DCNPs), reaching a size of approximately 8 nm. For bio-application, the hydrophobic oleic-acid-anchored DSNPs have been transferred to a hydrophilic state by adding amino phospholipids through the Van der Waals interaction of phosphate groups and lanthanide ions.[183] Lastly, the targeting peptide (a follicle-stimulating hormone peptide, FSHP) has been conjugated onto the surface of DSNPs (3 molecules of FSHP per particle), which reaches an average size of 12.6 nm and emits, with a higher quantum yield, at 1060 nm under 808 nm laser irradiation. After confirming the non-toxicity *in vitro* of DSNPs@FSHP (kit-8 assay), the FSHR-targeting ability has been evaluated *in vitro* on high FSHR-expressing ovarian cancer cell lines (CaOV3 cells). Differently from un-functionalized nanoprobes, DSNPs@FSHP have been able to efficiently enter inside the cells via endocytosis, and the nanoprobe internalization was consistent with the level of FSHR-expression of cells. DSNPs@FSHP have *in vivo* proved to specifically detect the subcutaneous tumor implants of murine models of ovarian cancer, showing the maximum accumulation after 12 h from IV injection (5 mg/kg). The nanoprobes undergo rapid hepatic and renal clearance, with a blood half-life of approximately 2.5 hours. According to *ex vivo* TEM analyses, the tumor lesions excised at 12 h post-injection revealed a nanoprobes heterogeneous distribution inside the malignant tissues, which, in addition, have shown a high targeting capability, in comparison with the unfunctionalized nanoprobes, used as a control. According to pathological analysis, the targeted nanoprobes have succeeded in clearly delineating the boundary between healthy and malignant tissues, and, once again, their accumulation showed consistency with FSHR level in tumor lesions. Moreover, DSNPs@FSHP have allowed a complete resection of tumor lesions in intraperitoneal murine models of metastatic ovarian cancer, detecting with a high TBR (~ 8.0) different-sized metastases diffused in the abdomen, that were invisible under the white light but appeared delineated by the NIR-II-fluorescence-emitting nanoprobes, under 808 nm laser irradiation. The significant outcomes obtained by DSNPs@FSHP proved the high potential of the nanoprobes in allowing the highly sensitive detection of both primary lesions and microscopic residual tumors and the subsequent complete surgical resection, which may help to reduce recurrence rates in ovarian cancer.[182]

3.11 Gonadotropin-releasing hormone receptor (GnRHR)

Gonadotropin-releasing hormone receptor (GnRHR) belongs to the G-protein-coupled receptors family, and it is primarily located in the anterior pituitary. Binding with GnRH triggers a conformation change, that activates intracellular pathways leading to the modulation of genes within a target cell, through phosphorylation events.[184] GnRH primarily acts on the pituitary gland, as the primary mediator of the hypothalamic-pituitary-gonadal axis, inducing the secretion of luteinizing hormone (LH) and follicle-stimulating hormone (FSH). In the past two decades, several studies have reported high and extra-pituitary expression of GnRHR in reproductive system tumors, including ovarian cancer.[185] Liu *et al.* have recently evaluated the potential of GnRHR as a reliable target for the imaging detection of human ovarian cancer. Based on an analysis of the cancer genome atlas (TCGA) datasets, the GnRHR mRNA expression has been found in 89.5% of 373 samples of serous ovarian cancer. According to an analysis of the genotype-tissue expression (GTEx) database, GnRHR expression among healthy tissues, the higher expression of GnRHR mRNA is primarily observed in ovaries, in comparison with other tissues in the abdominal and pelvic cavities. Furthermore, an immunohistochemical (IHC) analysis of 56 high-grade serous ovarian cancer tissue samples revealed that expression of GnRHR in 95% of samples was moderate in 10 cases (18%), and high in 43 cases (77%). Thus, these results suggest GnRHR may represent a good candidate as a target for targeted ovarian cancer imaging.[186]

GnRHa-ICG

Liu *et al.* have developed a fluorescent agent for *in vivo* GnRHR-targeted detection of ovarian cancer, constituted of a widely used GnRHR antagonist, GnRHa,[187] which presents in its structure several amino acid residues modified in comparison to the natural hypothalamic hormone (D-2-Nal-D-4-Cl-Phe-D-3-Pal-Ser-Tyr-D-Cit-Leu-Arg-Pro-D-Ala-NH_2). The peptide antagonist has been conjugated to indocyanine green (ICG), the first NIR fluorophore that received FDA approval for clinical application for angiography and lymphography. The conjugate obtained, GnRHa-ICG (Figure 25), exhibits an excitation wavelength of 795 nm and emitted light at 810 nm.

Figure 25.

GnRHa-ICG has shown *in vitro* high and specific capability to detect the target. Ovarian cancer cell lines characterized by different levels of GnRHR expression have been incubated with GnRHa-ICG at a concentration of 20 µmol/L, and a strong difference in fluorescence intensity has been observed. Detected by fluorescence microscopy, fluorescent signals were respectively 1.56- and 1.34-fold higher in GnRHR-positive cell lines (A2780 and OSE cells) than in GnRHR-negative cells (H1299 cells). Moreover, incubation with the simultaneous presence of unlabeled GnRHa and the contrast agent has induced a partial decrease in fluorescence intensity, confirming a specific interaction occurs between GnRHa-ICG and the target. Showing no cytotoxicity *in vitro* on GnRHR-positive A2780 cells, GnRHa-ICG has been evaluated *in vivo*, on intraperitoneal mice model of metastatic ovarian cancer (A2780 cells). After 2 hours from IP injection, GnRHa-ICG (1.5 mg/kg) specifically accumulates in peritoneal tumors. *Ex vivo* analyses of tumors and organs, excised at different time points after injection, revealed that GnRHa-ICG reached the maximum in contrast between 2 and 24 hours post-injection. In particular, the highest TBR value (approximately 8) has been obtained 24 hours post-administration, considering a healthy muscle as a background. Instead, considering the intestine as a background, the highest TBR (more than 4) has been registered after 2 hours. GnRHa-ICG allowed the detection of tiny tumor nodules (approximately 1mm) implanted on the mesentery, despite this latter exhibiting a weak fluorescence. TBR values remained stable from 2 to 24 hours post-injection, providing a time window feasible for clinical applications in cytoreductive surgery. Pathology confirmed the GnRHR overexpression of the tissues tracked by the contrast agent, which showed high efficiency and specificity in ovarian cancer detection. Blood panel hematology values, and histopathological analyses of excised organs, confirmed that GnRHR-ICG did not present *in vivo* significant side effects. Despite this, tumorigenic or endocrine potential effects of GnRHa-ICG must be investigated. Furthermore, the investigation must be conducted because the metabolic pathways of GnRHa-ICG are unclear, and its specificity and sensitivity should be more accurately determined.[186]

3.12 Lectin Receptors

Lectins are proteins that specifically bind to carbohydrate groups on glycolipids and glycoproteins, such as avidin and galactosylated protein.[188-191] β-D-galactose receptors are expressed on the cell surface of a wide variety of cancers, including ovarian cancer, which can spread in peritoneal space.[192] As a result, the β-D-galactose receptor has been considered a suitable target for the design of imaging and therapeutic specifically targeted probes.

*h*GSA-NMP1

Vinita *et al.* have developed an *in vivo* activatable NIR-fluorescent probe for targeted ovarian cancer intraoperative detection. The probe consists of a molecule of galactosyl human serum albumin (hGSA) conjugated with the synthetic dye NMP1 (in a ratio of hGSA: NMP1 of 1:1.8±0.3.).[193] Structurally constituted by a bacteriochlorin-core (tetrahydroporphyrin) functionalized with two phenylethynyl substituents (Figure 26), NMP1 exhibits two absorption peaks in the green region (λ_1=550 nm), and in the NIR region (λ_2=750 nm), and a single emission peak at λ=780 nm. The dual-band absorption profile of NMP1 allows the detection of both on-surface tumor nodules, via green excitation, and the deeper (below the surface) lesions by NIR excitation.[194-195]

Figure 26.

The targeting moiety of the probe constituted by hGSA has been obtained through a direct amidation reaction with human serum albumin and β-galactosamine. hGSA avidly binds to the receptor of β-D galactose (a lectin), highly expressed on the surface of ovarian cancer cells, permitting the internalization of the probe.[196-197] Once inside the tumor cell, hGSA-NMP1-probe undergoes dissociation in the two components by lysosomal proteases, and the probe fluorescence is turned on.[198-199] hGSA-NMP1 shows *in vitro* high quenching capabilities (>50) measured by adding 1% sodium dodecyl sulfate (SDS), an anionic detergent used for protein denaturation. Ovarian cancer cells (SHIN3 cells), incubated with 1 µg/mL of hGSA-NMP, have shown clustering of signal in the cytoplasm only after 3 hours, suggesting probe lysosomal accumulation. Moreover, the incubation with an excess of free-hGSA clearly showed to block binding between hGSA-NMP1 and the target, confirming that a specific interaction occurs. The hGSA-NMP1 feasibility *in vivo* was assessed in xenograft (intraperitoneal) murine models of ovarian cancer (SHIN3 cells), IP injected with 25 µg of the probe, and monitored by *in situ* spectral fluorescence imaging. Through fluorescence imaging, in small bowel mesentery, the first peritoneal metastases were already detectable following 1.5 hours of the injection. 3 hours post-injection, the fluorescence emitted by hGSA-NMP1 in tumors showed a great increase in intensity. Indeed, the mean TBR values of hGSA-NMP1, measured considering the tumor-adjacent intestine or mesenteric membrane as background, obtained using both green and NIR excitation lights went from 3.17 ± 2.02 and 2.95 ± 1.46 following 1.5 hours from the injection, to 22.21 ± 10.24 and 13.32 ± 8.27, 3 hours after the injection. Similar to TBR, two different values have been determined for the sensitivity and specificity of hGSA-NMP1, using excitation lights at the two absorption wavelengths of the probe, green (λ_1=550 nm) and NIR (λ_2=750 nm). While NIR images have shown hGSA-NMP1 to detect peritoneal lesions ≥0.8 mm with a sensitivity of 74.5% and a specificity of 92%, green images demonstrated that under green-light excitation, hGSA-NMP1 exhibits a sensitivity and specificity of 91% and 92%, respectively, in detecting ≥ 0.8 mm diffused metastases. Moreover, in addition to the high sensitivity and specificity exhibited, the dosage of hGSA-NMP1 required for fluorescence imaging-guided detection of ovarian cancer has been greatly low, considering that 25 µg of the probe contains less than 1µg of NMP1, for which the adult estimated dose is approximately 3 mg. Potentially, this results in lower toxicity of the agent. In conclusion, the evaluation in animal models suggests that hGSA-NMP1 could be a useful tool in the detection of peritoneal ovarian cancer lesions. Indeed, with low toxicity risk, hGSA-NMP1 has been shown to enable sensitive and specific detection of tumor metastases located both at the surface and at a depth in the abdominal cavity.[193]

4. Extracellular targets

4.1 Cluster of Differentiation 24 (CD24)

CD24 (cluster of differentiation 24) is a small, glycosylated molecule belonging to the CD protein family. CDs are surface antigens physiologically expressed in different types of cells, including premature lymphocytes (pre-B-cells), granulocytes (neutrophils), some epithelial (e.g., keratinocytes), neural, and pancreatic cells. Although CDs are mainly known as signaling molecules for intercellular communication, most CD proteins have other cellular functions (e.g., cell adhesion). CD24 is anchored to the cell surface by glycosylphosphatidylinositol (GPI). The overexpression of a membranous and cytoplasmatic isoform of CD24 has been observed in many cancer types, especially in solid tumors (68%), such as ovarian cancer, breast cancer, lung carcinoma, nasopharyngeal carcinoma, hepatocellular carcinoma, bladder carcinoma, and glioma. The presence of CD24 in cancer cells is associated with proliferation, growth, invasion, metastasis formation, and apoptosis inhibition. To date, the exact molecular mechanisms of CD24 in cancer cells have not been completely elucidated yet. However, its low physiologic expression in healthy tissues together with its overexpression in cancer cells makes CD24 a specific tumor biomarker with a wide clinical applicability. Several studies have identified CD24 as an ovarian cancer-specific biomarker. While the cytoplasmatic (59%) and membranous (84%) CD24 expression were observed in ovarian cancer by using immunohistochemistry (IHC), no expression was found in healthy ovarian tissue. Furthermore, a strong and independent correlation of a poor prognosis with cytoplasmatic overexpression of CD24 in ovarian cancer has been demonstrated. Indeed, the heterogeneous expression of CD24 has been observed in orthotopic and patient-derivate xenograft models of high-grade serous ovarian cancer (HGSOC), validating CD24 as an ovarian cancer biomarker, then used for both targeted therapy and nuclear imaging radiotracers development.[200-202]

CD24-AF680

In CD24-AF680, a near-infrared dye AlexaFluor 680 (Figure 27) has been conjugated to a mouse-derived monoclonal antibody against human CD24. The spectroscopic characteristics (λ_{abs}=678 nm; λ_{em}=706 nm) of the resulting contrast agent follow the detector range of most optical imaging systems. With no toxic effects on cellular proliferation and viability, this NIR probe has been pre-clinically evaluated in orthotopic and subcutaneous xenograft models of ovarian cancer. After 24 h from the injection (2 µg/g body weight) in the orthotopic xenograft models, the monoclonal antibody labelled with AF680 showed the highest fluorescence signal intensity, also with optimal TBR. CD24-AF680 was found to be an early-stage primary tumor-specific in xenograft mice; the probe can also identify disseminated metastasis in the high-grade serous ovarian cancer xenograft models. The specificity of

CD24-AF680 was evaluated with *ex vivo* imaging of tumor tissue. The CD24 grade of expression in the samples was confirmed with immunohistochemical (IHC) staining of the tumor implants. CD24-AF680 is an excellent candidate for a non-invasive fluorescence imaging contrast agent. Furthermore, CD24-AF680 has allowed the longitudinal *in vivo* visualization of the tumor progression and the pharmacological-treatment efficacy through the fluorescence imaging (FLI) approach in orthotopic humanized high-grade serous ovarian cancer mice, and patient-derived xenografts (PDX) models, even with low CD24 expression. Moreover, 24 hours after injection, CD24-AF680 allowed a real-time intraoperative detection of both primary tumor and metastatic lesions in both orthotopic and PXD xenograft models. Unfortunately, an autofluorescence signal at 700 nm wavelength range from gastrointestinal organs was detected, which could affect the procedure of intraoperative imaging.[203]
Figure 27.

CD24-AF750

In CD24-AF750, the mouse-derivate monoclonal antibody (mAb) against human CD24 has been conjugated to the NIR dye Alexa Fluor 750 (Figure 28).

Figure 28.

Indeed, the emission spectra of AF680, the dye previously employed, overlap autofluorescence signals emitted from the gastrointestinal tract cells. The fluorescence properties (λ_{abs}=753 ± 3 nm, λ_{em}=778 ± 2 nm) of the resulting labelled mAb allow its use in fluorescence-guided surgery. The fluorescent probe has no toxic effect on cellular proliferation even at increasing concentrations. CD24-AF750 has validated the CD24 heterogenous expression in epithelial ovarian cancer cell lines and patient-derived tumors. Furthermore, the probe revealed a significantly more elevated mean fluorescence intensity (MFI) than CD24-IRDye 800CW, the monoclonal antibody labelled with IRDye 800CW maleimide (λ_{abs}=774 nm, λ_{em}=789 nm in PBS, Figure 12). In ovarian cancer, orthotopic xenograft models, CD24-AF750 (3 μg/g of mouse body weight) was identified 48 hours after injection lesions with the highest MFI and TBR. However, this probe has a long circulation time and can detect the tumor up to 120 hours after administration. Finally, CD24-AF750 has been pre-clinically evaluated as a fluorescence imaging-guided surgery tracer in orthotopic high-grade serous ovarian cancer (HGSOC) models, showing more significant results than white light surgery. CD24-AF750 allowed both the identification and resection of a higher number of tumor lesions than white light surgery, which improve the cytoreduction phase. Furthermore, also in PXD models the probe has identified the primary tumor and small and disseminated metastatic lesions, 48 hours after the injection of 3μg/g of CD24-AF750, validating its potential clinical application in fluorescence imaging-guided surgery (Image 4).[204]

Image 4.

4.2 Matrix Metalloproteinase-3 (MMP-3)

Matrix metalloproteinases (MMPs) are a family of zinc-dependent extracellular endopeptidases,[205] involved in a variety of physiological processes such as tissue remodeling, organ development,[206] and the modulation of inflammatory syndrome.[207] In cancer, extracellular proteolytic process alteration is usually associated with an increase in the metastatic dissociation of tumor cells from the primary foci, consequently leading to local tissue invasion, angiogenesis, and blood or lymphatic system invasion.[208-209] It is known that among extracellular proteinases, MMPs represent the family primarily associated with tumorigenesis, mediating the majority of the changes occurring in the microenvironment during tumor progression, especially the destruction of extracellular matrix (ECM) and nonmatrix components.[210] In particular, MMP-3, -7, and -9 were found to be closely related to the promotion of metastasis.[211-214] Also known as stromelysin-1, MMP-3 is overexpressed in several tumor types, and despite being conducted numerous investigations on MMPs involvement in ovarian cancer, few are specifically focused on the MMP-3 role. Results reported by Sun *et al.* show a correlation between overexpression of MMP-3 and enhanced ovarian cancer invasiveness and metastasis.138 Indeed, as in other cancers, the ovarian cancer stroma expresses a multitude of molecules and macromolecules crucial for tumor progression, including MMP-3, such that, not infrequently, the mere presence of certain stromal components was reported to be related to poor survival in the advanced stage of the disease.[215-216] Wang *et al.* demonstrated that, while SKOV3 cells express minimal levels of MMP-3 when cultured alone, the MMP-3 expression of SKOV-3 cells shows a significant increase in the cocultures with fibroblast cell lines (WS1 cells), established to mimic the interaction of ovarian cancer cell with stromal cells.[217] However, further studies are required to confirm the activity of MMP-3 in ovarian cancer and its diagnostic and prognostic significance.

MMP-3-sensitive probe

Wang *et al.* have designed and characterized a fluorescent MMP-3-sensitive probe, connecting the NIR fluorophore Cy5.5 to the amino terminus of an MMP-3-specific peptide substrate (Figure 29).

Figure 29.

MMP-3-sensitive probe specifically detects the active MMP-3 enzyme, not only in cell cultures (co-cultivations of SKOV-3 and WS1 cell lines) but also *in vivo* in subcutaneous tumor-bearing mice models (SKOV-3 cells). Optical imaging has been performed at 610 – 650 nm excitation and 670 – 700 nm emission. IV injected (200 μL of 2nM) in mice, the fluorescence imaging has been performed on euthanized animals 2 hours post-injection, at days 3, 5, 7, and 11 after tumor implantation. The highest fluorescence intensity in tumor has been observed on day 5, decreasing in the following days, while on day 3 fluorescence detected was 4-fold lower than on day 5. This trend suggests that MMP-3 may have a “hit-and-run” role during early-stage tumor growth. Compared to control tissues (normal subcutaneous tissue adjacent to the tumor), NIR fluorescence observed in the tumors was significantly higher. Moreover, it is noteworthy the fact that the MMP-3-sensitive probe detects the target presence at the boundary of the tumor mass and the surrounding connective tissue, data confirmed by immunostaining (MMP-3 antibody) of tumors excised.[217] This finding is consistent with another study reporting that fibroblasts, endothelial cells, and immunocytes express MMP-3 exclusively in the tumor stroma.[218] Nevertheless, additional studies are necessary to validate the specificity of the probe in animal models which better reflect the complexities of ovarian cancer (intraperitoneal models) and to elucidate the role played by MMP-3 in early-stage ovarian cancer.[217]

4.3 Secreted Protein Acidic and Rich in Cysteine (SPARC)

Secreted protein acidic and rich in cysteine (SPARC) is a calcium-binding matricellular glycoprotein that mainly modulates interactions between cell and extracellular matrix, while not participating in the structural scaffold of the extracellular matrix.[219-220] Several studies have found SPARC overexpressed in cells and stroma of several tumors, demonstrating its contribution to the development and progression of a variety of tumors,[221] including ovarian cancer.[222-223] At the same time, some data demonstrated the opposite.[224] Chen *et al.* have demonstrated a strong correlation between the overexpression of SPARC and high-stage, low differentiation, lymph node metastasis, and poor prognosis in ovarian cancer.[219] On the contrary, in a more recent study, Peng *et al.* have suggested SPARC might inhibit angiogenesis and lymph-angiogenesis in ovarian cancer, by reducing the expression of vascular endothelial growth factors (VEGF)-C and (VEGF)-D, which favor the metastatic involvement of lymph nodes, promoting tumor lymphatic vessel growth.[225] Thus, the role of SPARC in ovarian cancer needs to be further investigated.

Single-walled carbon nanotubes (SWNT) probe

Ceppi *et al.* have developed a NIR-II fluorescent SWNTs-based nano-probe for real-time image-guided ovarian cancer-targeted surgery. The probe consists of the cylindrical non-lytic-M13-bacteriophage, characterized by a length of 880 nm and a diameter of ~ 5-6 nm, which acts as a carrier. The filamentous bacteriophage presents engineered coating-proteins, one of which (p3) mediates specific binding with SPARC, ovarian cancer over-expressed matricellular protein (targeting moiety). Instead, the other M13-coating protein, which represents the primary component, forms a multivalent SWNT (contrast moiety), the 500 nm long carbon nanotube with a diameter of 1 nm, endowed with intrinsic NIR-II fluorescence (900-1,400 nm range). When compared to other organic dyes, SWNTs exhibit more attractive features, such as a larger Stoke shift and a higher absorbance in the NIR I spectrum. The SWTNs probe feasibility has been *in vivo* evaluated in orthotopic mice models of ovarian cancer (A2780 cells). 24 Hours before the fluorescence-guided surgery, mice were IP injected with the fluorescent nanoprobe at 20-30 µg/ml concentration in 400 µl of 1× PBS. Based on the post-operative analyses performed on excised tissues, the nano tracer has shown a sensitivity of 97.2%, which corresponds to the percentage of the total of fluorescent tissues excised that were revealed to be malignant at biopsy (true positives). Instead, the SWNTs specificity has been assessed at 70.9%, due to the number of excised fluorescent tissues and negative for the biopsy (false positives, 29.1% of the total). Importantly, SWNTs have exhibited a high resolution, allowing the detection of sub-millimeter lesions, having an average size of 1.36 ± 1.01 mm (Image 5).[226]

Image 5.

According to *ex vivo* analyses, 93.5% of the malignant tissues tracked by SWNTs highly express SPARC, showing evidence of the effective *in vivo* targeting performed. Since SPARC not having been detected in 10 of the 16 false positive tissues analyzed, SWNTs-based nanoprobe presents a little non-specific binding. On the contrary, the presence of 6 target-expressing lesions, on a total of 16 false positives, indicates that SPARC is expressed also in other tissues, despite at a low level.[226] Indeed, a previous study reported that SPARC is expressed in fibroblasts and adipocytes.[227] In the SWNTs *in vivo* evaluation, the nano tracer has identified an ectopic expression of SPARC in pancreatic stromal structures and pericolic fat tissues. Summarily, the fluorescent imaging nano-agent developed allows accurate ovarian cancer detection and subsequent surgical resection, despite some limitations in the targeting effectiveness.[226]

4.4 Tumor-associated macrophages (TAMs)

Being the major component of the leukocyte infiltrate inside the stroma of several solid tumors, in some cases, tumor-associated macrophages (TAMs) represent up to 50% of the tumor mass and play a key role in tumor development.[228-229] These innate immunity cells constitute the mononuclear phagocyte system, and they are involved in defense mechanisms, tissue development, and maintenance of homeostasis. Macrophages have primarily phagocytic and bactericidal activity, but they can also produce inflammatory cytokines fundamental in adaptive immune responses. Depending on signals received from the microenvironment, macrophages can exhibit a wide spectrum of activation states, that range from classical activation (M_1 macrophages) to alternative activation (M_2 macrophages). While M1 macrophages inhibit cell proliferation and induce tissue damage, M_2 macrophages promote cell proliferation and tissue repair.[230-231] Despite previous studies reporting that macrophages can exert both anti- and pro-tumoral functions, high TAMs content is mostly associated with a poor prognosis, at least in 80% of tumors.[232-233] Indeed, TAMs possess tumor-supportive properties, making the tumor microenvironment immunosuppressive, and they support metastasis development, promoting neo-angiogenesis and tumor-spheroids formation *via* detached-cancer-cells dissemination.[232,234-236] Robinson-Smith *et al.* reported intraperitoneal inflammation enhances the risk for peritoneal metastasis dissemination in ovarian cancer. Indeed, the depletion of peritoneal macrophages, but not neutrophils and natural killer cells, has reduced the chance of peritoneal metastasis.[237] Yin *et al.* demonstrated the correlation between TAMs and intraperitoneal metastasis, in an intraperitoneal murine model of ovarian cancer (SKOV-3 cells). Localized in the center of spheroids, TAMs M_2 macrophage-like secrete EGF, which upregulates integrin $\alpha_M\beta_2$ on TAMs and ICAM-1 on tumor cells, promoting association between tumor cells and TAMs. Moreover, the activation of EGFR by EGR on tumor cells, in turn, up-regulates the VEGF/VEGFR signalling pathway which supports tumor cell proliferation and migration, in the surrounding environment.[238]

Fluorescent SiNPs

Haber *et al.* have synthesized fluorophore-loaded silica nanoparticles (SiNPs) for *in vivo* ovarian cancer tumor-targeted detection. The tumor-targeting capability of SiNPs depends upon the used route of administration, and NPs size and charge. The anionic SiNPs capable of targeting ovarian cancer cells exhibit a hydroxyl surface and include a red fluorescent dye (structure not available). The tumors were imaged at an excitation of 570 nm and an emission of 610 nm. In addition, for high and specific tumor accumulation, the nanoparticles must have an average size of 500 nm and be administered by IP injection. In intraperitoneal murine models of metastatic (stage III) ovarian cancer (human OVCAR8.EGFP cell line), SiNPs (1 mg NPs/mL) have selectively detected ovarian cancer metastases, after 4 days of IP injection, accumulating on tumor surfaces but not on healthy ones. The red fluorescent silica NPs have shown a high sensitivity, tracking even sub-millimeter metastases (0.5 mm). Confocal images of the excised and dissected animal tissues, which included both the malignant lesions and surrounding the healthy tissue, have revealed that SiNPs identified 94% of malignant tissues, and only 3% of labelled tissues were healthy. The specific tumor localization of SiNPs requires several days. The nanoparticles likely circulate in the intraperitoneal cavity and slowly accumulate on the tumor surfaces, according to confocal microscopy at high magnification images. Flow cytometry analyses have shown that 72% of SiNPs-containing cells were positive for the TAMs markers CD45, CD11b, and F4/80. More specifically, 87 % of the total TAMs population includes the SiNPs, and only 2.1% of silica nanoparticles entered inside the cancer cells. The high SiNPs-uptake by TAMs has been observed in freshly excised patients-derived samples obtained as well. Similarly, to that observed in animal models, the highest SiNPs accumulation in tumors has been achieved on day 4 post-injection, even if a strong signal is still present on day 7, and no accumulation has been observed in healthy tissues. Although the use of SiNPs demonstrated significant advantages in the selective and sensitive *in vivo* detection of ovarian cancer, red fluorescent particles are not ideal for surgery application, since they emit in the visible spectrum, and their fluorescence is not easily distinguishable from blood and tissue.[239]

Silica-coated up-converting nanoparticles (UCNPs)

Marotta *et al.* have developed silica-coated UCNPs (Yb-Ho-SiO_2-2) for *in vivo* ovarian cancer detection, combining the high TAMs-targeting ability of SiNPs and the advantageous spectroscopic properties of the up-converting inorganic nanoparticles.[240] Excited by multiple photons, with a longer wavelength (NIR), UCNPs can emit a single, high-energy photon, with a shorter wavelength (UV-Vis).[20] Indeed, despite the inorganic nanoparticles' toxicity profile needing further investigations, UCNPs offer the possibility of using a low-energy and less invasive light source, reducing irradiation patient exposure. These inorganic nano-tracers consist of three primary components: a sensitizer (Yb^{3+}) which absorbs the light energy, an emitter (Ho^{3+}), and a hexagonal host matrix ($NaYF_4$). Specifically, UCNPs have been synthesized by increasing the lanthanoid core sequentially by adding layers of varying compositions until obtaining a specific multilayer core@shell structure of $NaY{:}Yb{:}Ho(10{:}89{:}1)F_4@NaYb{:}Y(9{:}1)F_4@NaNd{:}Y(9{:}1)F_4$. Lastly, to increase their biocompatibility and targeting capability, the lanthanoid-based UCNPs were coated with silica (Yb-Ho-SiO_2-2), using the reverse micro-emulsion process, reaching a size over 150 nm. With an absorption in the NIR window (λ_{abs}=980 nm), Yb-Ho-SiO_2-2 exhibits a strong green fluorescence emission (λ_{em}=545 nm). Evaluated *in vivo* on intraperitoneally xenografted mice model of ovarian cancer (OVCAR8-GFP cells), silica-coated UCNPs proved to selectively detect tumor lesions, sparing non-cancerous tissues, following 4 days from the IP injection (1.37×10^{10} NPs in 1 mL PBS). According to fluorescence imaging analyses of organs and tumor lesions excised from the animal models, the inorganic fluorescent nano-traces highlight cancerous tissues with a very high contrast value. Measured as the maximum pixel count of the tumor (or non-malignant tissue) divided by the average mean pixel count of the background, the average value of TBRs for malignant tissues was found to be 397, whereas the mean of TBRs values measured for healthy tissues was 4. Moreover, compared to a surgical resection guided by naked-eye visual inspection, the UCNPs-guided detection allowed to reduce the residual tumor mass after surgery to 0.2%, against the ~10.7% that remained after visual-guided surgical removal. Additional guided-surgical investigations and analysis to confirm TAMs as the primary target, further research, and in-depth analysis to strengthen the use of UCNPs as a potential contrast agent for targeted ovarian cancer imaging is needed.[240]

Table 1.

5. Conclusion and final remarks

Complete resection of all visible diseases (R0 resection) is critical for the treatment of ovarian cancer patients, and accurate real-time guidance provided by intraoperative near-infrared (NIR) fluorescence images is beneficial for achieving complete resection of all visible diseases. Several fluorescent probes have been developed. Noteworthy is Cytalux, the first targeted imaging agent, approved by the FDA last year, designed to "highlight" ovarian and lung cancer in the body, helping surgeons to see it in real-time, as they operate. Cytalux is a pafolacyanine ligand of Folate receptor alpha. However, adverse reactions including nausea, vomiting, abdominal pain, flushing, allergic reaction, elevation in blood pressure, indigestion, and chest discomfort were reported during the administration of Cytalux. Consequently, more probes must be identified with a better safety profile. The targeting unit (antibody, nanobody, small molecules etc) as well as the fluorophore selected to build a fluorescent probe affect the liability of the final compounds, consequently it is not yet possible to identify a general rule. Thus, the main aim of this review is the describe a selection of fluorescent probes that are classified based on their biological target. Details about their mechanism of action are also reported.

Declarations

Conflit of Interest. The authors declare that they have no competing interests.

Compliance with Ethics Guidelines. This article is based on previously conducted studies and does not contain any new studies with human participants or animals performed by any of the authors.

Data availability. Data sharing is not applicable for this article, as no datasets were generated or analyzed during the current study.

Authorship. All named authors meet the international criteria for authorship for this article, take responsibility for the integrity of the work, and have given their approval for this version to be published.

ACKNOWLWDGEMENT

This work was funded by (a) the Ministry of Economic Development (MISE) funded project "GENESI" code 092-Prog n. F/180003/03/X43 for the development of innovative radiopharmaceuticals and biomarkers for the diagnosis of cancers of the male and female reproductive system (2021–2023); and (b) First AIRC-MFAG2015 Grant (Project Id. 17566).

References

1. Perrone MG, Luisi O, De Grassi A, Ferorelli S, Cormio G, Scilimati A. Translational Theragnosis of Ovarian Cancer: where do we stand? *Curr Med Chem*. 2020;27(34):5675-5715.
2. Scarberry KE, Dickerson EB, Zhang ZJ, Benigno BB, McDonald JF. Selective removal of ovarian cancer cells from human ascites fluid using magnetic nanoparticles. *Nanomedicine*. 2010;6(3):399-408.
3. Zalfa F, Perrone MG, Ferorelli S, et al. Genome-Wide Identification and Validation of Gene Expression Biomarkers in the Diagnosis of Ovarian Serous Cystadenocarcinoma. *Cancers (Basel)*. 2022;14(15):3764.
4. Buys SS, Partridge E, Black A, et al. Effect of screening on ovarian cancer mortality: the Prostate, Lung, Colorectal and Ovarian (PLCO) Cancer Screening Randomized Controlled Trial. *JAMA*. 2011;305(22):2295-2303.
5. Ozols RF, Bundy BN, Greer BE, et al. Phase III trial of carboplatin and paclitaxel compared with cisplatin and paclitaxel in patients with optimally resected stage III ovarian cancer: a Gynecologic Oncology Group study. *J Clin Oncol*. 2003;21(17):3194-3200.
6. Bast RC Jr, Hennessy B, Mills GB. The biology of ovarian cancer: new opportunities for translation. Nat Rev Cancer. 2009;9(6):415-428.
7. Zhang S, Balch C, Chan MW, et al. Identification and characterization of ovarian cancer-initiating cells from primary human tumors. *Cancer Res*. 2008;68(11):4311-4320.

8. Desfeux P, Camatte S, Chatellier G, Blanc B, Querleu D, Lécuru F. Impact of surgical approach on the management of macroscopic early ovarian borderline tumors. *Gynecol Oncol*. 2005;98(3):390-395.
9. Lécuru F, Desfeux P, Camatte S, Bissery A, Blanc B, Querleu D. Impact of initial surgical access on staging and survival of patients with stage I ovarian cancer. *Int J Gynecol Cancer*. 2006;16(1):87-94.
10. Vahrmeijer AL, Hutteman M, van der Vorst JR, van de Velde CJ, Frangioni JV. Image-guided cancer surgery using near-infrared fluorescence. *Nat Rev Clin Oncol*. 2013;10(9):507-518.
11. De Ravin E, Venkatesh S, Harmsen S, et al. Indocyanine green fluorescence-guided surgery in head and neck cancer: A systematic review. *Am J Otolaryngol*. 2022;43(5):103570.
12. Corbin IR, Ng KK, Ding L, Jurisicova A, Zheng G. Near-infrared fluorescent imaging of metastatic ovarian cancer using folate receptor-targeted high-density lipoprotein nanocarriers. *Nanomedicine (Lond)*. 2013;8(6):875-890.
13. Kobayashi M, Sawada K, Kimura T. Potential of Integrin Inhibitors for Treating Ovarian Cancer: A Literature Review. *Cancers (Basel)*. 2017;9(7):83.
14. Tan D, Chen KE, Khoo T, Walker AM. Prolactin increases survival and migration of ovarian cancer cells: importance of prolactin receptor type and therapeutic potential of S179D and G129R receptor antagonists. *Cancer Lett*. 2011;310(1):101-108.
15. Bhartiya D, Singh J. FSH-FSHR3-stem cells in ovary surface epithelium: basis for adult ovarian biology, failure, aging, and cancer. *Reproduction*. 2015;149(1):R35-R48.
16. Zhang J, Cheng P, Pu K. Recent Advances of Molecular Optical Probes in Imaging of β-Galactosidase. *Bioconjug Chem*. 2019;30(8):2089-2101.
17. Perrone MG, Malerba P, Uddin J, et al. PET radiotracer [^{18}F]-P6 selectively targeting COX-1 as a novel biomarker in ovarian cancer: preliminary investigation. *Eur J Med Chem*. 2014;80:562-568.
18. Barth CW, Gibbs SL. Fluorescence Image-Guided Surgery - a Perspective on Contrast Agent Development. *Proc SPIE Int Soc Opt Eng*. 2020;11222:112220J.
19. Borlan R, Tatar AS, Soritau O, et al. Design of fluorophore-loaded human serum albumin nanoparticles for specific targeting of NIH:OVCAR3 ovarian cancer cells. *Nanotechnology*. 2020;31(31):315102.
20. Loo JF, Chien Y, Yin F, Kong SK, Ho H, Yong K. Upconversion and downconversion nanoparticles for biophotonics and nanomedicine. *Coord Chem Rev.* 2019;400(400):213042.
21. Mochida A, Ogata F, Nagaya T, Choyke PL, Kobayashi H. Activatable fluorescent probes in fluorescence-guided surgery: Practical considerations. *Bioorg Med Chem*. 2018;26(4):925-930.
22. Xu D, Li L, Chu C, Zhang X, Liu G. Advances and perspectives in near-infrared fluorescent organic probes for surgical oncology. *Wiley Interdiscip Rev Nanomed Nanobiotechnol*. 2020;12(5):e1635.
23. Chen Y, Xue L, Zhu Q, Feng Y, Wu M. Recent Advances in Second Near-Infrared Region (NIR-II) Fluorophores and Biomedical Applications. *Front*. 2021;9.
24. Rouzer CA, Marnett LJ. Cyclooxygenases: structural and functional insights. *J Lipid Res*. 2009;50 Suppl(Suppl):S29-S34.
25. Smith WL, Garavito RM, DeWitt DL. Prostaglandin endoperoxide H synthases (cyclooxygenases)-1 and -2. *J Biol Chem*. 1996;271(52):33157-33160.
26. Arend R, Martinez A, Szul T, Birrer MJ. Biomarkers in ovarian cancer: To be or not to be. *Cancer*. 2019;125 Suppl 24:4563-4572.
27. Wilson AJ, Fadare O, Beeghly-Fadiel A, et al. Aberrant over-expression of COX-1 intersects multiple pro-tumorigenic pathways in high-grade serous ovarian cancer. *Oncotarget*. 2015;6(25):21353-21368.
28. Scilimati A, Ferorelli S, Iaselli MC, et al. Targeting COX-1 by mofezolac-based fluorescent probes for ovarian cancer detection. *Eur J Med Chem*. 2019;179:16-25.
29. Perrone MG, Vitale P, Miciaccia M, et al. Fluorochrome Selection for Imaging Intraoperative Ovarian Cancer Probes. *Pharmaceuticals (Basel)*. 2022;15(6):668.
30. Malerba P, Crews BC, Ghebreselasie K, et al. Targeted Detection of Cyclooxygenase-1 in Ovarian Cancer. *ACS Med Chem Lett*. 2019;11(10):1837-1842.
31. Uddin MJ, Crews BC, Blobaum AL, et al. Selective visualization of cyclooxygenase-2 in inflammation and cancer by targeted fluorescent imaging agents. *Cancer Res*. 2010;70(9):3618-3627.

32. Uddin MJ, Crews BC, Ghebreselasie K, Marnett LJ. Design, synthesis, and structure-activity relationship studies of fluorescent inhibitors of cycloxygenase-2 as targeted optical imaging agents. *Bioconjug Chem*. 2013;24(4):712-723.
33. Zhang K, Chen D, Ma K, Wu X, Hao H, Jiang S. NAD(P)H:Quinone Oxidoreductase 1 (NQO1) as a Therapeutic and Diagnostic Target in Cancer. J Med Chem. 2018;61(16):6983-7003.
34. Nioi P, Hayes JD. Contribution of NAD(P)H:quinone oxidoreductase 1 to protection against carcinogenesis, and regulation of its gene by the Nrf2 basic-region leucine zipper and the arylhydrocarbon receptor basic helix-loop-helix transcription factors. Mutat Res. 2004;555(1-2):149-171.
35. Prawan A, Buranrat B, Kukongviriyapan U, Sripa B, Kukongviriyapan V. Inflammatory cytokines suppress NAD(P)H:quinone oxidoreductase-1 and induce oxidative stress in cholangiocarcinoma cells. J Cancer Res Clin Oncol. 2009;135(4):515-522.
36. Kolesar JM, Pritchard SC, Kerr KM, Kim K, Nicolson MC, McLeod H. Evaluation of NQO1 gene expression and variant allele in human NSCLC tumors and matched normal lung tissue. Int J Oncol. 2002;21(5):1119-1124.
37. Cresteil T, Jaiswal AK. High levels of expression of the NAD(P)H:quinone oxidoreductase (NQO1) gene in tumor cells compared to normal cells of the same origin. Biochem Pharmacol. 1991;42(5):1021-1027.
38. Siegel D, Ross D. Immunodetection of NAD(P)H:quinone oxidoreductase 1 (NQO1) in human tissues. Free Radic Biol Med. 2000;29(3-4):246-253.
39. Cui X, Li L, Yan G, et al. High expression of NQO1 is associated with poor prognosis in serous ovarian carcinoma. BMC Cancer. 2015;15:244.
40. Nakamura Y, Shen Z, Harada T, et al. Characteristics of ovarian cancer detection by a near-infrared fluorescent probe activated by human NAD(P)H: quinone oxidoreductase isozyme 1 (hNQO1). Oncotarget. 2017;8(37):61181-61192.
41. Mitsunaga M, Kosaka N, Choyke PL, et al. Fluorescence endoscopic detection of murine colitis-associated colon cancer by topically applied enzymatically rapid-activatable probe. Gut. 2013;62(8):1179-1186.
42. Nakamura Y, Harada T, Nagaya T, et al. Dynamic fluorescent imaging with the activatable probe, γ-glutamyl hydroxymethyl rhodamine green in the detection of peritoneal cancer metastases: Overcoming the problem of dilution when using a sprayable optical probe. Oncotarget. 2016;7(32):51124-51137.
43. Pauli BU, Knudson W. Tumor invasion: a consequence of destructive and compositional matrix alterations. *Hum Pathol*. 1988;19(6):628-639.
44. Asanuma D, Sakabe M, Kamiya M, et al. Sensitive β-galactosidase-targeting fluorescence probe for visualizing small peritoneal metastatic tumours in vivo. *Nat Commun*. 2015;6:6463.
45. Guo W, Hiratake J, Ogawa K, Yamamoto M, Ma SJ, Sakata K. Beta-D-glycosylamidines: potent, selective, and easily accessible 1-glycosidase inhibitors. *Bioorg Med Chem Lett*. 2001;11(4):467-470.
46. Hama Y, Urano Y, Koyama Y, et al. A target cell-specific activatable fluorescence probe for in vivo molecular imaging of cancer based on a self-quenched avidin-rhodamine conjugate. *Cancer Res*. 2007;67(6):2791-2799.
47. Chen JA , Pan H , Wang Z , et al. Imaging of ovarian cancers using enzyme activatable probes with second near-infrared window emission. *Chem Commun (Camb)*. 2020;56(18):2731-2734.
48. Della-Longa S, Arcovito A. Structural and functional insights on folate receptor α (FRα) by homology modeling, ligand docking and molecular dynamics. *J Mol Graph*. 2013;44:197-207.
49. Scaranti M, Cojocaru E, Banerjee S, Banerji U. Exploiting the folate receptor α in oncology. *Nat Rev Clin Oncol*. 2020;17(6):349-359.
50. Cheung A, Bax HJ, Josephs DH, et al. Targeting folate receptor alpha for cancer treatment. *Oncotarget*. 2016;7(32):52553-52574.
51. Chen J, Corbin IR, Li H, Cao W, Glickson JD, Zheng G. Ligand conjugated low-density lipoprotein nanoparticles for enhanced optical cancer imaging in vivo. *J Am Chem Soc*. 2007;129(18):5798-5799.
52. Corbin IR, Chen J, Cao W, Li H, Lund-Katz S, Zheng G. Enhanced Cancer-Targeted Delivery Using Engineered High-Density Lipoprotein-Based Nanocarriers. *J Biomed Nanotechnol*. 2007;3(4):367-376.

53. Lee H, Kim J, Kim H, Kim Y, Choi Y. A folate receptor-specific activatable probe for near-infrared fluorescence imaging of ovarian cancer. *Chem Commun (Camb)*. 2014;50(56):7507-7510.
54. Van Dam GM, Themelis G, Crane LMA, et al. Intraoperative tumor-specific fluorescence imaging in ovarian cancer by folate receptor-α targeting: first in-human results. *Nat Med*. 2011;17(10):1315-1319.
55. Tummers QR, Hoogstins CE, Gaarenstroom KN, et al. Intraoperative imaging of folate receptor alpha positive ovarian and breast cancer using the tumor specific agent EC17. *Oncotarget*. 2016;7(22):32144-32155.
56. ClinicalTrials.gov Identifier: NCT02000778.
57. ClinicalTrials.gov Identifier: NCT01511055.
58. Hekman MCH, Boerman OC, Bos DL, et al. Improved Intraoperative Detection of Ovarian Cancer by Folate Receptor Alpha Targeted Dual-Modality Imaging. *Mol Pharm*. 2017;14(10):3457-3463.
59. Borlan R, Focsan M, Perde-Schrepler M, et al. Antibody-functionalized theranostic protein nanoparticles for the synergistic deep red fluorescence imaging and multimodal therapy of ovarian cancer. *Biomater Sci*. 2021;9(18):6183-6202.
60. Numasawa K, Hanaoka K, Saito N, et al. A Fluorescent Probe for Rapid, High-Contrast Visualization of Folate-Receptor-Expressing Tumors In Vivo. *Angew Chem Int Ed Engl*. 2020;59(15):6015-6020.
61. Lukinavičius G, Umezawa K, Olivier N, et al. A near-infrared fluorophore for live-cell super-resolution microscopy of cellular proteins. *Nat Chem*. 2013;5(2):132-139.
62. Chen C, Ke J, Zhou XE, et al. Structural basis for molecular recognition of folic acid by folate receptors. *Nature*. 2013;500(7463):486-489.
63. Hada AM, Craciun AM, Focsan M, et al. Folic acid functionalized gold nanoclusters for enabling targeted fluorescence imaging of human ovarian cancer cells. *Talanta*. 2021;225:121960.
64. Hoogstins CE, Tummers QR, Gaarenstroom KN, et al. A Novel Tumor-Specific Agent for Intraoperative Near-Infrared Fluorescence Imaging: A Translational Study in Healthy Volunteers and Patients with Ovarian Cancer. *Clin Cancer Res*. 2016;22(12):2929-2938.
65. García de Jalón E, Kleinmanns K, Fosse V, et al. Comparison of Five Near-Infrared Fluorescent Folate Conjugates in an Ovarian Cancer Model. *Mol Imaging Biol*. 2023;25(1):144-155.
66. Potara M, Nagy-Simon T, Focsan M, et al. Folate-targeted Pluronic-chitosan nanocapsules loaded with IR780 for near-infrared fluorescence imaging and photothermal-photodynamic therapy of ovarian cancer. *Colloids Surf B Biointerfaces*. 2021;203:111755.
67. Song J, Ye H, Jiang S, Yang Y, Li X. An Acid Response IR780-Based Targeted Nanoparticle for Intraoperative Near-Infrared Fluorescence Imaging of Ovarian Cancer. *Int J Nanomedicine*. 2022;17:4961-4974.
68. Song J, Zhang N, Zhang L, et al. IR780-loaded folate-targeted nanoparticles for near-infrared fluorescence image-guided surgery and photothermal therapy in ovarian cancer. *Int J Nanomedicine*. 2019;14:2757-2772.
69. Li X, Schumann C, Albarqi HA, et al. A Tumor-Activatable Theranostic Nanomedicine Platform for NIR Fluorescence-Guided Surgery and Combinatorial Phototherapy. *Theranostics*. 2018;8(3):767-784.
70. Zhang L, Yi H, Song J, et al. Mitochondria-Targeted and Ultrasound-Activated Nanodroplets for Enhanced Deep-Penetration Sonodynamic Cancer Therapy. *ACS Appl Mater Interfaces*. 2019;11(9):9355-9366.
71. Wang Y, Liu T, Zhang E, Luo S, Tan X, Shi C. Preferential accumulation of the near infrared heptamethine dye IR-780 in the mitochondria of drug-resistant lung cancer cells. *Biomaterials*. 2014;35(13):4116-4124.
72. Mangeolle T, Yakavets I, Marchal S, et al. Fluorescent Nanoparticles for the Guided Surgery of Ovarian Peritoneal Carcinomatosis. *Nanomaterials (Basel)*. 2018;8(8):572.
73. Randall LM, Wenham RM, Low PS, Dowdy SC, Tanyi JL. A phase II, multicenter, open-label trial of OTL38 injection for the intra-operative imaging of folate receptor-alpha positive ovarian cancer. *Gynecol Oncol*. 2019;155(1):63-68.
74. Tanyi JL, Randall LM, Chambers SK, et al. A Phase III Study of Pafolacianine Injection (OTL38) for Intraoperative Imaging of Folate Receptor-Positive Ovarian Cancer (Study 006). *J Clin Oncol*. 2023;41(2):276-284.

75. Zhang K, Chen J. The regulation of integrin function by divalent cations. *Cell Adh Migr*. 2012;6(1):20-29.
76. Hynes RO. Integrins: bidirectional, allosteric signaling machines. *Cell*. 2002;110(6):673-687.
77. Charo IF, Nannizzi L, Smith JW, Cheresh DA. The vitronectin receptor alpha v beta 3 binds fibronectin and acts in concert with alpha 5 beta 1 in promoting cellular attachment and spreading on fibronectin. *J Cell Biol*. 1990;111(6 Pt 1):2795-2800.
78. Landen CN, Kim TJ, Lin YG, et al. Tumor-selective response to antibody-mediated targeting of alphavbeta3 integrin in ovarian cancer. *Neoplasia*. 2008;10(11):1259-1267.
79. Mery E, Jouve E, Guillermet S, et al. Intraoperative fluorescence imaging of peritoneal dissemination of ovarian carcinomas. A preclinical study. *Gynecol Oncol*. 2011;122(1):155-162.
80. Dutour A, Josserand V, Jury D, et al. Targeted imaging of α(v)β(3) expressing sarcoma tumor cells in vivo in pre-operative setting using near infrared: a potential tool to reduce incomplete surgical resection. *Bone*. 2014;62:71-78.
81. Dumy P, Favrot MC, Boturyn D, Coll JL. Synthesis and characterization of novel system for guidance and vectorization of molecules of therapeutic interest towards target cells US Patent US2006/0173160, 2006.
82. Sani S, Messe M, Fuchs Q, et al. Biological Relevance of RGD-Integrin Subtype-Specific Ligands in Cancer. *Chembiochem*. 2021;22(7):1151-1160.
83. Boturyn D, Coll JL, Garanger E, Favrot MC, Dumy P. Template assembled cyclopeptides as multimeric system for integrin targeting and endocytosis. *J Am Chem Soc*. 2004;126(18):5730-5739.
84. Garanger E, Boturyn D, Jin Z, Dumy P, Favrot MC, Coll JL. New multifunctional molecular conjugate vector for targeting, imaging, and therapy of tumors. *Mol Ther*. 2005;12(6):1168-1175.
85. Apparao KB, Murray MJ, Fritz MA, et al. Osteopontin and its receptor alphavbeta(3) integrin are coexpressed in the human endometrium during the menstrual cycle but regulated differentially. *J Clin Endocrinol Metab*. 2001;86(10):4991-5000.
86. Mery E, Golzio M, Guillermet S, et al. Fluorescence-guided surgery for cancer patients: a proof of concept study on human xenografts in mice and spontaneous tumors in pets. *Oncotarget*. 2017;8(65):109559-109574.
87. Josserand V, Bernard C, Michy T, et al. Tumor-Specific Imaging with Angiostamp800 or Bevacizumab-IRDye 800CW Improves Fluorescence-Guided Surgery over Indocyanine Green in Peritoneal Carcinomatosis. *Biomedicines*. 2022;10(5):1059.
88. van Manen L, Handgraaf HJM, Diana M, et al. A practical guide for the use of indocyanine green and methylene blue in fluorescence-guided abdominal surgery. *J Surg Oncol*. 2018;118(2):283-300.
89. Josserand V, Kéramidas M, Lavaud J, et al. Electrochemotherapy guided by intraoperative fluorescence imaging for the treatment of inoperable peritoneal micro-metastases. *J Control Release*. 2016;233:81-87.
90. Mery E, Jouve E, Guillermet S, et al. Intraoperative fluorescence imaging of peritoneal dissemination of ovarian carcinomas. A preclinical study. *Gynecol Oncol*. 2011;122(1):155-162.
91. Harlaar NJ, Kelder W, Sarantopoulos A, et al. Real-time near infrared fluorescence (NIRF) intra-operative imaging in ovarian cancer using an α(v)β(3-)integrin targeted agent. *Gynecol Oncol*. 2013;128(3):590-595.
92. Shaw SK, Schreiber CL, Roland FM, et al. High expression of integrin αvβ3 enables uptake of targeted fluorescent probes into ovarian cancer cells and tumors. *Bioorg Med Chem*. 2018;26(8):2085-2091.
93. Cao Q, Li ZB, Chen K, et al. Evaluation of biodistribution and anti-tumor effect of a dimeric RGD peptide-paclitaxel conjugate in mice with breast cancer. *Eur J Nucl Med Mol Imaging*. 2008;35(8):1489-1498.
94. Ruoslahti E, Bhatia SN, Sailor MJ. Targeting of drugs and nanoparticles to tumors. *J Cell Biol*. 2010;188(6):759-768.
95. Serrano-Olvera A, Dueñas-González A, Gallardo-Rincón D, Candelaria M, De la Garza-Salazar J. Prognostic, predictive and therapeutic implications of HER2 in invasive epithelial ovarian cancer. *Cancer Treat Rev*. 2006;32(3):180-190.
96. Schlessinger J. Cell Signaling by Receptor Tyrosine Kinases. *Cell*. 2000;103(2):211-225.
97. Graus-Porta D, Beerli RR, Daly JW, Hynes NE. ErbB-2, the preferred heterodimerization partner of all ErbB receptors, is a mediator of lateral signaling. *The EMBO Journal*. 1997;16(7):1647-1655.

98. Mendelsohn J, Baselga J. Status of Epidermal Growth Factor Receptor Antagonists in the Biology and Treatment of Cancer. *J Clin Oncol.* 2003;21(14):2787-2799.
99. Chavez-Blanco A, Pérez-Sánchez V, Gonzalez-Fierro A, et al. HER2 expression in cervical cancer as a potential therapeutic target. *BMC Cancer*. 2004;4(1).
100. Zhang HY, Wang Q, Greene MI, Murali R. New perspectives on anti-HER2/neu therapeutics. *PubMed*. 2000;13(6):325-329.
101. Park HK, Kim IY, Kim JK, Nam TJ. Induction of apoptosis and the regulation of ErbB signaling by laminarin in HT-29 human colon cancer cells. *Int J Mol Med*. 2013;32(2):291-295.
102. Chung YW, Kim SM, Hong JT, et al. Overexpression of HER2/HER3 and clinical feature of ovarian cancer. *J Gynecol Oncol*. 2019;30(5).
103. Høgdall EV, Christensen L, Kjaer SK, et al. Distribution of HER-2 overexpression in ovarian carcinoma tissue and its prognostic value in patients with ovarian carcinoma: from the Danish MALOVA Ovarian Cancer Study. *Cancer*. 2003;98(1):66-73.
104. Asar M, Newton-Northup J, Deutscher S, Soendergaard M. Ovarian Cancer Targeting Phage for In Vivo Near-Infrared Optical Imaging. *Diagnostics (Basel)*. 2019;9(4):183.
105. Soendergaard M, Newton-Northup JR, Deutscher SL. In vivo phage display selection of an ovarian cancer targeting peptide for SPECT/CT imaging. *Am J Nucl Med Mol Imaging*. 2014;4(6):561-570.
106. Choi JH, Choi KC, Auersperg N, Leung PC. Gonadotropins upregulate the epidermal growth factor receptor through activation of mitogen-activated protein kinases and phosphatidyl-inositol-3-kinase in human ovarian surface epithelial cells. *Endocr Relat Cancer*. 2005;12(2):407-421.
107. Choi JH, Choi KC, Auersperg N, Leung PC. Gonadotropins activate proteolysis and increase invasion through protein kinase A and phosphatidylinositol 3-kinase pathways in human epithelial ovarian cancer cells. *Cancer Res*. 2006;66(7):3912-3920.
108. Ellerbroek SM, Halbleib JM, Benavidez M, et al. Phosphatidylinositol 3-kinase activity in epidermal growth factor-stimulated matrix metalloproteinase-9 production and cell surface association. *Cancer Res*. 2001;61(5):1855-1861.
109. Anido J, Matar P, Albanell J, et al. ZD1839, a specific epidermal growth factor receptor (EGFR) tyrosine kinase inhibitor, induces the formation of inactive EGFR/HER2 and EGFR/HER3 heterodimers and prevents heregulin signaling in HER2-overexpressing breast cancer cells. *Clin Cancer Res*. 2003;9(4):1274-1283.
110. Soendergaard M, Newton-Northup JR, Deutscher SL. In vitro high throughput phage display selection of ovarian cancer avid phage clones for near-infrared optical imaging. *Comb Chem High Throughput Screen*. 2014;17(10):859-867.
111. Ma C, Yin G, Yan D, et al. A novel peptide specifically targeting ovarian cancer identified by in vivo phage display. *J Pept Sci*. 2013;19(12):730-736.
112. Li SD, Huang L. Pharmacokinetics and Biodistribution of Nanoparticles. *Mol Pharm*. 2008;5(4):496-504.
113. Wang M, Thanou M. Targeting nanoparticles to cancer. *Pharmacological Research*. 2010;62(2):90-99.
114. Newton JR, Kelly KA, Mahmood U, Weissleder R, Deutscher SL. In vivo selection of phage for the optical imaging of PC-3 human prostate carcinoma in mice. *Neoplasia*. 2006;8(9):772-780.
115. Yip YL, Hawkins NJ, Smith G, Ward RL. Biodistribution of filamentous phage-Fab in nude mice. *J Immunol Methods*. 1999;225(1-2):171-178.
116. Smith MW, Al-Jayyoussi G, Gumbleton M. Peptide sequences mediating tropism to intact blood-brain barrier: an in vivo biodistribution study using phage display. *Peptides*. 2012;38(1):172-180.
117. Zou J, Dickerson MT, Owen NK, Landon LA, Deutscher SL. Biodistribution of filamentous phage peptide libraries in mice. *Mol Biol Rep*. 2004;31(2):121-129.
118. Vankayala R, Bahena E, Guerrero Y, et al. Virus-Mimicking Nanoparticles for Targeted Near Infrared Fluorescence Imaging of Intraperitoneal Ovarian Tumors in Mice. *Ann Biomed Eng*. 2021;49(2):548-559.
119. Guerrero YA, Bahmani B, Singh SP, Vullev VI, Kundra V, Anvari B. Virus-resembling nano-structures for near infrared fluorescence imaging of ovarian cancer HER2 receptors. *Nanotechnology*. 2015;26(43):435102.

120. Guerrero Y, Singh SP, Mai T, et al. Optical Characteristics and Tumor Imaging Capabilities of Near Infrared Dyes in Free and Nano-Encapsulated Formulations Comprised of Viral Capsids. *ACS Appl Mater Interfaces*. 2017;9(23):19601-19611.
121. Matsumura Y, Maeda H. A new concept for macromolecular therapeutics in cancer chemotherapy: mechanism of tumoritropic accumulation of proteins and the antitumor agent smancs. *Cancer Res*. 1986;46(12 Pt 1):6387-6392.
122. Nakamura Y, Mochida A, Choyke PL, Kobayashi H. Nanodrug Delivery: Is the Enhanced Permeability and Retention Effect Sufficient for Curing Cancer?. *Bioconjug Chem*. 2016;27(10):2225-2238.
123. Rangel LB, Agarwal R, D'Souza T, et al. Tight junction proteins claudin-3 and claudin-4 are frequently overexpressed in ovarian cancer but not in ovarian cystadenomas. *Clin Cancer Res*. 2003;9(7):2567-2575.
124. Hough CD, Sherman-Baust CA, Pizer ES, et al. Large-scale serial analysis of gene expression reveals genes differentially expressed in ovarian cancer. *Cancer Res*. 2000;60(22):6281-6287.
125. Morita K, Furuse M, Fujimoto K, Tsukita S. Claudin multigene family encoding four-transmembrane domain protein components of tight junction strands. *Proc Natl Acad Sci U S A*. 1999;96(2):511-516.
126. Santin AD, Cané S, Bellone S, et al. Treatment of chemotherapy-resistant human ovarian cancer xenografts in C.B-17/SCID mice by intraperitoneal administration of Clostridium perfringens enterotoxin. *Cancer Res*. 2005;65(10):4334-4342.
127. Cocco E, Casagrande F, Bellone S, et al. Clostridium perfringens enterotoxin carboxy-terminal fragment is a novel tumor-homing peptide for human ovarian cancer. *BMC Cancer*. 2010;10:349.
128. Cocco E, Shapiro EM, Gasparrini S, et al. Clostridium perfringens enterotoxin C-terminal domain labeled to fluorescent dyes for in vivo visualization of micrometastatic chemotherapy-resistant ovarian cancer. *Int J Cancer*. 2015;137(11):2618-2629.
129. Goodison S, Urquidi V, Tarin D. CD44 cell adhesion molecules. *J Clin Pathol*. 1999;52(4):189-196.
130. Wang L, Zhi X, Lu Y, et al. Identification of microRNA expression profiles of CD44$^+$ ovarian cancer stem cells. *Arch Gynecol Obstet*. 2022;306(2):461-472.
131. Bhattacharya R, Mitra T, Ray Chaudhuri S, Roy SS. Mesenchymal splice isoform of CD44 (CD44s) promotes EMT/invasion and imparts stem-like properties to ovarian cancer cells. *J Cell Biochem*. 2018;119(4):3373-3383.
132. Sacks Suarez J, Gurler Main H, Muralidhar GG, et al. CD44 Regulates Formation of Spheroids and Controls Organ-Specific Metastatic Colonization in Epithelial Ovarian Carcinoma. *Mol Cancer Res*. 2019;17(9):1801-1814.
133. Dang X, Gu L, Qi J, et al. Layer-by-layer assembled fluorescent probes in the second near-infrared window for systemic delivery and detection of ovarian cancer. *Proc Natl Acad Sci U S A*. 2016;113(19):5179-5184.
134. Huang X, Feng B, Liu M, Liu Z, Li S, Zeng W. Preclinical detection of lysophosphatidic acid: A new window for ovarian cancer diagnostics. *Talanta*. 2022;247:123561.
135. Jonkers J, Moolenaar WH. Mammary tumorigenesis through LPA receptor signaling. *Cancer Cell*. 2009;15(6):457-459.
136. Xu Y, Shen Z, Wiper DW, et al. Lysophosphatidic acid as a potential biomarker for ovarian and other gynecologic cancers. *JAMA*. 1998;280(8):719-723.
137. Cui R, Bai H, Cao G, Zhang Z. The Role of Lysophosphatidic Acid Receptors in Ovarian Cancer: A Minireview. *Crit Rev Eukaryot Gene Expr*. 2020;30(3):265-272.
138. Yao D, Lin Z, Wu J. Near-Infrared Fluorogenic Probes with Polarity-Sensitive Emission for in Vivo Imaging of an Ovarian Cancer Biomarker. *ACS Appl Mater Interfaces*. 2016;8(9):5847-5856.
139. Guo HF, Feng J, Zhang H, Yao Y, Cheng HY. *Zhonghua Fu Chan Ke Za Zhi*. 2005;40(9):614-618.
140. Chen J, Zhang C, Guo Y, et al. Evaluation of a novel ovarian cancer-specific fluorescent antibody probe for targeted near-infrared fluorescence imaging. *World J Surg Oncol*. 2020;18(1):66.
141. Chen J, Guo Y, Li H, et al. Near-infrared dye-labeled antibody COC183B2 enables detection of tiny metastatic ovarian cancer and optimizes fluorescence-guided surgery. *J Surg Oncol*. 2020;122(6):1207-1217.

142. Yin BW, Lloyd KO. Molecular cloning of the CA125 ovarian cancer antigen: identification as a new mucin, MUC16. *J Biol Chem*. 2001;276(29):27371-27375.
143. Duraisamy S, Ramasamy S, Kharbanda S, Kufe D. Distinct evolution of the human carcinoma-associated transmembrane mucins, MUC1, MUC4 AND MUC16. *Gene*. 2006;373:28-34.
144. Gipson IK. The ocular surface: the challenge to enable and protect vision: the Friedenwald lecture. *Invest Ophthalmol Vis Sci*. 2007;48(10):4390-4398.
145. Perez BH, Gipson IK. Focus on Molecules: human mucin MUC16. *Exp Eye Res*. 2008;87(5):400-401.
146. Blalock TD, Spurr-Michaud SJ, Tisdale AS, et al. Functions of MUC16 in corneal epithelial cells. *Invest Ophthalmol Vis Sci*. 2007;48(10):4509-4518.
147. Rump A, Morikawa Y, Tanaka M, et al. Binding of ovarian cancer antigen CA125/MUC16 to mesothelin mediates cell adhesion. *J Biol Chem*. 2004;279(10):9190-9198.
148. Thériault C, Pinard M, Comamala M, et al. MUC16 (CA125) regulates epithelial ovarian cancer cell growth, tumorigenesis and metastasis. *Gynecol Oncol*. 2011;121(3):434-443.
149. Boivin M, Lane D, Piché A, Rancourt C. CA125 (MUC16) tumor antigen selectively modulates the sensitivity of ovarian cancer cells to genotoxic drug-induced apoptosis. *Gynecol Oncol*. 2009;115(3):407-413.
150. Bast RC Jr, Xu FJ, Yu YH, Barnhill S, Zhang Z, Mills GB. CA 125: the past and the future. *Int J Biol Markers*. 1998;13(4):179-187.
151. Marotta CB, Haber T, Berlin JM, Grubbs RH. Surgery-Guided Removal of Ovarian Cancer Using Up-Converting Nanoparticles. *ACS Appl Mater Interfaces*. 2020;12(43):48371-48379.
152. Köbel M, Kalloger SE, Boyd N, et al. Ovarian carcinoma subtypes are different diseases: implications for biomarker studies. *PLoS Med*. 2008;5(12):e232.
153. Punzón-Jiménez P, Lago V, Domingo S, Simón C, Mas A. Molecular Management of High-Grade Serous Ovarian Carcinoma. *Int J Mol Sci*. 2022;23(22):13777.
154. Sharma SK, Wuest M, Wang M, et al. Immuno-PET of epithelial ovarian cancer: harnessing the potential of CA125 for non-invasive imaging. *EJNMMI Res*. 2014;4(1):60.
155. Fung K, Sharma SK, Keinänen O, Roche KL, Lewis JS, Zeglis BM. A Molecularly Targeted Intraoperative Near-Infrared Fluorescence Imaging Agent for High-Grade Serous Ovarian Cancer. *Mol Pharm*. 2020;17(8):3140-3147.
156. Hisatsune A, Nakayama H, Kawasaki M, et al. Anti-MUC1 antibody inhibits EGF receptor signaling in cancer cells. *Biochem Biophys Res Commun*. 2011;405(3):377-381.
157. McQuarrie SA, Baum RP, Niesen A, et al. Pharmacokinetics and radiation dosimetry of 99Tcm-labelled monoclonal antibody B43.13 in ovarian cancer patients. *Nucl Med Commun*. 1997;18(9):878-886.
158. Schultes BC, Baum RP, Niesen A, Noujaim AA, Madiyalakan R. Anti-idiotype induction therapy: anti-CA125 antibodies (Ab3) mediated tumor killing in patients treated with Ovarex mAb B43.13 (Ab1). *Cancer Immunol Immunother*. 1998;46(4):201-212.
159. Noujaim AA, Schultes BC, Baum RP, Madiyalakan R. Induction of CA125-specific B and T cell responses in patients injected with MAb-B43.13--evidence for antibody-mediated antigen-processing and presentation of CA125 in vivo. *Cancer Biother Radiopharm*. 2001;16(3):187-203.
160. Gordon AN, Schultes BC, Gallion H, et al. CA125- and tumor-specific T-cell responses correlate with prolonged survival in oregovomab-treated recurrent ovarian cancer patients. *Gynecol Oncol*. 2004;94(2):340-351.
161. Salouti M, Babaei MH, Rajabi H, Rasaee Mj. Preparation and biological evaluation of (177)Lu conjugated PR81 for radioimmunotherapy of breast cancer. *Nucl Med Biol*. 2011;38(6):849-855.
162. Hughes OD, Bishop MC, Perkins AC, et al. Preclinical evaluation of copper-67 labelled anti-MUC1 mucin antibody C595 for therapeutic use in bladder cancer. *Eur J Nucl Med*. 1997;24(4):439-443.
163. Brewer M, Angioli R, Scambia G, et al. Front-line chemo-immunotherapy with carboplatin-paclitaxel using oregovomab indirect immunization in advanced ovarian cancer: A randomized phase II study. *Gynecol Oncol*. 2020;156(3):523-529.
164. Bernard V, Young J, Binart N. Prolactin - a pleiotropic factor in health and disease. *Nat Rev Endocrinol*. 2019;15(6):356-365.

165. Ramírez-de-Arellano A, Villegas-Pineda JC, Hernández-Silva CD, Pereira-Suárez AL. The Relevant Participation of Prolactin in the Genesis and Progression of Gynecological Cancers. *Front Endocrinol (Lausanne)*. 2021;12:747810.
166. Bernichtein S, Touraine P, Goffin V. New concepts in prolactin biology. *J Endocrinol*. 2010;206(1):1-11.
167. Asai-Sato M, Nagashima Y, Miyagi E, et al. Prolactin inhibits apoptosis of ovarian carcinoma cells induced by serum starvation or cisplatin treatment. *Int J Cancer*. 2005;115(4):539-544.
168. Levina VV, Nolen B, Su Y, et al. Biological significance of prolactin in gynecologic cancers. *Cancer Res*. 2009;69(12):5226-5233.
169. Sundaram KM, Zhang Y, Mitra AK, et al. Prolactin Receptor-Mediated Internalization of Imaging Agents Detects Epithelial Ovarian Cancer with Enhanced Sensitivity and Specificity. *Cancer Res*. 2017;77(7):1684-1696.
170. Elkins PA, Christinger HW, Sandowski Y, et al. Ternary complex between placental lactogen and the extracellular domain of the prolactin receptor. *Nat Struct Biol*. 2000;7(9):808-815.
171. Lu JC, Scott P, Strous GJ, Schuler LA. Multiple internalization motifs differentially used by prolactin receptor isoforms mediate similar endocytic pathways. *Mol Endocrinol*. 2002;16(11):2515-2527.
172. Bhartiya D, Patel H. An overview of FSH-FSHR biology and explaining the existing conundrums. *J Ovarian Res*. 2021;14(1):144.
173. Sun D, Bai M, Jiang Y, et al. Roles of follicle stimulating hormone and its receptor in human metabolic diseases and cancer. *Am J Transl Res*. 2020;12(7):3116-3132.
174. Zhang Z, Zhu Y, Lai Y, et al. Follicle-stimulating hormone inhibits apoptosis in ovarian cancer cells by regulating the OCT4 stem cell signaling pathway. *Int J Oncol*. 2013;43(4):1194-1204.
175. Zhang Z, Jia L, Feng Y, Zheng W. Overexpression of follicle-stimulating hormone receptor facilitates the development of ovarian epithelial cancer. *Cancer Lett*. 2009;278(1):56-64.
176. Yang Y, Zhang J, Zhu Y, Zhang Z, Sun H, Feng Y. Follicle-stimulating hormone induced epithelial-mesenchymal transition of epithelial ovarian cancer cells through follicle-stimulating hormone receptor PI3K/Akt-Snail signaling pathway. *Int J Gynecol Cancer*. 2014;24(9):1564-1574.
177. Chen J, Bai M, Ning C, et al. Gankyrin facilitates follicle-stimulating hormone-driven ovarian cancer cell proliferation through the PI3K/AKT/HIF-1α/cyclin D1 pathway. *Oncogene*. 2016;35(19):2506-2517.
178. Tao X, Zhao N, Jin H, et al. FSH enhances the proliferation of ovarian cancer cells by activating transient receptor potential channel C3. *Endocr Relat Cancer*. 2013;20(3):415-429.
179. Zhang Z, Wang Q, Ma J, et al. Reactive oxygen species regulate FSH-induced expression of vascular endothelial growth factor via Nrf2 and HIF1α signaling in human epithelial ovarian cancer. *Oncol Rep*. 2013;29(4):1429-1434.
180. Wang P, Fan Y, Lu L, et al. NIR-II nanoprobes in-vivo assembly to improve image-guided surgery for metastatic ovarian cancer. *Nat Commun*. 2018;9(1):2898.
181. Zhong Y, Dai H. A mini-review on rare-earth down-conversion nanoparticles for NIR-II imaging of biological systems. *Nano Res*. 2020;13(5):1281-1294.
182. Wang P, Jiang S, Li Y, et al. Corrigendum to "Downshifting nanoprobes with the follicle stimulating hormone peptide fabrication for highly efficient NIR II fluorescent bioimaging guided ovarian tumor surgery" *Nanomedicine: NBM*. 28(2020)102198.
183. Yao C, Wang P, Zhou L, et al. Highly biocompatible zwitterionic phospholipids coated upconversion nanoparticles for efficient bioimaging. *Anal Chem*. 2014;86(19):9749-9757.
184. Casteel CO, Singh G. *Physiology, Gonadotropin-Releasing Hormone*. *StatPearls;* 2022.
185. Limonta P, Montagnani Marelli M, Mai S, Motta M, Martini L, Moretti RM. GnRH receptors in cancer: from cell biology to novel targeted therapeutic strategies. *Endocr Rev*. 2012;33(5):784-811.
186. Liu Q, Zhou X, Feng W, et al. Gonadotropin-Releasing Hormone Receptor-Targeted Near-Infrared Fluorescence Probe for Specific Recognition and Localization of Peritoneal Metastases of Ovarian Cancer. *Front Oncol*. 2020;10:266.
187. Reissmann T, Schally AV, Bouchard P, Riethmiiller H, Engel J. The LHRH antagonist cetrorelix: a review. *Hum Reprod Update*. 2000;6(4):322-331.

188. Yao Z, Zhang M, Sakahara H, Saga T, Arano Y, Konishi J. Avidin targeting of intraperitoneal tumor xenografts. *J Natl Cancer Inst*. 1998;90(1):25-29.

189. Yao Z, Zhang M, Sakahara H, et al. Imaging of intraperitoneal tumors with technetium-99m GSA. *Ann Nucl Med*. 1998;12(2):115-118.

190. Hama Y, Urano Y, Koyama Y, et al. In vivo spectral fluorescence imaging of submillimeter peritoneal cancer implants using a lectin-targeted optical agent. *Neoplasia*. 2006;8(7):607-612.

191. Lotan R, Raz A. Lectins in cancer cells. *Ann N Y Acad Sci*. 1988;551:385-398.

192. Hama Y, Urano Y, Koyama Y, Choyke PL, Kobayashi H. Targeted optical imaging of cancer cells using lectin-binding BODIPY conjugated avidin. *Biochem Biophys Res Commun*. 2006;348(3):807-813.

193. Alexander VM, Sano K, Yu Z, et al. Galactosyl human serum albumin-NMP1 conjugate: a near infrared (NIR)-activatable fluorescence imaging agent to detect peritoneal ovarian cancer metastases. *Bioconjug Chem*. 2012;23(8):1671-1679.

194. Kee HL, Nothdurft R, Muthiah C, et al. Examination of chlorin-bacteriochlorin energy-transfer dyads as prototypes for near-infrared molecular imaging probes. *Photochem Photobiol*. 2008;84(5):1061-1072.

195. Krayer M, Ptaszek M, Kim HJ, et al. Expanded scope of synthetic bacteriochlorins via improved acid catalysis conditions and diverse dihydrodipyrrin-acetals. *J Org Chem*. 2010;75(4):1016-1039.

196. Regino CA, Ogawa M, Alford R, et al. Two-step synthesis of galactosylated human serum albumin as a targeted optical imaging agent for peritoneal carcinomatosis. *J Med Chem*. 2010;53(4):1579-1586.

197. Hama Y, Urano Y, Koyama Y, et al. In vivo spectral fluorescence imaging of submillimeter peritoneal cancer implants using a lectin-targeted optical agent. *Neoplasia*. 2006;8(7):607-612.

198. Harada T, Sano K, Sato K, et al. Activatable organic near-infrared fluorescent probes based on a bacteriochlorin platform: synthesis and multicolor in vivo imaging with a single excitation. *Bioconjug Chem*. 2014;25(2):362-369.

199. Ogawa M, Kosaka N, Choyke PL, Kobayashi H. In vivo molecular imaging of cancer with a quenching near-infrared fluorescent probe using conjugates of monoclonal antibodies and indocyanine green. *Cancer Res*. 2009;69(4):1268-1272.

200. Tarhriz V, Bandehpour M, Dastmalchi S, Ouladsahebmadarek E, Zarredar H, Eyvazi S. Overview of CD24 as a new molecular marker in ovarian cancer. *J Cell Physiol*. 2019;234(3):2134-2142.

201. Kleinmanns K, Fosse V, Bjørge L, McCormack E. The Emerging Role of CD24 in Cancer Theranostics-A Novel Target for Fluorescence Image-Guided Surgery in Ovarian Cancer and Beyond. *J Pers Med*. 2020;10(4):255.

202. Tarhriz V, Bandehpour M, Dastmalchi S, Ouladsahebmadarek E, Zarredar H, Eyvazi S. Overview of CD24 as a new molecular marker in ovarian cancer. *J Cell Physiol*. 2019;234(3):2134-2142.

203. Kleinmanns K, Bischof K, Anandan S, et al. CD24-targeted fluorescence imaging in patient-derived xenograft models of high-grade serous ovarian carcinoma. *EBioMedicine*. 2020;56:102782.

204. Kleinmanns K, Fosse V, Davidson B, et al. CD24-targeted intraoperative fluorescence image-guided surgery leads to improved cytoreduction of ovarian cancer in a preclinical orthotopic surgical model. *EBioMedicine*. 2020;56:102783.

205. Kessenbrock K, Plaks V, Werb Z. Matrix metalloproteinases: regulators of the tumor microenvironment. *Cell*. 2010;141(1):52-67.

206. Page-McCaw A, Ewald AJ, Werb Z. Matrix metalloproteinases and the regulation of tissue remodelling. *Nat Rev Mol Cell Biol*. 2007;8(3):221-233.

207. Wilson CL, Ouellette AJ, Satchell DP, et al. Regulation of intestinal alpha-defensin activation by the metalloproteinase matrilysin in innate host defense. *Science*. 1999;286(5437):113-117.

208. Chambers AF, Groom AC, MacDonald IC. Dissemination and growth of cancer cells in metastatic sites. *Nat Rev Cancer*. 2002;2(8):563-572.

209. Steeg PS. Tumor metastasis: mechanistic insights and clinical challenges. *Nat Med*. 2006;12(8):895-904.

210. Egeblad M, Werb Z. New functions for the matrix metalloproteinases in cancer progression. *Nat Rev Cancer*. 2002;2(3):161-174.
211. Choi JW, Ahn SE, Rengaraj D, et al. Matrix metalloproteinase 3 is a stromal marker for chicken ovarian cancer. *Oncol Lett*. 2011;2(6):1047-1051.
212. Chakravarty D, Roy SS, Babu CR, et al. Therapeutic targeting of PELP1 prevents ovarian cancer growth and metastasis [published correction appears in Clin Cancer Res. 2013 Mar 1;19(5):1305]. *Clin Cancer Res*. 2011;17(8):2250-2259.
213. Zhao H, Yang Z, Wang X, et al. Triptolide inhibits ovarian cancer cell invasion by repression of matrix metalloproteinase 7 and 19 and upregulation of E-cadherin. *Exp Mol Med*. 2012;44(11):633-641.
214. Sun N, Zhang Q, Xu C, et al. Molecular regulation of ovarian cancer cell invasion. *Tumour Biol*. 2014;35(11):11359-11366.
215. Davidson B, Trope CG, Reich R. The role of the tumor stroma in ovarian cancer. *Front Oncol*. 2014;4:104.
216. Labiche A, Heutte N, Herlin P, Chasle J, Gauduchon P, Elie N. Stromal compartment as a survival prognostic factor in advanced ovarian carcinoma. *Int J Gynecol Cancer*. 2010;20(1):28-33.
217. Wang KH, Wang YM, Chiu LH, et al. Optical imaging of ovarian cancer using a matrix metalloproteinase-3-sensitive near-infrared fluorescent probe [published correction appears in PLoS One. 2018 Aug 14;13(8):e0202610]. *PLoS One*. 2018;13(2):e0192047.
218. Nagase H, Woessner JF Jr. Matrix metalloproteinases. *J Biol Chem*. 1999;274(31):21491-21494.
219. Chen J, Wang M, Xi B, et al. SPARC is a key regulator of proliferation, apoptosis and invasion in human ovarian cancer. *PLoS One*. 2012;7(8):e42413.
220. Bornstein P, Sage EH. Matricellular proteins: extracellular modulators of cell function. *Curr Opin Cell Biol*. 2002;14(5):608-616.
221. Tai IT, Tang MJ. SPARC in cancer biology: its role in cancer progression and potential for therapy. *Drug Resist Updat*. 2008;11(6):231-246.
222. Brown TJ, Shaw PA, Karp X, Huynh MH, Begley H, Ringuette MJ. Activation of SPARC expression in reactive stroma associated with human epithelial ovarian cancer. *Gynecol Oncol*. 1999;75(1):25-33.
223. Paley PJ, Goff BA, Gown AM, Greer BE, Sage EH. Alterations in SPARC and VEGF immunoreactivity in epithelial ovarian cancer. *Gynecol Oncol*. 2000;78(3 Pt 1):336-341.
224. Yiu GK, Chan WY, Ng SW, et al. SPARC (secreted protein acidic and rich in cysteine) induces apoptosis in ovarian cancer cells. *Am J Pathol*. 2001;159(2):609-622.
225. Peng F, Zhong Y, Liu Y, et al. SPARC suppresses lymph node metastasis by regulating the expression of VEGFs in ovarian carcinoma. *Int J Oncol*. 2017;51(6):1920-1928.
226. Ceppi L, Bardhan NM, Na Y, et al. Real-Time Single-Walled Carbon Nanotube-Based Fluorescence Imaging Improves Survival after Debulking Surgery in an Ovarian Cancer Model. *ACS Nano*. 2019;13(5):5356-5365.
227. Yan Q, Sage EH. SPARC, a matricellular glycoprotein with important biological functions. *J Histochem Cytochem*. 1999;47(12):1495-1506.
228. Szebeni GJ, Vizler C, Kitajka K, Puskas LG. Inflammation and Cancer: Extra- and Intracellular Determinants of Tumor-Associated Macrophages as Tumor Promoters. *Mediators Inflamm*. 2017;2017:9294018.
229. Kim J, Bae JS. Tumor-Associated Macrophages and Neutrophils in Tumor Microenvironment. *Mediators Inflamm*. 2016;2016:6058147.
230. Sica A, Erreni M, Allavena P, Porta C. Macrophage polarization in pathology. *Cellular and Molecular Life Sciences*. 2015;72(21):4111-4126.
231. Mills CD. M1 and M2 Macrophages: Oracles of Health and Disease. *Crit Rev Immunol*. 2012;32(6):463-488.
232. Franklin RA, Li MO. Ontogeny of Tumor-associated Macrophages and Its Implication in Cancer Regulation. *Trends Cancer*. 2016;2(1):20-34.
233. Laoui D, Van Overmeire E, De Baetselier P, Van Ginderachter JA, Raes G. Functional Relationship between Tumor-Associated Macrophages and Macrophage Colony-Stimulating Factor as Contributors to Cancer Progression. *Front Immunol*. 2014;5:489.

234. Zhang W, Zhang C, Li W, et al. CD8+ T-cell immunosurveillance constrains lymphoid premetastatic myeloid cell accumulation. *Eur J Immunol*. 2015;45(1):71-81.

235. Caronni N, Savino B, Bonecchi R. Myeloid cells in cancer-related inflammation. *Immunobiology*. 2015;220(2):249-253.

236. Biswas SK, Allavena P, Mantovani A. Tumor-associated macrophages: functional diversity, clinical significance, and open questions. *Semin Immunopathol*. 2013;35(5):585-600.

237. Robinson-Smith TM, Isaacsohn I, Mercer CA, et al. Macrophages mediate inflammation-enhanced metastasis of ovarian tumors in mice. *Cancer Res*. 2007;67(12):5708-5716.

238. Yin M, Li X, Tan S, et al. Tumor-associated macrophages drive spheroid formation during early transcoelomic metastasis of ovarian cancer. *J Clin Invest*. 2016;126(11):4157-4173.

239. Haber T, Cornejo YR, Aramburo S, et al. Specific targeting of ovarian tumor-associated macrophages by large, anionic nanoparticles. *Proc Natl Acad Sci U S A*. 2020;117(33):19737-19745.

240. Marotta CB, Haber T, Berlin JM, Grubbs RH. Surgery-Guided Removal of Ovarian Cancer Using Up-Converting Nanoparticles. *ACS Appl Mater Interfaces*. 2020;12(43):48371-48379.

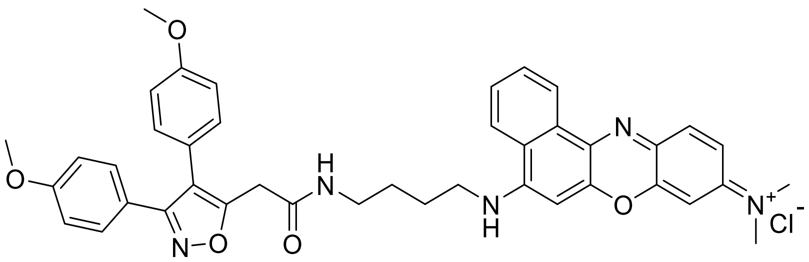

Figure 1. Chemical structure of RR11 probe.

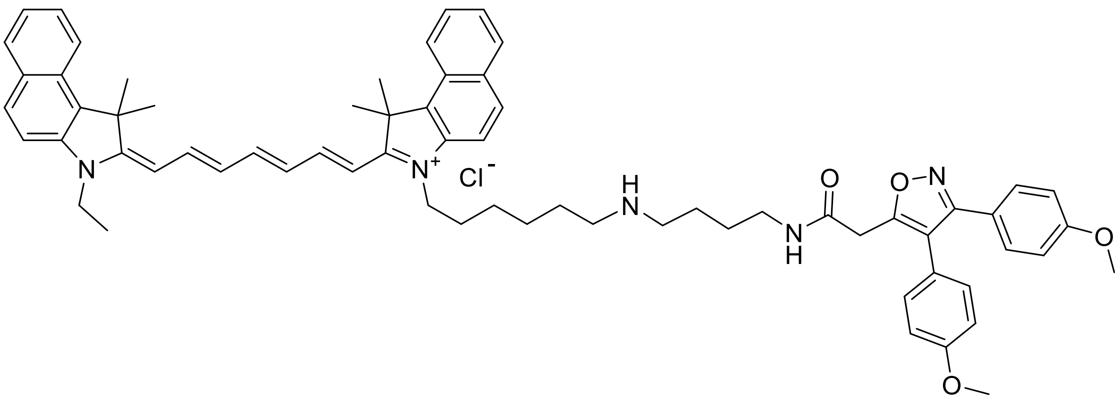

Figure 2. Chemical structure of MSA14 probe.

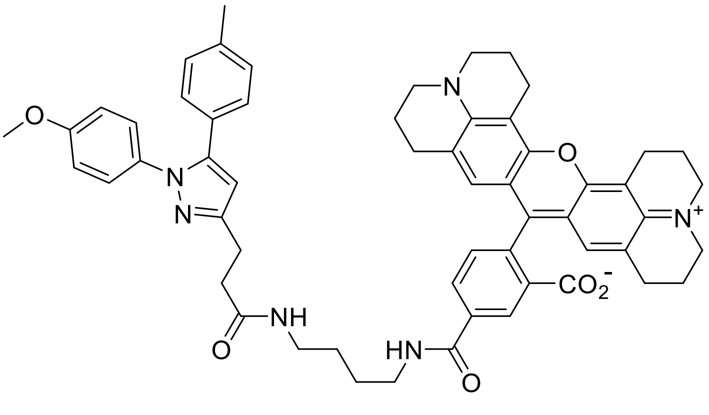

Figure 3. Chemical structure of CMP probe.

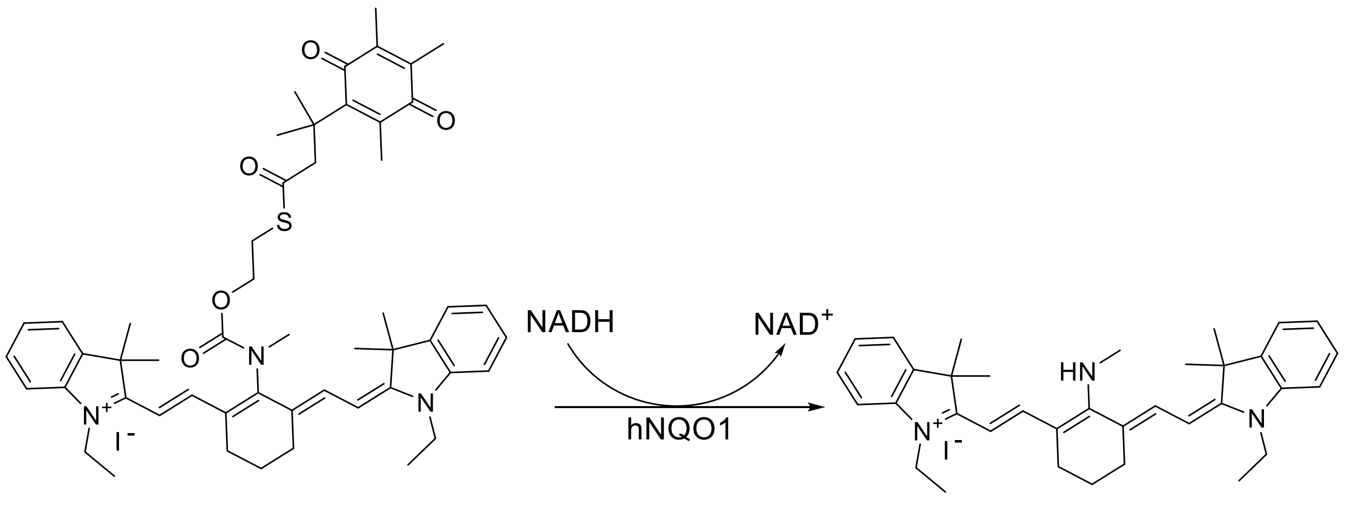

Figure 4. Simplified activation mechanism of Q_3STCy.

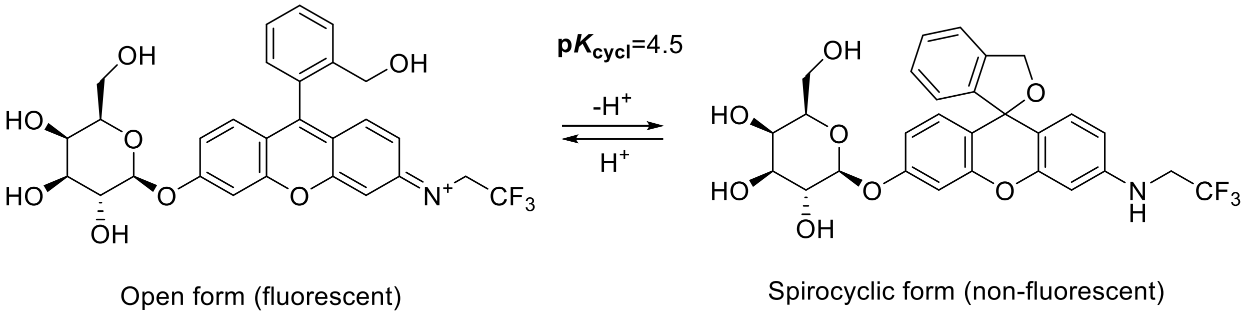

Open form (fluorescent)

Spirocyclic form (non-fluorescent)

Figure 5. Cyclization equilibrium of HMRef-βGal.

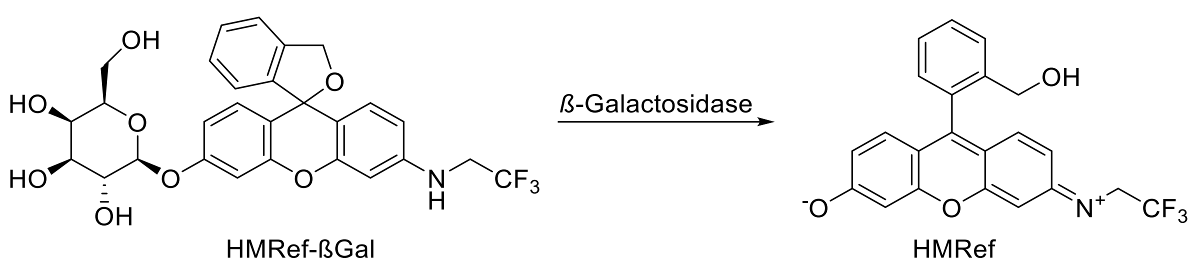

Figure 6. HMRef-βGal activation by specific action of *β*-Galactosidase.

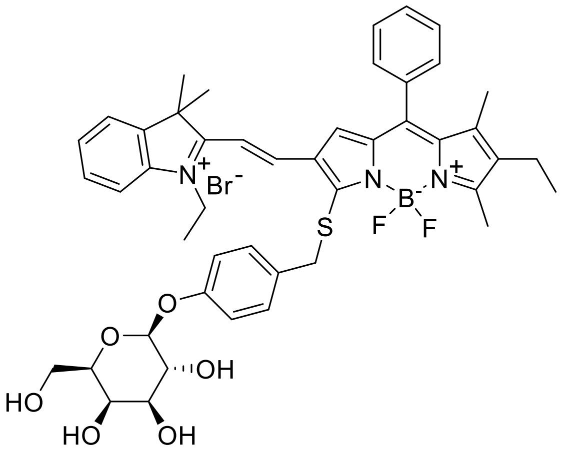

Figure 7. Chemical structure of BOD-M-βGal.

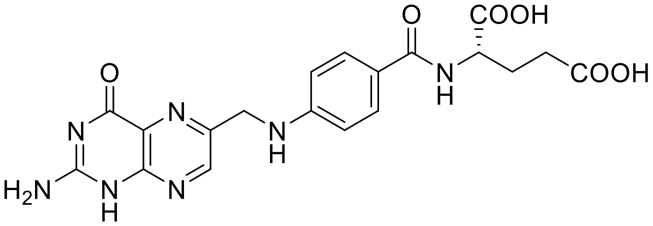

Figure 8. Folic acid (FA) chemical structure.

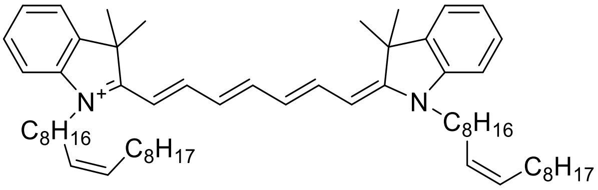

Figure 9. Chemical structure of 1,1'-dioctadecyl-3,3,3',3'-tetramethylindo-tricarbocyanine iodide bis-oleate (DiR-BOA).

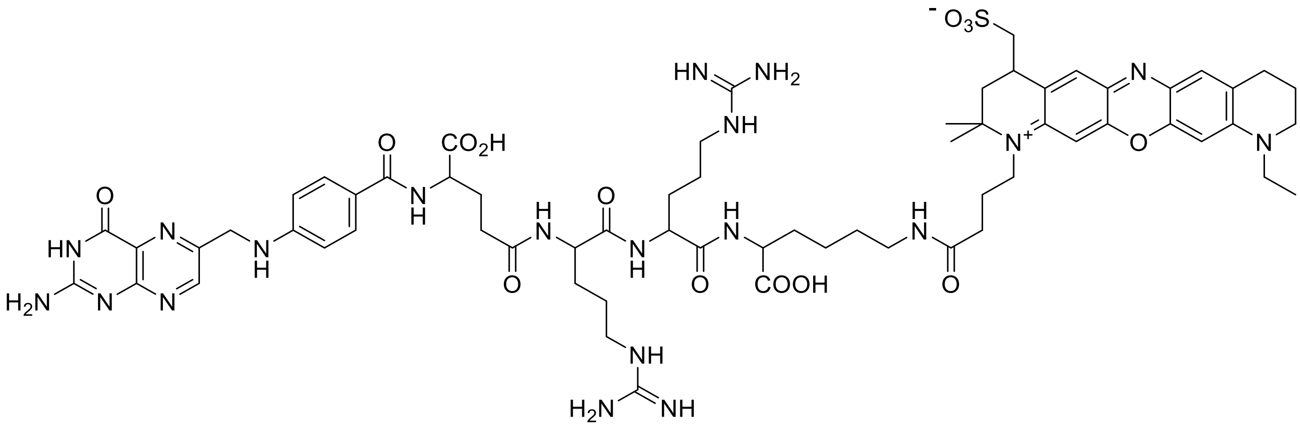

Figure 10. Chemical structure of the folate-specific activatable probe (FSA).

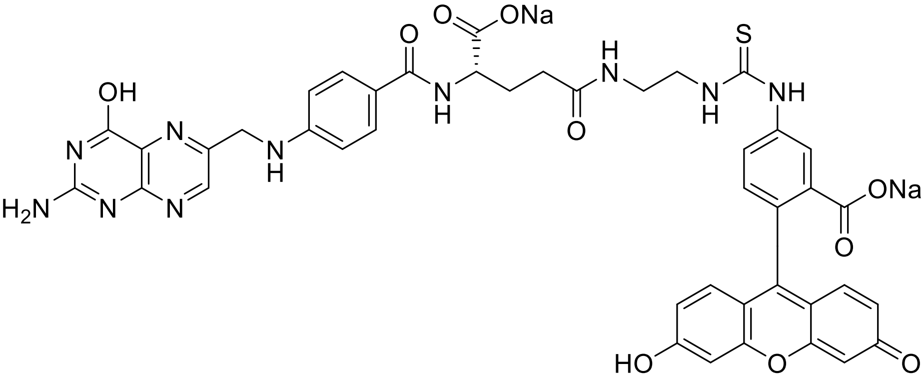

Figure11. EC17 chemical structure.

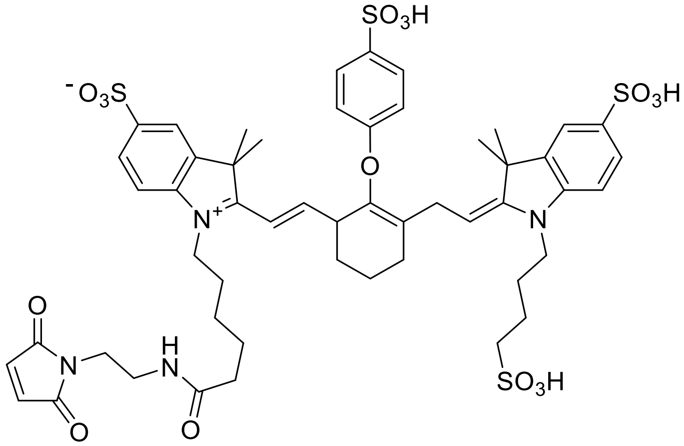

Figure 12. Chemical structure of IRDye 800CW maleimide.

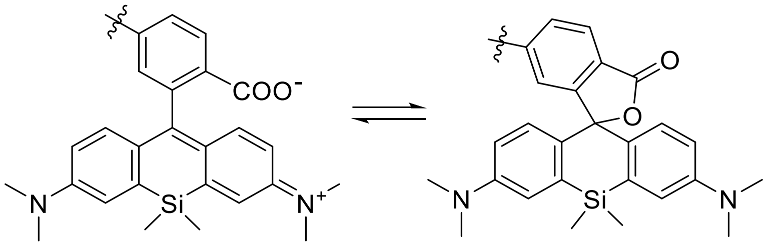

Figure13. Intramolecular spiro cyclization of 2-COOH SiR650.

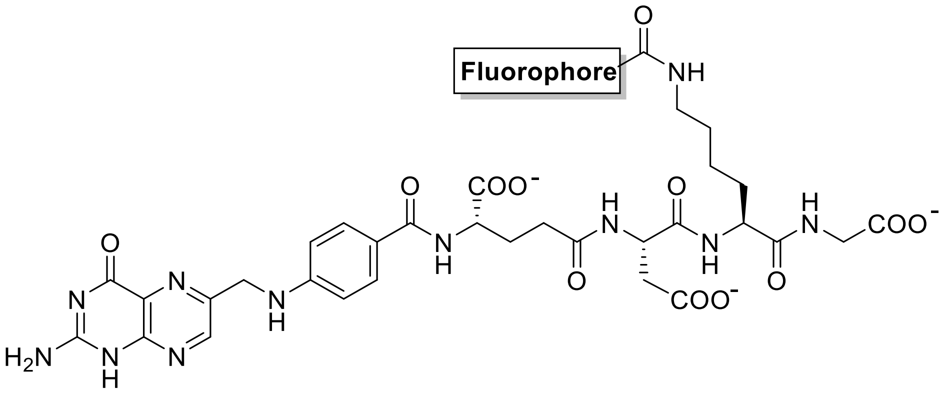

Figure 14. Structure of FolateSiR 1.

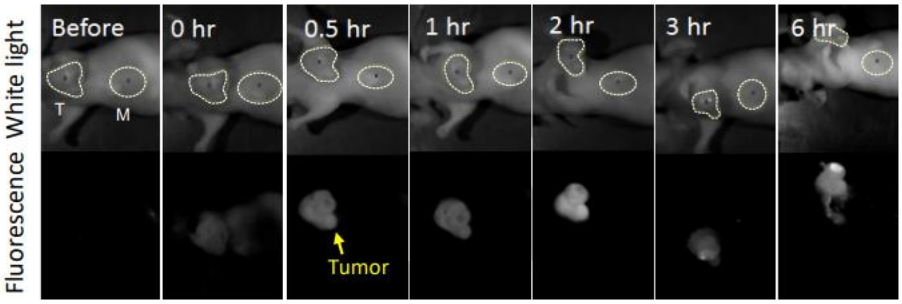

Image 1. Time-lapse fluorescence images of KB tumor-bearing mouse injected with 100 μM FolateSiR-1.

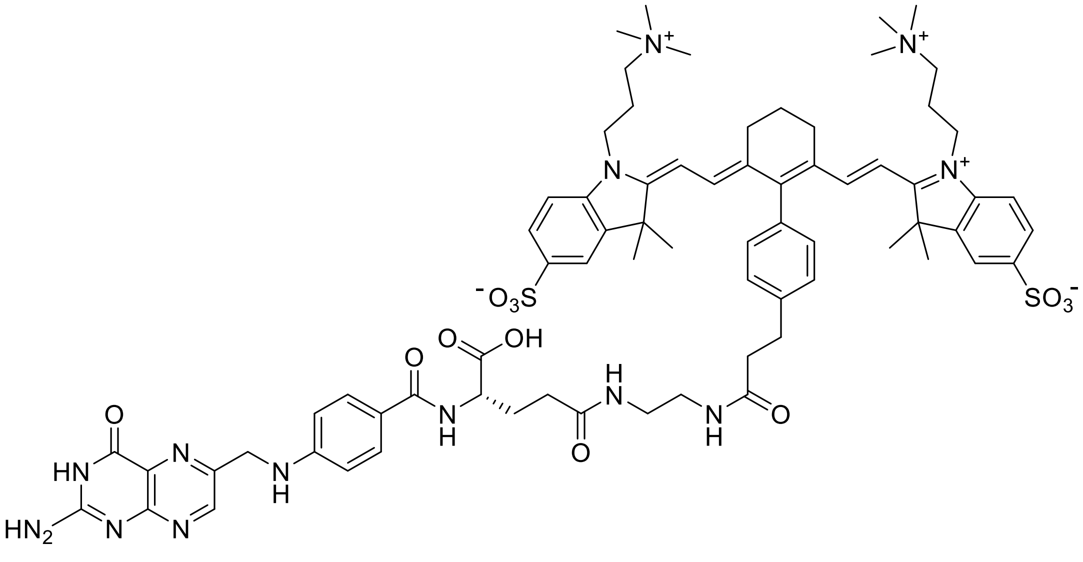

Figure 15. Chemical structure of FA-ZW800-1-Forte.

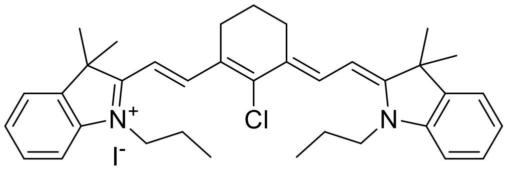

Figure 16. IR780 chemical structure.

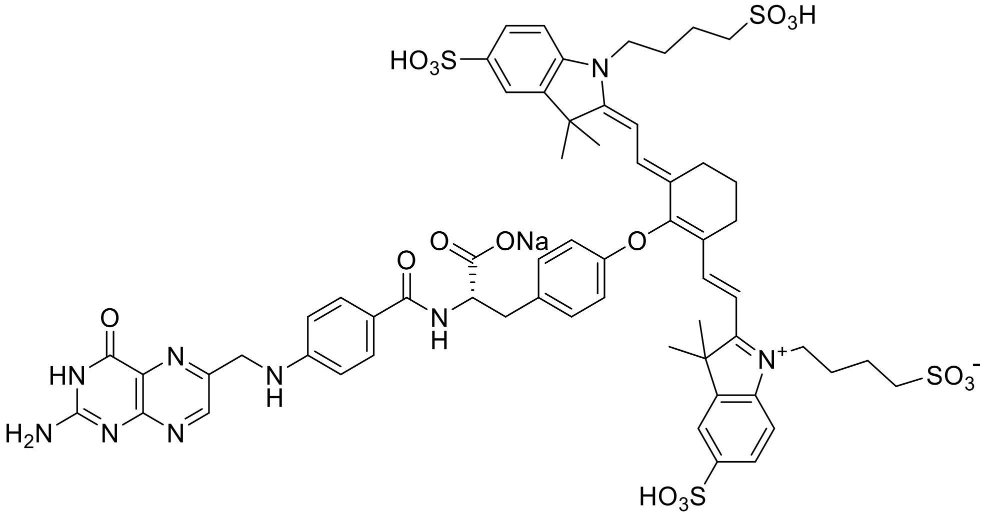

Figure 17. Pafolacianine (Cytalux) structure.

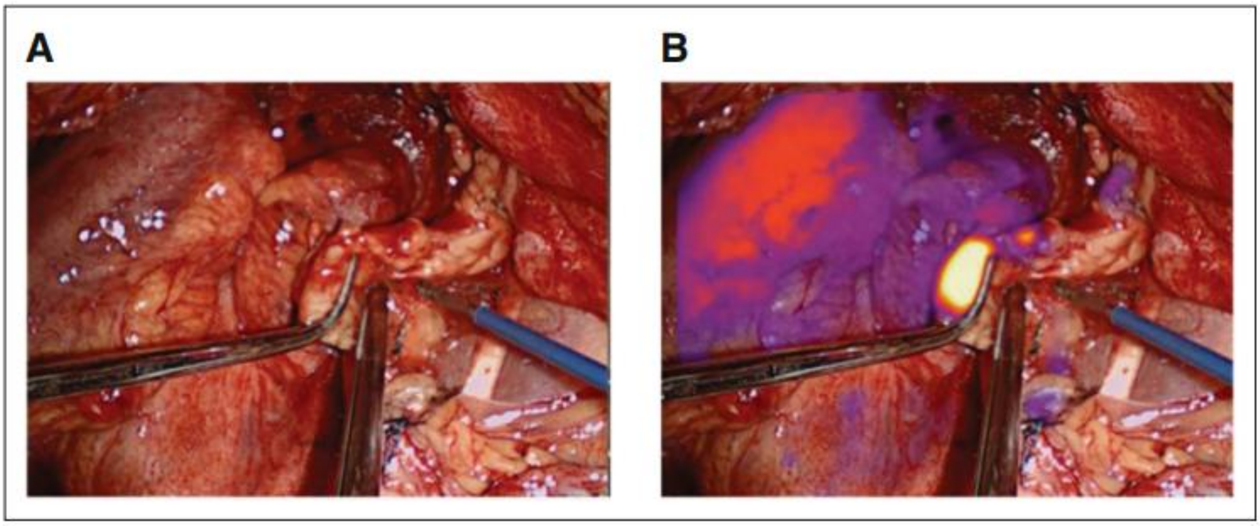

Image 2. Visualization of ovarian cancer lesions in the right paracolic gutter using (A) normal white light compared with (B) NIR fluorescence imaging following pafolacianine injection.[74]

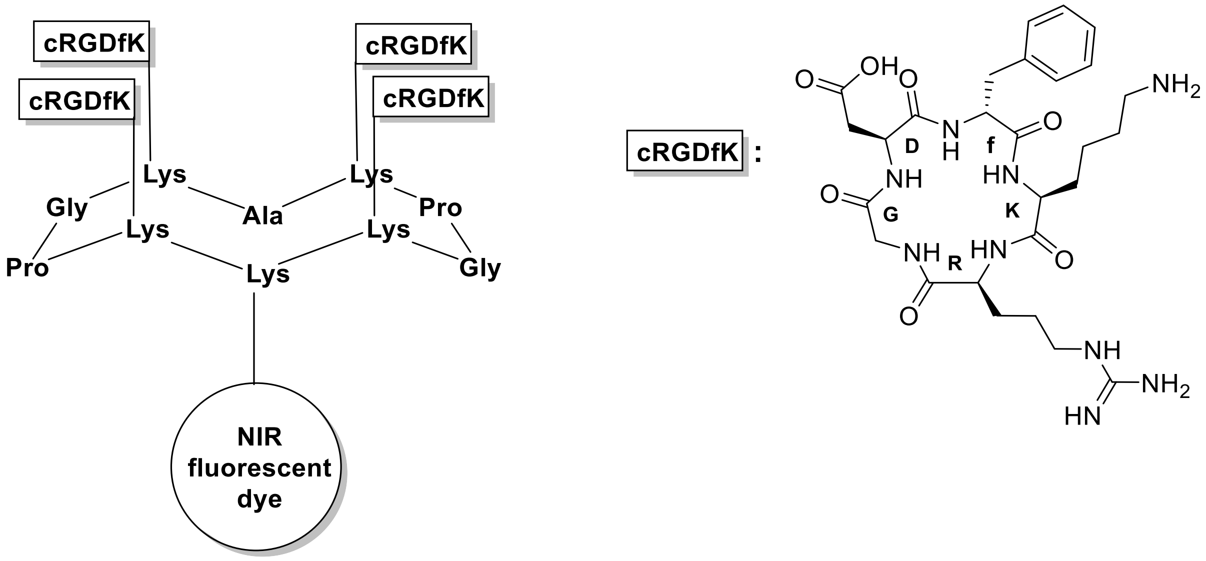

Figure 18. Structure of AngioStamp®.

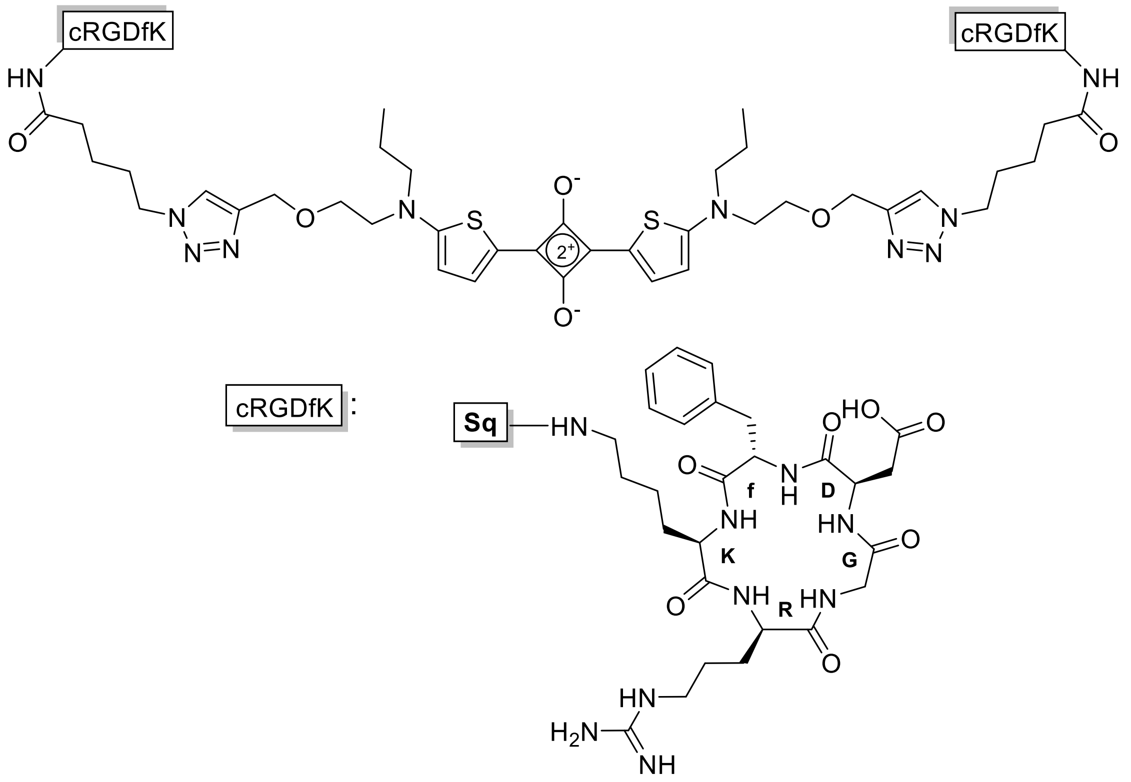

Figure 19. Chemical structure of SqRGD2.

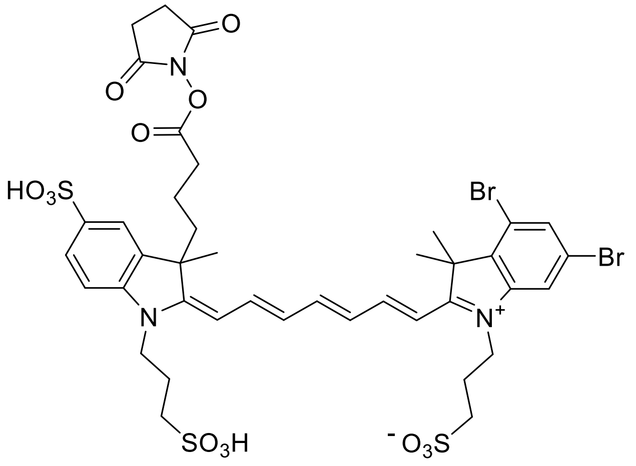

Figure 20. Chemical structure of BrCy106-NHS.

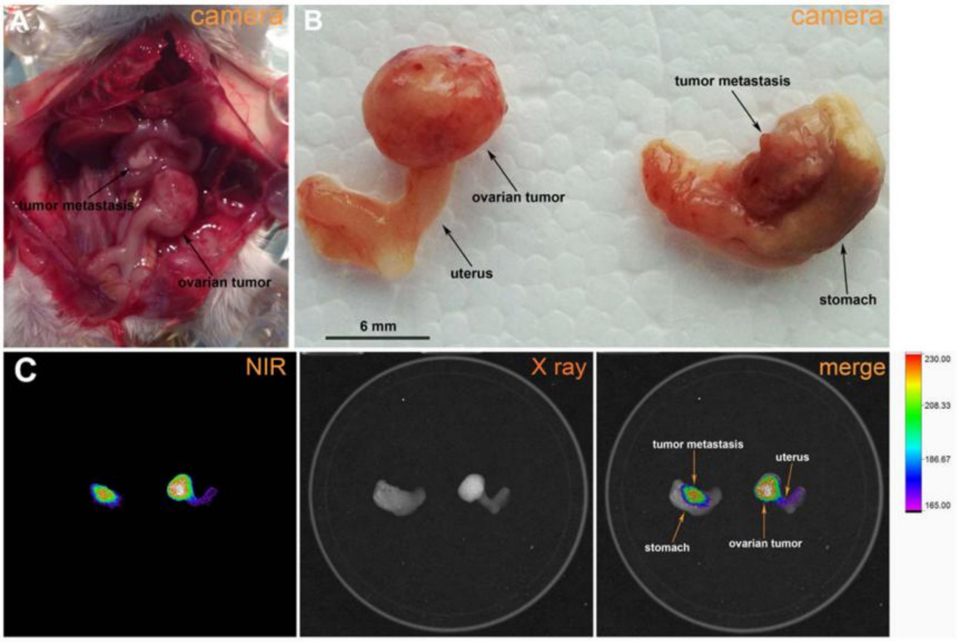

Image 3. Fluorescence the ovarian tumor and metastasis of few millimeters detected on the lesser curvature of the stomach of the tumor bearing mouse (Image 2B–C).[128]

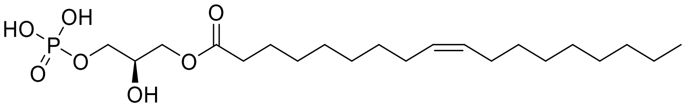

Figure 21. Chemical structure of LPA.

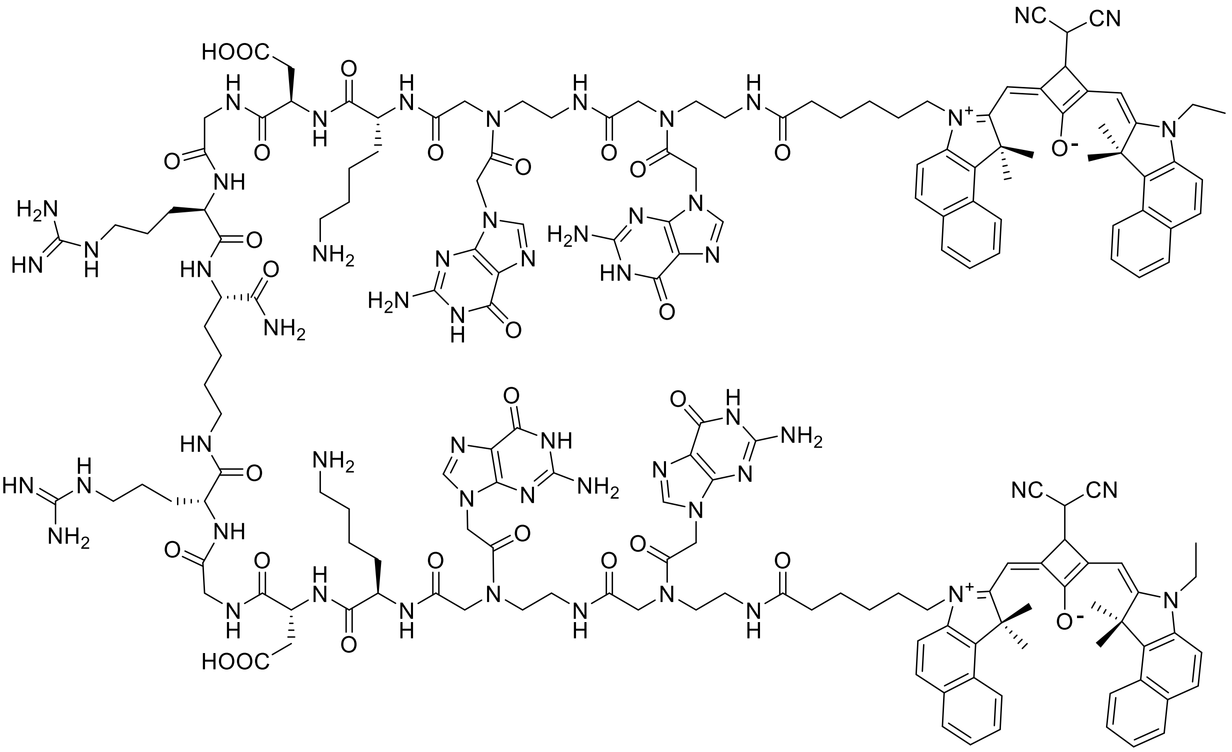

Figure 22. Chemical structure of G4RGDSq2.

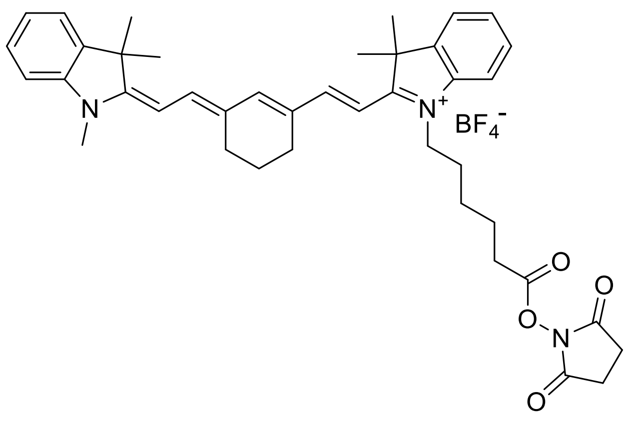

Figure 23. Chemical structure of Cy7 NHS.

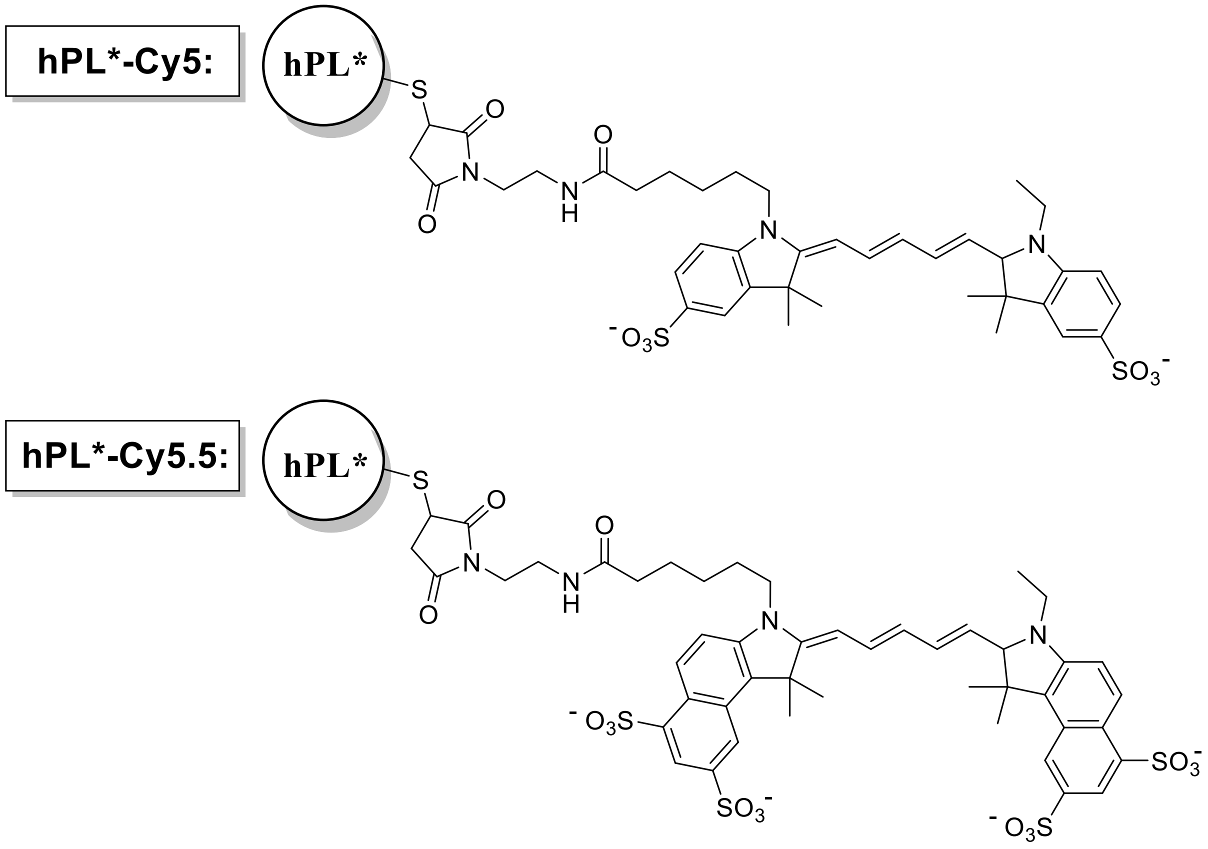

Figure 24. Structure of hPL*-Cy5 and hPL*-Cy5.5.

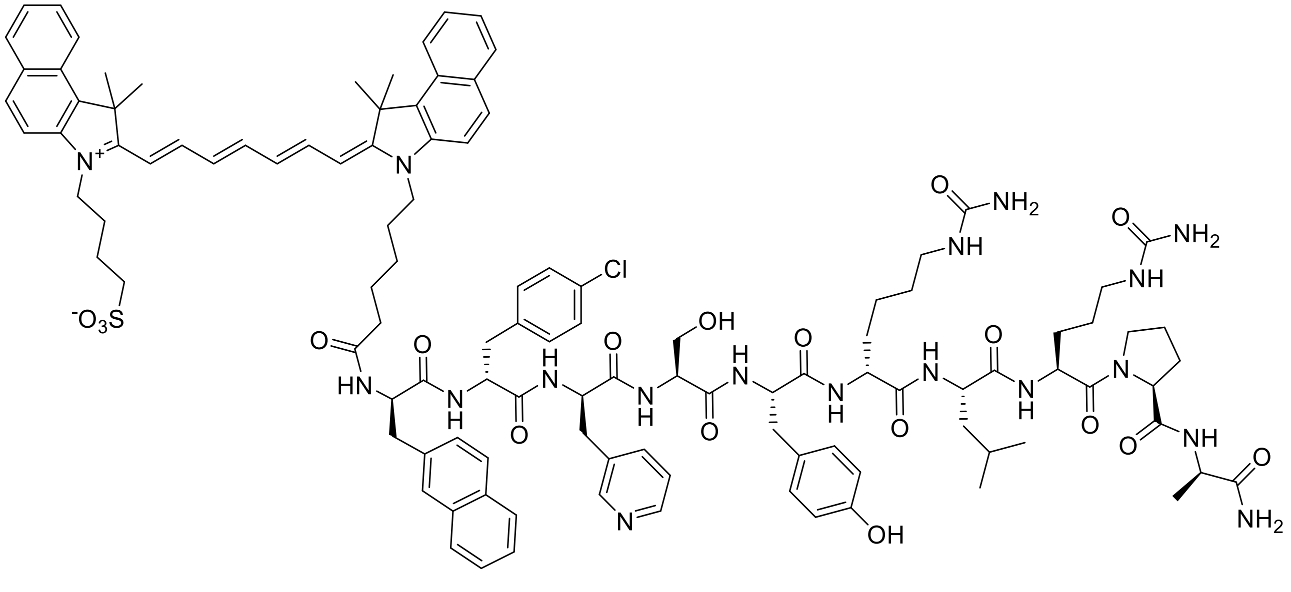

Figure 25. Chemical structure of GnRHa-ICG.

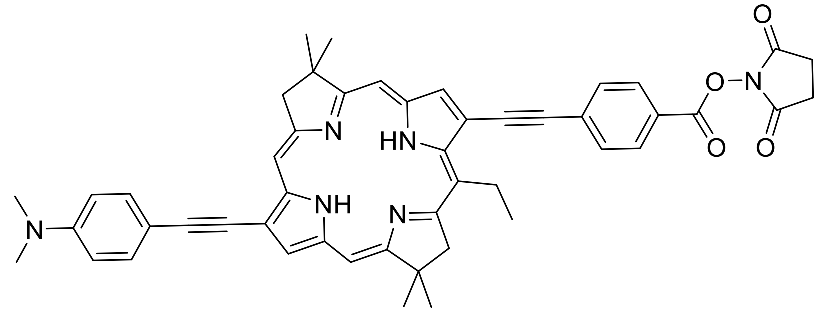

Figure 26. Chemical structure of NMP1.

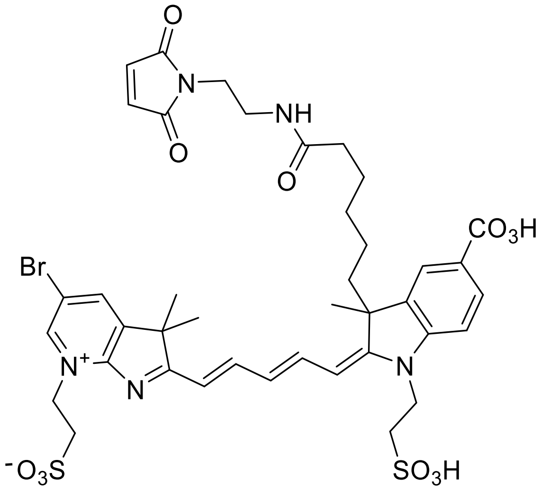

Figure 27. Chemical structure of AlexaFluor 680.

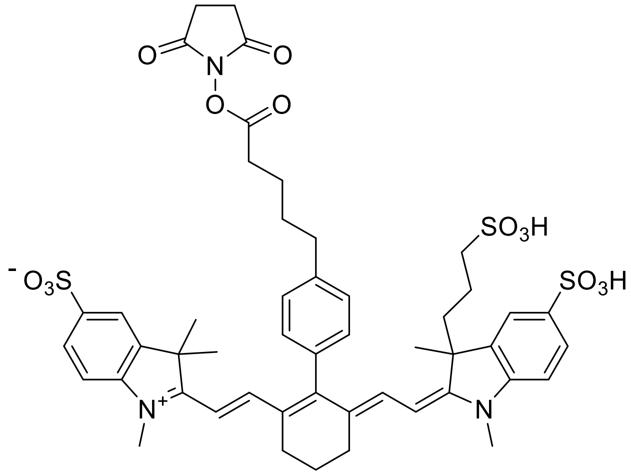

Figure 28. Chemical structure of AlexaFluor 750.

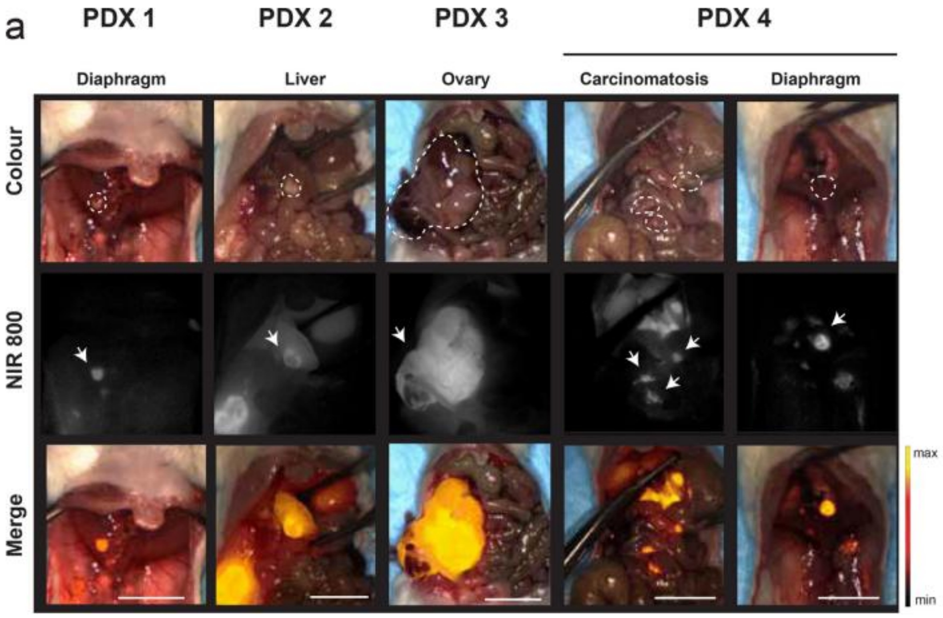

Image 4. Intraoperative white light (colour), near infrared (NIR 800) fluorescent and pseudo-colorued fluorescence intensity merge images show positive identification of primary tumor and small metastatic lesions in four separate, orthotopically implanted PDX models of HGSOC.[204]

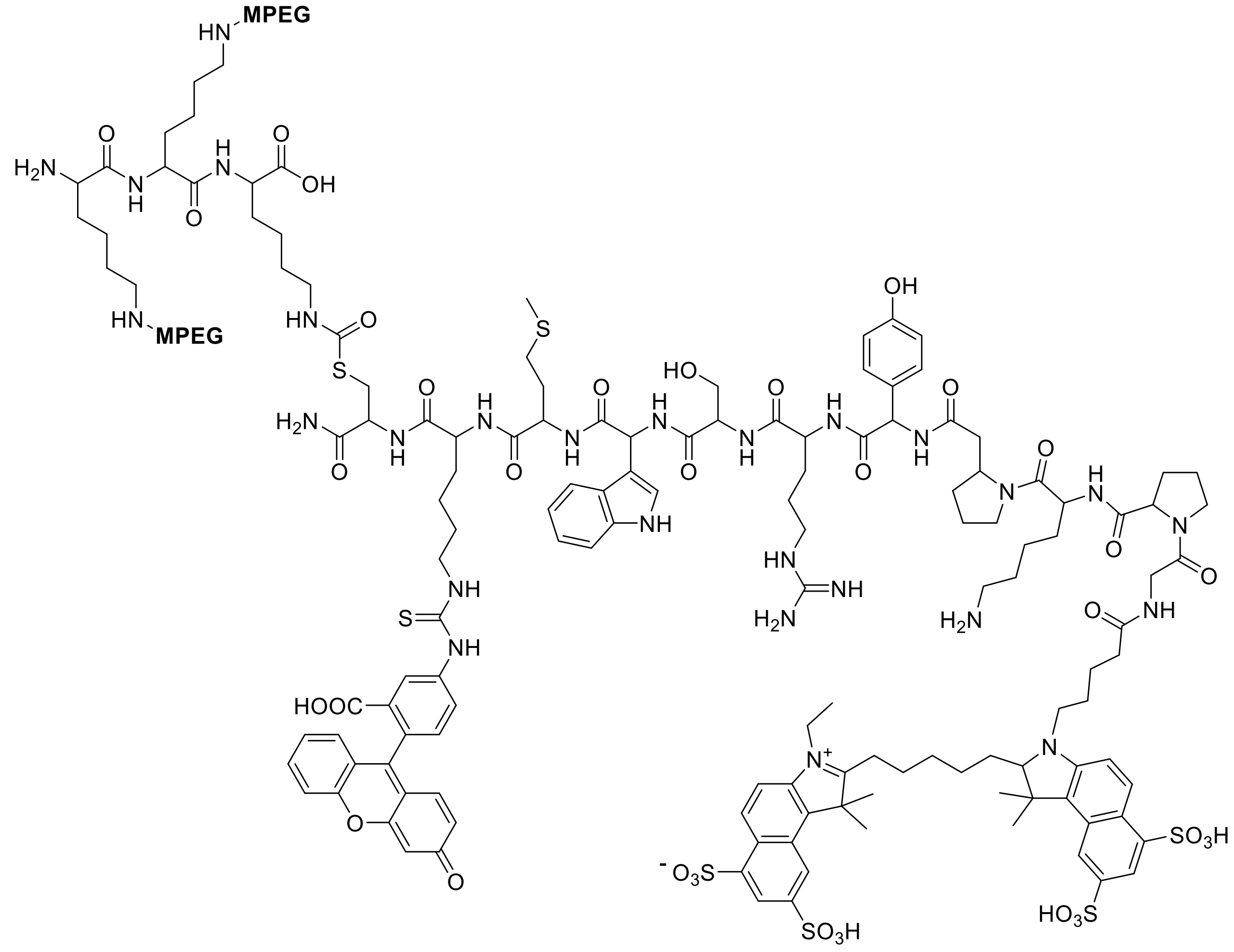

Figure 29. Chemical structure of MMP-3-sensitive probe.

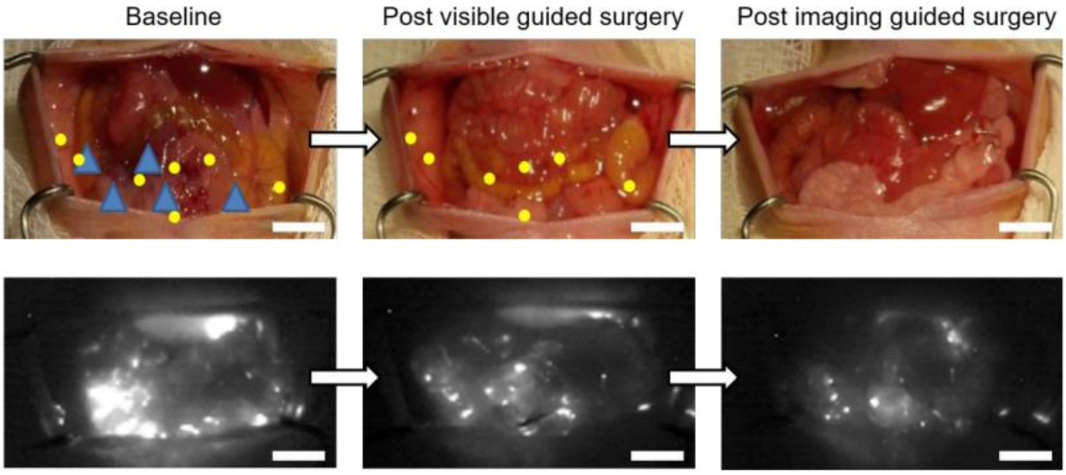

Image 5. Steps of surgery. Visible pictures (top) and corresponding fluorescent images with representative visible (blue arrowheads) and microscopic tissues (yellow dots). After visible surgical resection, no visible disease is observed; the remaining fluorescence-labelled tissues are removed with SWINTs guidance.[226]

Table 1. Summary of covered fluorescent-imaged guided surgery probes of ovarian cancer.

Probe	Target	Target recognizing moiety	Fluorophore	Reference
RR11	COX-1	Mofezolac	Nile Blue	[28-29]
MSA14	COX-1	Mofezolac	NIR cyanine	[29]
CMP	COX-1	SC-560	Carboxy-X-rhodamine fluorophore	[30]
Q_3STCy	hNQO1	2-mercaptoethanol	NIR fluorophore	[40]
HMRef-βGal	β-Galactosidase (β-Gal)	*β*-galactose	HMR-Ref	[44]
BOD-M-βGal	β-Galactosidase (β-Gal)	*β*-galactose	Boron dipyrromethene (BODIPY)-based fluorophore	[47]
FA-HDL(DiR-BOA) NPs	FRα	Folic Acid	NIR fluorescent dye DiR-BOA	[12]
Folate-specific activatable probe (FSA)	FRα	Folic Acid	NIR dye ATT655	[53]
EC17	FRα	Folic Acid	Fluorescein (FITC)	[54-57]
^{111}In-farletuzumab-IRDye800CW	FRα	Farletuzumab	IRDye800CW	[58]
HSA&ICG-FA NPs HSA&FITC-FA NPs	FRα	Folic Acid	ICG FITC	[19]
HSA&phthaloNO2-AB NPs	FRα	AB	Phthalocyanine fluorescent dye (phthaloNO_2)	[59]
FolateSiR 1	FRα	Folic Acid	Si-Rhodamine (2-COOH SiR650)	[60]
FA-BSA-AuNCs	FRα	Folic Acid	BSA-AuNCs	[63]
FA-ZW800-1-Forte	FRα	Folic Acid	ZW800-1-Forte	[65]
Plu-IR780-chit-FA	FRα	Folic Acid	IR780	[66]

FA-IR780&PFOB-SNPs	FRα	Folic Acid	IR780	[67]
OTL38	FRα	Folic Acid	Indocyanine Green-like NIR dye	[64,73-74]
AngioStamp®	$\alpha_v\beta_3$-integrin	RAFT-(cRGDfK)$_4$	Not available	[79]
AngioStamp800	$\alpha_v\beta_3$-integrin	RAFT-(cRGDfK)$_4$	IRDye800CW	[83]
IntegriSense 680	$\alpha_v\beta_3$-integrin	$\alpha_v\beta_3$-integrin nonpeptidic antagonist	NIR fluorophore	[91]
SqRGD2	$\alpha_v\beta_3$-integrin	cRGDfK	NIR-emitting squaraine dye (Sq)	[92]
AF680-labeled phage-J18	EGFR	biotinylated-peptide J18	AF680	[104]
BrCy106-NHS-doped optical viral ghosts (OVGs)	HER-2	Antibodies against HER-2	NIR bromo-cyanine dye BrCy106-NHS	[118]
FITC-conjugated CPE peptide	Claudin 3/4	cCPE	Fluorescein isothiocyanate (FITC)	[127-128]
CW800-cCPE	Claudin 3/4	cCPE	IRDye800CW	[132]
LbL DCNPs	CD44	Hyaluronic Acid (HA)	Inorganic fluorescent dye DCNPs	[133]
G4RGDSq2	LPA	G4RGD	NIR-emitting squaraine dye (Sq)	[138]
COC183B2-Cy7	OC183B2	COC183B2	Cy7	[140-141]
COC183B2-800	OC183B2	COC183B2	IRDye800CW	[141]
^{ss}B43.13-IR800	Cancer antigen 125 (CA125)	mAb-based targeting moiety (B43.13)	IRDye800CW	[155]
NIR fluorescent hPL*-conjugates	Prolactin receptor (PRLR)	Recombinant human placental lactogen* (hPL*)	Cy5 Cy5.5	[169]
DCNPs-$L_{1/2}$-FSH_β	FSHR	FSH_β	NIR-II-emitting inorganic down-shifting nanoparticles (DCNPs)	[180]
DSNPs@FSHP	FSHR	Follicle-Stimulating	NIR-II fluorescent lanthanide-based	[182]

		Hormone Peptide (FSHP)	down-shifting nanoparticles (DSNPs)	
GnRHa-ICG	GnRHR	The peptidic antagonist of GnRHR (GnRHa)	Indocyanine Green (ICG)	[186]
*h*GSA-NMP1	Lectin receptors	*human* Galactosyl Serum Albumin (hGSA)	Synthetic dye (NMP1)	[193]
CD24-AF680	CD24	Mouse-derived monoclonal antibody against human-CD24	AF680	[203]
CD24-AF750	CD24	Mouse-derived monoclonal antibody against human-CD24	AF750	[204]
Metalloproteinase-3 (MMP-3)-sensitive probe	MMP-3	MMP-3-specific peptide substrate	NIR fluorophore Cy5.5	[217]
Single-walled carbon nanotubes (SWNT) probe	Secreted Protein Acidic and Rich in Cysteine (SPARC)	cylindrical non-lytic-M13-bacteriophage	intrinsic NIR-II fluorescence	[226]
Fluorescent Silica Nanoparticles (SiNPs)	Tumor-Associated Macrophages (TAMs)	Anionic SiNPs capable of targeting	Red fluorescent dye (structure not available)	[239]
Silica-coated Up-Converting Nanoparticles (UCNPs)	Tumor-Associated Macrophages (TAMs)	Specific multilayer core@shell structure	Intrinsic NIR Fluorescence of UCNPs	[240]

Dr. Roberta Solidoro graduated cum laude in Pharmacy (2020) is currently attending her PhD in Pharmaceutical Sciences at the University of Bari with Prof. Antonio Scilimati. Her project concerns the development of novel diarylisoxazole-based COX-1 inhibitors and COX-1-targeting selective fluorescent probes for *in vivo* ovarian cancer detection.

Dr. Antonella Centonze graduated in Pharmaceutical Chemistry and Technology. Subsequently, after obtaining her PhD in Medicinal Chemistry developing fluorescent organic nanoparticles (FONPs) targeting children midline gliomas, she was employed at Merck Group as a quality control analyst.

Dr. Morena Miciaccia is a Researcher at the Department of Pharmacy-Pharmaceutical Sciences, University of Bari. Her main research interests focus on the biopharmaceutical evaluation of small molecules with potential applications in oncology.

Dr. Olga Maria Baldelli graduated cum laude in Pharmacy (2022). After, one-year research grant under the supervision of Prof. Antonio Scilimati she is currently PhD student in Medicinal Chemistry developing positron emission tomography agents for tumor imaging.

Dr. Domenico Armenise graduated cum laude in Pharmaceutical Chemistry and Technology (2022). He is currently a PhD student in Medicinal Chemistry at the University Aldo Moro of Bari under the supervision of Prof. Antonio Scilimati. He is currently involved in the synthesis of putative compounds targeting children's gliomas.

Prof. Savina Ferorelli Associate Professor of Medicinal Chemistry at University of Bari-Italy. Her research interests are devoted to study structure-affinity and structure-activity relationships for serotonergic, dopaminergic, and sigma receptors. Currently, she is developing highly selective COX inhibitors for PET and fluorescence imaging.

Prof. Maria Grazia Perrone is an Associate professor at the University of Bari. Her scientific interest concerns the design, preparation, and biopharmaceutical characterization of compounds with potential application in cancer and cardiovascular diseases. She develops in vitro methods for testing their activity and their ADME properties.

Prof. Antonio Scilimati researcher at the University of Bari (Italy) and University of Wisconsin (USA) (1984-1994). Top Manager of the Biotech Industry Merck-Serono producing recombinant reproductive hormones-drugs (1994-1998); since 1998 Associate Professor of Medicinal Chemistry at the University of Bari, where he is responsible of the "Research Laboratory for the Woman and Child Health" focusing is research interest on developing new drugs targeting onco-biomolecules.